# CHALMERS



# Fracture deformation when grouting in hard rock

In situ measurements in tunnels under Gothenburg and Hallandsås

*Master of Science Thesis in the Master's Programme Geo and Water Engineering*

## EDWARD RUNSLÄTT & JOHAN THÖRN

Department of Civil and Environmental Engineering
*Division of GeoEngineering*
*Engineering Geology Research Group*
CHALMERS UNIVERSITY OF TECHNOLOGY
Gothenburg, Sweden 2010
Master's Thesis 2010:87

# Fracture deformation when grouting in hard rock

In situ measurements in tunnels under Gothenburg and Hallandsås

*Master of Science Thesis in the Master's Programme Geo and Water Engineering*

EDWARD RUNSLÄTT & JOHAN THÖRN

Department of Civil and Environmental Engineering
*Division of GeoEngineering*
*Engineering Geology Research Group*
CHALMERS UNIVERSITY OF TECHNOLOGY

Gothenburg, Sweden 2010

Fracture deformation when grouting in hard rock
In situ measurements in tunnels under Gothenburg and Hallandsås
*Master of Sceince Thesis in the Master's Programme Geo and Water Engineering*
EDWARD RUNSLÄTT & JOHAN THÖRN

Department of Civil and Environmental Engineering
Division of GeoEngineering
Engineering Geology Research Group
Chalmers University of Technology
SE-412 96 Göteborg
Sweden
Telephone: + 46 (0)31-772 1000

Cover:
Deformation measurement equipment installed in Hallandsås (see further Section 2.3).

Fracture deformation when grouting in hard rock
In situ measurements in tunnels under Gothenburg and Hallandsås
*Master of Science Thesis in the Master's Programme Geo and Water Engineering*
EDWARD RUNSLÄTT & JOHAN THÖRN
Department of Civil and Environmental Engineering
*Division of GeoEngineering*
*Engineering Geology Research Group*
Chalmers University of Technology

ABSTRACT

When grouting fracture systems in crystalline rock the grout is pumped with a substantial overpressure. The force that the pressurised grout induces onto the fracture surfaces may change the aperture and deform the rock mass. If one grouted fracture is deformed, the interaction between blocks in the rock mass may cause another fracture to close, open, or shear along its fracture plane. Such effects may reduce the grouting efficiency as new paths for water leakage is opened. The objective of this project is to measure and evaluate the results from such deformations in situ.

The measurements have been performed with newly developed equipment from Chalmers University of Technology. Initially the equipment was tested in a service tunnel under Gothenburg, but due to various reasons no deformation measurements were conducted and the work was continued in Hallandsås. The results are compared to calculations of rock stress and estimates of fracture stiffness based on hydraulic tests and grouting.

Deformation was successfully measured seven times in one borehole. For six measurements the magnitude of deformation was 30-60 μm. The largest part of the deformations occurred at a pump pressure between 1-1.4 MPa, which is lower than the estimated rock stress. Fracture stiffness showed some scatter but generally the stiffness is lower in Hallandsås than for the service tunnel.

Key words:  Deformation measurements, fracture stiffness, hydromechanical coupling, hydraulic testing, rock stresses

Sprickdeformation vid injektering i hårt berg
Fältmätningar i Göteborg och Hallandsås
*Examensarbete inom Mastersprogrammet Geo and Water Engineering*
EDWARD RUNSLÄTT & JOHAN THÖRN
Institutionen för bygg- och miljöteknik
*Avdelningen för Geologi och Geoteknik*
*Forskargrupp Geologi*
Chalmers tekniska högskola

SAMMANFATTNING

När spricksystem i kristallint berg injekteras pumpas bruket med ett betydande övertryck. Kraften som bruket utövar på sprickornas ytor kan komma att ändra vidden och deformera berget. Om en injekterad spricka deformeras kan interaktionen mellan block i bergmassan leda till att andra sprickor stängs, öppnas eller skjuvas. Sådana effekter kan reducera injekteringseffektiviteten eftersom nya flödesvägar skapas. Syftet med examensarbetet är att mäta och utvärdera resultatet från sådana deformationer in situ.

Mätningarna har utförts med en nyutvecklad mätutrustning från Chalmers tekniska högskola. Inledningsvis testades utrustningen i en installationstunnel under Göteborg, men av olika anledningar kunde ingen deformationsmätning utföras och arbetet fortsatte istället i Hallandsåstunneln. Resultaten jämförs med beräkningar av berg-spänningar och skattningar av sprickstyvhet, baserade på data från hydrauliska tester och injektering.

Deformation uppmättes framgångsrikt sju gånger i ett och samma borrhål. Sex av dessa mätningar uppvisade deformationer i storleksordningen 30-60 μm. Majoriteten av deformationerna skedde vid ett pumptryck på 1-1.4 MPa, vilket är lägre än den beräknade bergspänningen. Sprickstyvhetsuppskattningar uppvisar viss spridning men generellt är styvheten lägre i Hallandsåstunneln än i Göteborgstunneln.

Nyckelord: Deformationsmätning, sprickstyvhet, hydromekanisk koppling, hydrauliska tester, bergspänning

# Contents

# List of Appendices

# Preface by supervisors

Detta examensarbete förenar teori och praktik. Arbetet är omfattande och väl genomfört. Centralt är deformation av sprickor i en tunnels nävområde som följd av spänningsändringar vid hydrauliska tester och injektering. En ny utrustning för mätning av deformation har testats och utvecklats under fältarbetet i två tunnelprojekt. Mätningar har använts för att skatta sprickstyvheter och resultatet har jämförts med data från litteraturen. En ökad förståelse för det spruckna bergets kopplade hydromekaniska egenskaper och metoder för att mäta detta kan komma att bli värdefullt för framtida tunnelprojekt.
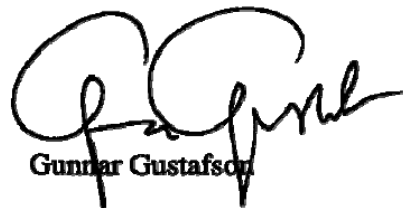
Göteborg i juni 2010

Johan Funehag                    Åsa Fransson                    Gunnar Gustafson

# Preface

This master thesis project was carried out at the Department of Civil and Environmental Engineering, Division of GeoEngineering, Engineering Geology Research Group, Chalmers University of Technology, Sweden. Supervisor was Johan Funehag, Chalmers University of Technology and examiner was Gunnar Gustafson, Chalmers University of Technology.

We wish to extend our sincere thanks to Johan Funehag, Åsa Fransson and Gunnar Gustafson for invaluable support and guidance during the work. Great thanks to Aaro Pirhonen and Peter Hedborg for all help with the practical and technical solutions with the test equipment. Also, thanks to our opponent Sara Kvartsberg for reading and commenting on our work.

Finally we would like to thank the staff at Bergavdelningen Tyrens, for company and support during the work. A special thank goes to the staff from Skanska/Vinci and Banverket at the Hallandsås tunnel, and Telia and Besab at the service tunnel, for providing us with the sites for in situ measurements.

Gothenburg June 2010

Edward Runslätt                         Johan Thörn

# Notations

## Roman letters

| | | |
|---|---|---|
| $a$ | (m) | Radius of circular opening |
| $b$ | (m) | Fracture aperture |
| $b_{hyd}$ | (m) | Hydraulic aperture |
| $dh$ | (m) | Pressure change |
| $g$ | (m/s$^2$) | Gravity |
| $I_{max}$ | (m) | Maximum penetration length |
| $I_{max}^{Cement}$ | (m) | Maximum penetration length for cementitous grout |
| $I_{max}^{Silica}$ | (m) | Maximum penetration length for silica sol |
| $k$ | (-) | Ratio $\sigma_h/\sigma_v$ |
| $k_n^{hyd}$ | (Pa/m) | Fracture stiffness based on hydraulic aperture |
| $k_n^{meas}$ | (Pa/m) | Fracture stiffness based on measured deformation |
| $k_n^S$ | (Pa/m) | Fracture stiffness based on storativity |
| $L$ | (m) | Length |
| $p$ | (Pa) | Pressure |
| $p_g$ | (Pa) | Grout overpressure |
| $Q$ | (m$^3$/s or l/min) | Flow |
| $Q/dh$ | (m$^2$/s) | Specific capacity |
| $Q_{inner}$ | (m$^3$/s or l/min) | Flow from inside packer |
| $Q_{out}$ | (m$^3$/s or l/min) | Flow from outer 2-3 m of drilled hole |
| $Q_{tot}$ | (m$^3$/s or l/min) | Total flow from drilled hole |
| $r$ | (m) | Distance from centre of circular opening |
| $r_w$ | (m) | Borehole radius |
| $S$ | (-) | Storativity |
| $T$ | (m$^2$/s) | Transmissivity |
| $T_f$ | (m$^2$/s) | Fracture transmissivity |
| $t$ | (s) | Time |
| $t'$ | (s) | Recovery time |
| $t_e$ | (s) | Equivalent recovery time |
| $t_g$ | (-) | Gel induction time |
| $t_p$ | (s) | Flow period pressure build up test |
| $u_n$ | (m) | Normal deformation |
| $z$ | (m) | Depth |

## Greek letters

| | | |
|---|---|---|
| $\Delta a_i$ | (m) | Initial deformation |
| $\Delta a_J$ | (m) | Jacking |
| $\Delta a_u$ | (m) | Deformation due to redistribution of stresses |
| $\Delta b_{hyd}$ | (m) | Change in hydraulic aperture |
| $\Delta b_{meas}$ | (m) | Measured deformation |
| $\Delta b_n$ | (m) | Normal deformation |

| | | |
|---|---|---|
| $\Delta h$ | (m) | Hydraulic head |
| $\Delta p$ | (Pa) | Overpressure |
| $\Delta s$ | (m) | Pressure change during PBT |
| $\Delta u_n$ | (m) | Deformation |
| $\theta$ | (°) | Angle from vertical |
| $\kappa$ | (°) | Angle between tunnel wall and fracture |
| $\mu$ | (Pas) | Viscosity |
| $\mu_0$ | (Pas) | Viscosity silica sol |
| $\mu_w$ | (Pas) | Viscosity of water |
| $\rho$ | (kg/m$^3$) | Density |
| $\rho_f$ | (kg/m$^3$) | Density of fluid |
| $\rho_w$ | (kg/m$^3$) | Density water |
| $\sigma_{\parallel}$ | (Pa) | Principal horizontal stress, parallel to tunnel wall |
| $\sigma_L$ | (Pa) | Principal horizontal stress, perpendicular to tunnel wall |
| $\sigma_1$ | (Pa) | Largest principal stress |
| $\sigma_2$ | (Pa) | Intermediate principal stress |
| $\sigma_3$ | (Pa) | Smallest principal stress |
| $\sigma_h$ | (Pa) | Smallest horizontal principal stress |
| $\sigma_H$ | (Pa) | Largest horizontal principal stress |
| $\sigma_n$ | (Pa) | Normal stress upon a fracture |
| $\sigma'_n$ | (Pa) | Effective normal stress |
| $\sigma_r$ | (Pa) | Radial stress around circular opening |
| $\sigma_\theta$ | (Pa) | Tangential stress around circular opening |
| $\sigma_v$ | (Pa) | Vertical rock stress |
| $\sigma_x$ | (Pa) | Horizontal stress in Kirsch equations |
| $\sigma_z$ | (Pa) | Vertical stress in Kirsch equations |
| $\tau$ | (Pa) | Shear stress |
| $\tau_0$ | (Pa) | Yield stress of grout |
| $\tau_{r\theta}$ | (Pa) | Shear stress around circular opening |

## Abbreviations

| | |
|---|---|
| BH | Borehole, used for percussion drilled holes |
| CFL | Chalmers flow logger, equipment for 0.5 m section inflow tests |
| KBH | Cored borehole, from Swedish: Kärnborrhål |
| NIT | Natural inflow test |
| PBT | Pressure buildup test |
| PFL | Posiva flow logger |
| PL | Pressure loss |
| WPT | Water pressure test |

# 1 Introduction

When grouting fracture systems in crystalline rock the grout is pumped with a substantial overpressure. The force that the pressurised grout induces onto the fracture surfaces may change the aperture and deform the rock mass. If one grouted fracture is deformed, the interaction between blocks in the rock mass may cause another fracture to close, open, or shear along its fracture surface. Such effects may reduce the grouting efficiency as new paths for water leakage is opened.

Previous works carried out in this area, for example Barton (2004ab), Cornet (2003) and Gothäll (2009) indicates that deformation occur in fractures when pressurized. However there seems to be little work carried out by measuring total deformation of a fractured rock mass when grouted or injected with water. This report, written as a master's thesis in the Geo and Water engineering programme at Chalmers University of Technology, aims at predicting, measuring and evaluating such water or grout induced deformations.

## 1.1 Objective

The objective of this project is to measure and evaluate the result from deformations that occur in the rock mass close to a tunnel wall when grouting. These measurements are compared to theoretical calculations of rock stresses and fracture stiffness in order to assess the plausibility of the measurements.

## 1.2 Scope of work

The work is carried out in two tunnels which were post grouted with silica sol during the spring 2010. The first tunnel is a service tunnel under Gothenburg which were built in the early 1970s in a sparsely fractured granodiorite. The second tunnel is a railroad tunnel through Hallandsås, a highly fractured gneiss horst, close to Båstad. The studied part of this tunnel was constructed in 1993-1995. The deformations are measured with newly developed equipment from Chalmers University of Technology.

The deformation measured is the effective component aligned with the measurement equipment. The method does not allow analysis of deformations in other directions. A combined action of reduced normal stress and shear stress could deform a fracture. A deeper analysis of this failure mode might be possible to perform with the calculated stresses, and data from the fracture mapping. But such analysis is beyond the scope of this thesis.

## 1.3 Hypotheses

This section is an account for the general assumptions under which the work is carried out. It shall be regarded as a starting point, from which the further work emerges.

When grouting a hydraulic open fracture a deformation might occur. In the zone closest to the tunnel wall the radial rock stresses are small, which increases the probability for deformation.

In order to visualize the interaction between the stress situation in the rock mass, and the stresses that grout induces onto sides of grouted fractures, a schematic model is built. The model represents a part of the horizontal plane at mid-height of the tunnel wall (see Figure 1.1). The scale of the model is a couple of meters, and the boundary conditions applied are the in situ stress situation. The rock stress close to the tunnel wall is assumed to be small. Therefore it is probable that the grout pressure onto the fracture sides will cause a measurable deformation.
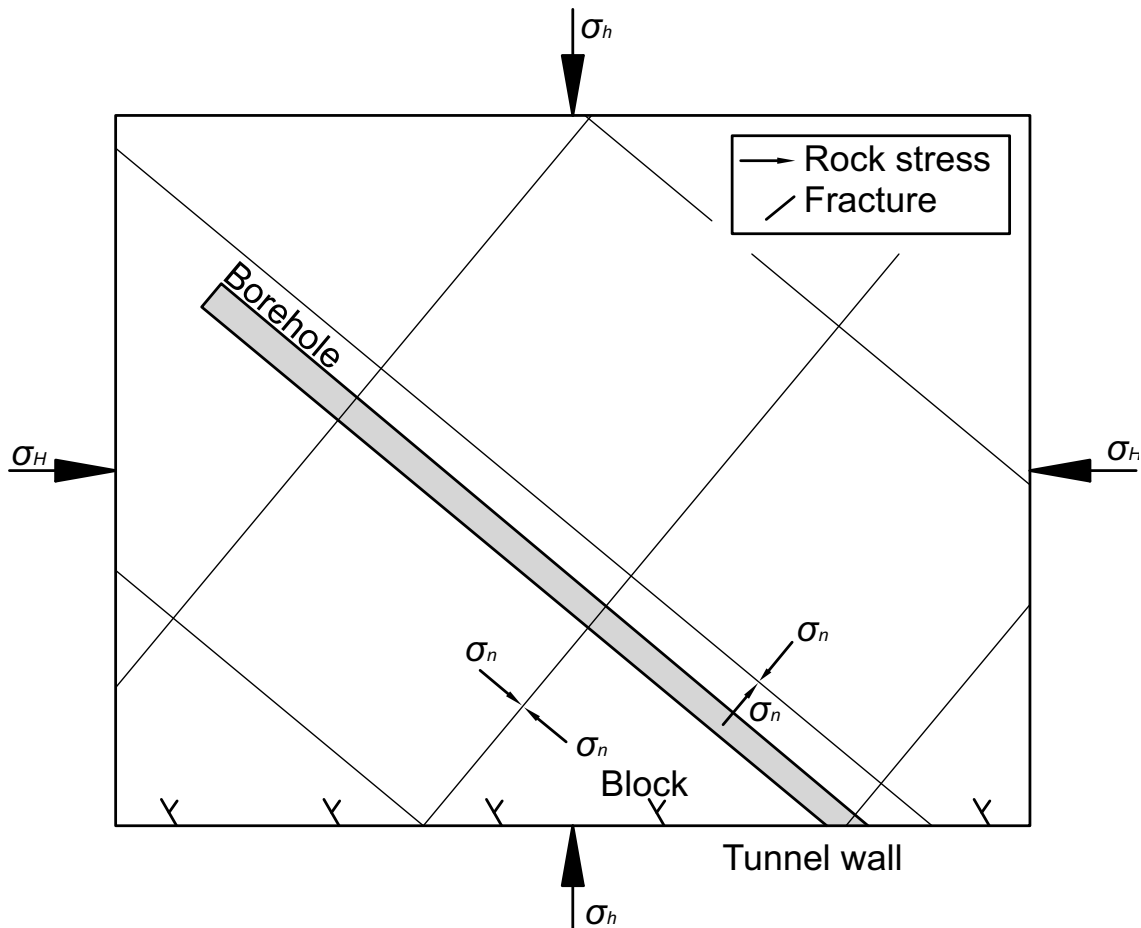


*Figure 1.1: A simple model of the in situ stresses. $\sigma_H$ and $\sigma_h$ is the principal in situ stresses, $\sigma_h$ is zero at the tunnel wall, and grows with distance from tunnel. $\sigma_n$ is the normal stress on the fractures.*

# 2 Method

The method to achieve the scope of this thesis consists of three different approaches in order to describe the deformation of a fracture. A theoretical global stress model is performed in order to estimate the normal stress on a single fracture. The global stress situation is described with both measured and empirical data. The stress field due to an opening (tunnel) in the rock mass is calculated with a software called Examine2D and the Kirsch equations (Kirsch 1898). A low stress is assumed to indicate a low stiffness. The second approach utilizes data from hydraulic testing to assess the fracture normal stiffness. Fracture transmissivity is evaluated from the tests and a fracture normal stiffness is then calculated.

In the third approach mapping and geometric modelling were tools for finding fractures with possible contact between two boreholes in a sparsely fractured rock mass. For a highly fractured rock mass it was assumed that a contact was present in any two boreholes close to each other. Hydraulic tests were conducted in order to prove such a fracture connection. When a connection was proved deformation measurements during hydraulic tests and grouting were conducted. The test setup for deformation measurement was mounted, with an anchor (see Section 2.3), in one of the two boreholes. The other borehole was grouted and the deformation was logged.

First, the theory needed for understanding the tests and analyses performed is presented together with a background to fracture deformations. A conceptual model utilizes the theory described and combines it into a set of assumptions of the fracture behaviour, and how to explain it. The equipment and the test setup used for deformation measurements are described and last the procedure for the work carried out in the two cases is presented.

## 2.1 Theory

In this section a description of the theory, that is needed as a basis for the analysis performed in the thesis, is presented. The description is subdivided into seven paragraphs that sum up to a conceptual model presented in Section 2.2.

### 2.1.1 Stress field

Rock stresses are the concept of forces applied by tectonic activity and the weight of overlying rock mass. When constructing a tunnel in rock the stress field is redistributed in the direct vicinity of the tunnel. Lindblom (2001) describes the stress situation around a tunnel with three sets of stresses; primary, secondary and tertiary stresses. The primary stresses are the stress situation before excavation of the tunnel. The secondary stresses are due to the excavation, support and maintenance of the tunnel, and the tertiary stressed are induced by support forces, pressure and temperature conditions in the tunnel.

### 2.1.1.1 Primary stresses

The direction of the primary or principal stresses, $\sigma_1$, $\sigma_2$ and $\sigma_3$, can be determined by measurements in situ or estimated with empirical equations. For a general case in Scandinavia with a horizontal ground level at a low depth the smallest principal stress, $\sigma_3$ is oriented vertically, and $\sigma_1$ and $\sigma_2$ are horizontal (Lindblom 2001).

The vertical rock stress, $\sigma_v$, can be calculated as the product of gravity, $g$, density, $\rho$, and depth, $z$, (Lindblom 2001 and Hoek 2006) as described in Eq. 2.1. However, measurements around the world have shown a substantial scatter from this equation (Hoek 2006). The horizontal stresses are described by Eq. 2.2 and Eq. 2.3 (Stephanson, Ljunggren and Jing 1991).

$$\sigma_v = \rho \cdot g \cdot z \qquad\qquad \text{Eq. 2.1}$$

$$\sigma_H = 2.8 + 0.04 \cdot z \qquad\qquad \text{Eq. 2.2}$$

$$\sigma_h = 2.2 + 0.024 \cdot z \qquad\qquad \text{Eq. 2.3}$$

Lindblom (2001) suggests that Eq. 2.2 and Eq. 2.3 only shall be used as a first approximation of the stress situation, since the formulas are based on few measurements with one single method; hydraulic fracturing. An accurate estimate of stresses is achieved by measuring the stresses in situ. Such measurements have previously been performed in Hallandsås and Gothenburg area; those results are used in the analysis (section 3.1 and 3.3).

For the case with a hilly topography the horizontal principal stresses are parallel with the ground surface and the vertical stress perpendicular to it. This is valid at surface and shallow depth, but the effect diminishes rapidly with increased depth (Lindblom 2001). For a valley with depth $z$, with gravity loadings only, Amadei & Stephansson (1997) indicate that the majority of the stress direction anomaly at surface on the slope of the valley has disappeared at depth $z$ below the valley floor.

### 2.1.1.2 Secondary stresses

The stress situation around an opening in rock, for example a tunnel is of importance for calculation of the stability of walls and roof. Another application is that fractures loaded with high stress rates tend to be tighter (Eriksson & Stille 2005), and only allow channel-like flow of water. Therefore the grouting performance is affected by the stress situation around a tunnel.

Kirsch suggested in 1898 a solution to the secondary stresses around a circular opening in a plate (see Figure 2.1 and Eq. 2.4-Eq. 2.6). The general feature of this is that a disturbance in the stress field occurs around the opening, and decreases with distance from it.
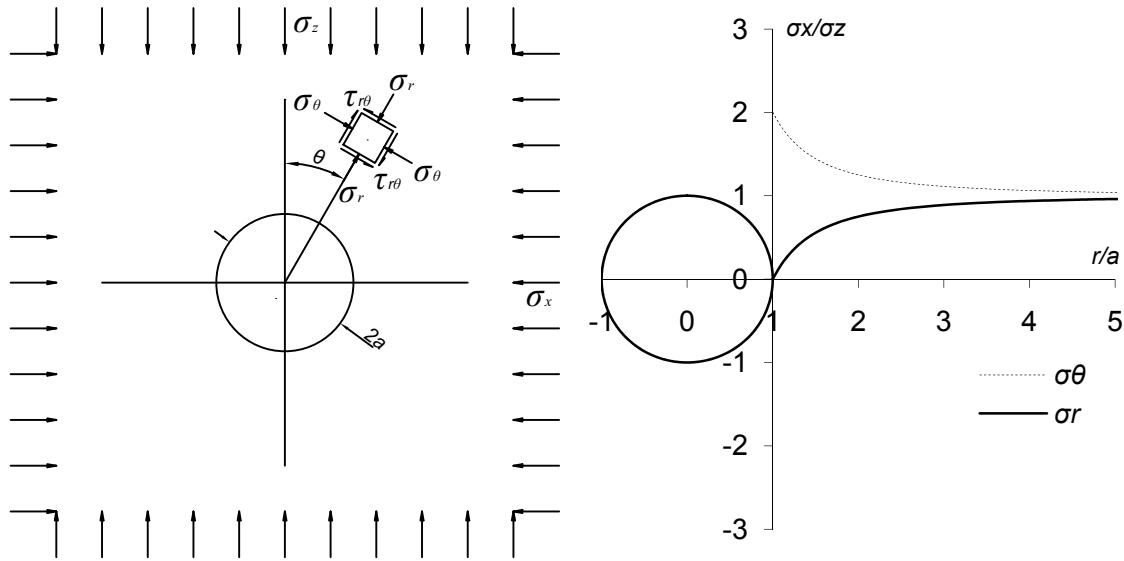
*Figure 2.1: Left: The stress field in a plate with a circular opening, according to Kirsch (1898) (Redrawn from Lindblom 2001). Right: A plot of the radial stress, $\sigma_r$ and the tangential stress, $\sigma_\theta$, and their variation with distance from the tunnel wall.*

$$\sigma_r = \frac{1}{2}\sigma_z\left((1+k)\left(1-\frac{a^2}{r^2}\right)+(1-k)\left(1-4\frac{a^2}{r^2}+3\frac{a^4}{r^4}\right)\cdot\cos 2\theta\right) \qquad \text{Eq. 2.4}$$

$$\sigma_\theta = \frac{1}{2}\cdot\sigma_z\left((1+k)\left(1+\frac{a^2}{r^2}\right)-(1-k)\left(1+3\frac{a^4}{r^4}\right)\cos 2\theta\right) \qquad \text{Eq. 2.5}$$

$$\tau_{r\theta} = \frac{1}{2}\cdot\sigma_z\left(-(1-k)\left(1+2\frac{a^2}{r^2}-3\frac{a^4}{r^4}\right)\sin 2\theta\right) \qquad \text{Eq. 2.6}$$

Where $\sigma_r$ is the radial stress, $\sigma_\theta$ is the tangential stress, $\tau_{r\theta}$ is the shear stress, $k$ is the ratio $\sigma_h/\sigma_v$, $a$ is the tunnel radius, $r$ is the radius to the calculated point and $\theta$ is the angle between the vertical centreline and the calculated point, see Figure 2.1.

A software called Examine2D, developed by Hoek, was used for analyzing noncircular tunnel geometries. Input parameters are the principal stresses, and output is a graphical description of the stress field as well as a table of the stress values in each point. The software applies some simplifications, which is described in the documentation of the software. For example the material is assumed to be homogenous, linearly elastic and isotropic or transversely isotropic.
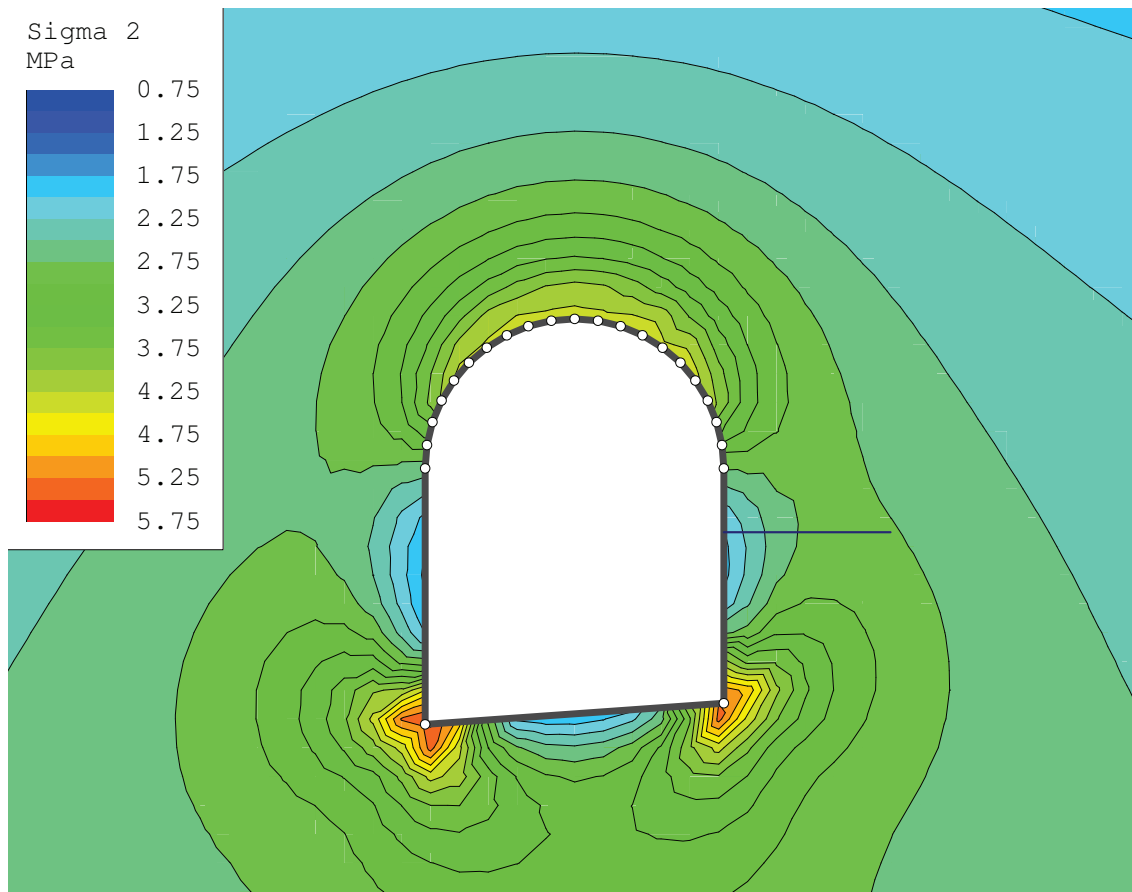
*Figure 2.2: An example of the second principal stress in Hallandsås, calculated in Examine2D.*

### 2.1.2 Fracture characteristics

This paragraph describes the fracture characteristics applicable for the topic of this thesis. The relevant parameters are fracture aperture, *b*, hydraulic aperture, $b_{hyd}$ and transmissivity, *T*.

A fracture can be described as two surfaces with an aperture, *b*, which varies due to the roughness of the surfaces, see Figure 2.3. The area of contact points varies widely, from 1-70 % of the fracture surface area (Jansson 1998). This depends on the rock stress and rock quality. Increased rock stress due to increased depth leads to larger contact areas. According to Hernqvist (2009) aperture and contact area have the largest influence on the flow in fracture networks.
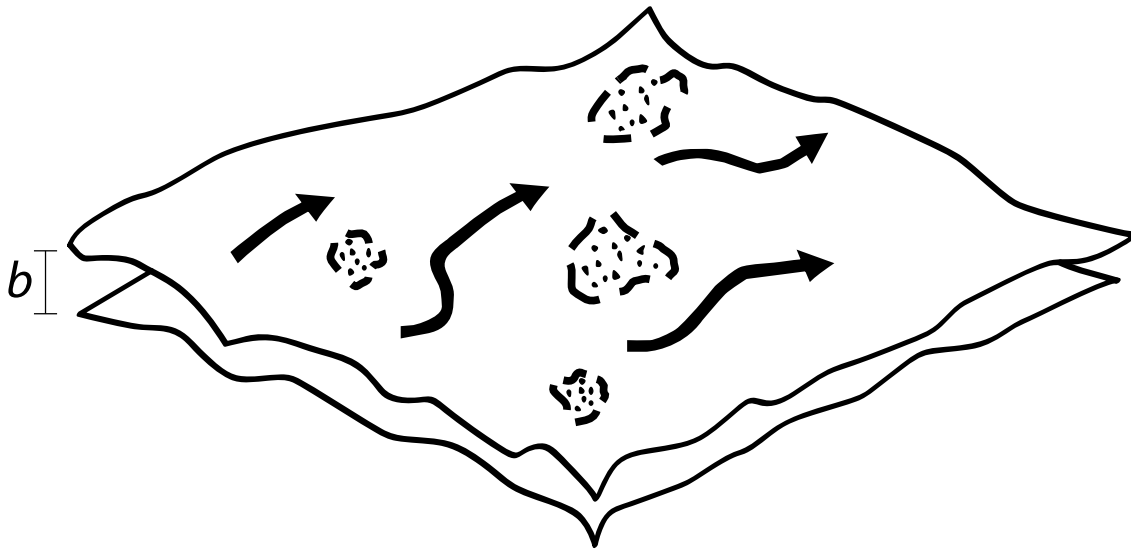
*Figure 2.3: The concept of a fracture regarded as two rough surfaces, with contact points and an aperture, b. The arrows represent the water flow, which has to flow around the contact points (Modified from Hakami 1995).*

The hydraulic aperture, $b_{hyd}$, is described by Snow (1968) with Eq. 2.7 and is known as the cubic law, where $T$ is the fracture transmissivity, $\rho_w$ is the density of water, $g$ the earth acceleration and $\mu_w$ the viscosity of water. The cubic law is valid for both entirely open fractures, and fractures with contacts points (Witherspoon et al, 1980).

$$b_{hyd} = \sqrt[3]{\frac{12 \cdot \mu_w \cdot T}{\rho_w \cdot g}}$$
Eq. 2.7

As seen in Eq. 2.7 the flow is proportional to the cube of the hydraulic aperture. This means that the hydraulic aperture is of great importance when considering fracture characteristics.

The fracture transmissivity describes the ability of a fracture to transmit water. According to Fransson (2001) the specific capacity (Eq. 2.8, where $Q$ is the flow and $dh$ is the difference in hydraulic head) is a good estimation for the transmissivity for a short duration test.

$$T \approx \frac{Q}{dh}$$
Eq. 2.8

The hydraulic aperture distribution of fractures in a rock mass can be described with a Pareto distribution. This means that most of the fractures have small apertures and low transmissivity and only few fractures have large apertures but constitutes a major part of the total transmissivity of a borehole (Gustafson 2009).

Fracture orientation is interesting to get an idea of the direction (strike) and inclination (dip) of the fracture planes. Data can be obtained in several ways, either with mapping of cored boreholes, tunnel wall mapping or surface mapping of outcrops. Fracture

length is, according to Vermilye and Scholz (1995), linked to aperture and may be described with the Pareto analogy. Fractures with large apertures tend to be long and small aperture fractures tend to be short. Fracture intensity is the amount of fractures in a rock mass. A common way to measure the intensity is to count the fractures from a rock core. This is preferable because it is a scale independent parameter (Hernqvist 2009).

### 2.1.3 Fracture stiffness

Fracture stiffness is a measure of a fractures resistance to deformation. There are several ways to estimate the stiffness of a fracture and in this paragraph two different methods is presented. The first one, presented in Rutqvist (1995), describes the fracture normal stiffness as a ratio between change in normal stress and change in aperture. The other method, presented by Fransson (2009) utilizes a relation between fracture normal stiffness and hydraulic storativity, evaluated from hydraulic tests (Rhén et al 2008). The fracture stiffness, $k_n$, can according to Rutqvist (1995) be expressed as the change in effective normal stress, $\Delta\sigma_n'$, divided by the joint normal deformation, $\Delta u_n$:

$$k_n = \frac{\Delta\sigma_n'}{\Delta u_n}$$

Eq. 2.9

The change in effective normal stress is expressed as:

$$\Delta\sigma_n' = \Delta\sigma_n - \Delta p$$

Eq. 2.10

Where $\Delta\sigma_n$ is the change in total normal stress and $\Delta p$ is the change in fluid pressure. Fransson et al. (2010) states that a linear approximation of the fracture stiffness may be done for an incremental displacement $\Delta u_n$, see Figure 2.4 and that the change in effective normal stress in the fracture is $\Delta p/3$. Small values of effective normal stress will result in large deformations if the stress is changed (Rutqvist 1995).
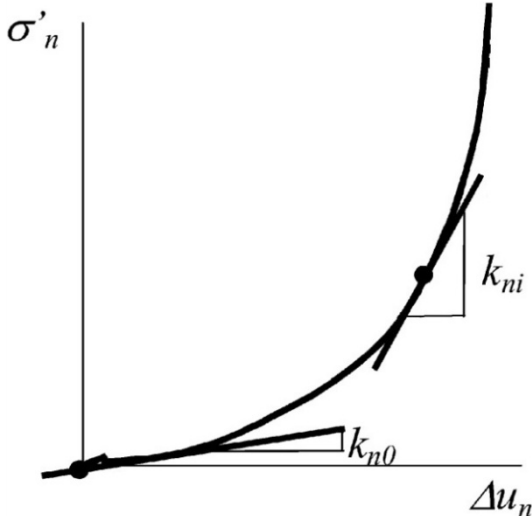


*Figure 2.4: Shows the relation between effective stress and aperture for a normal closure test. The slope of the curve describes the fracture normal stiffness. Modified from Rutqvist (1995).*

Storativity, or coefficient of storage, *S*, is a dimensionless coefficient that describes the quantity of water that is stored in an aquifer. According to empirical studies performed in granitic rock by Rhén et al (2008) the relation between storativity and transmissivity can be expressed as Eq. 2.11. According to Doe and Geier (1990) in Fransson (2009) the storativity of a fracture can be described as Eq. 2.12. Fransson (2009) suggested that it is possible to combine Eq. 2.11 and Eq. 2.12 which gives Eq. 2.13, an estimation of the fracture stiffness with data from hydraulic tests.

$$S = 0.0109T^{0.71}$$ 
Eq. 2.11

$$S = \rho_f g \left( \frac{1}{k_n} \right)$$ 
Eq. 2.12

$$k_n^S = \frac{\rho_f g}{0.0109T^{0.71}}$$ 
Eq. 2.13

### 2.1.4 Fracture flow dimensionality

The flow regime of a fluid in a rock mass can be described in three ways; channel, radial and spherical flow, as shown in Figure 2.5. Gustafson and Stille (2005) introduced an equation (Eq. 2.14) that can determine the flow dimension with an analysis of data from a grouting session, where $Q$ is the instantaneous flow, $t$ is the accumulated time and $V$ accumulated volume at time $t$. The data is plotted in a lin-log diagram, see Figure 2.6, and is compared to three different values. Channel flow (1D) gives a value of about 0.45 and radial flow (2D) a value of 0.8 according to Gustafson and Stille (2005) and Butron (2010) suggest a value of 1 or higher for a 3D flow.

**Linear flow, 1D**   **Radial flow, 2D**   **Spherical flow, 3D**
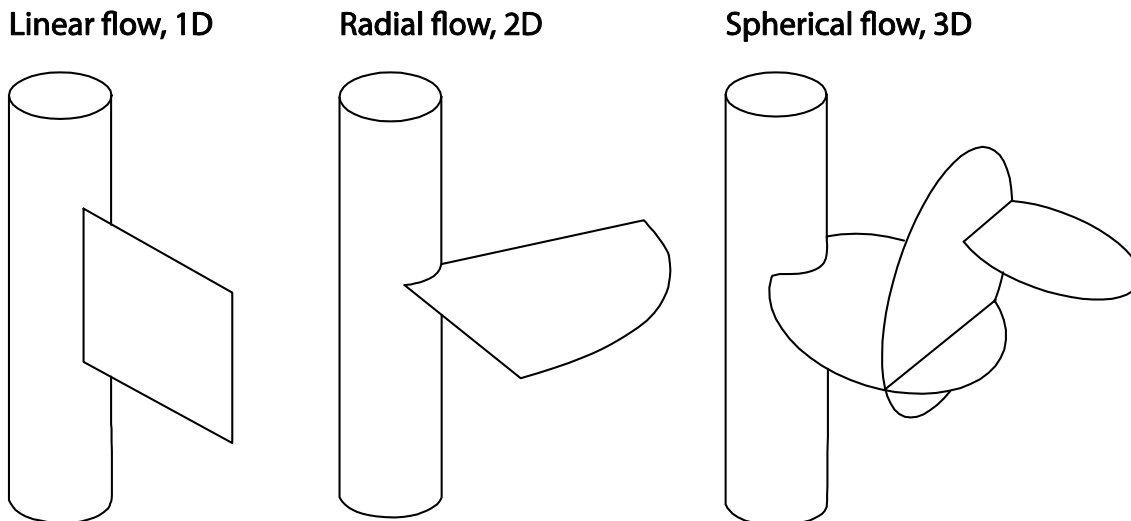


*Figure 2.5: The concepts of flow dimensions. A linear, or 1D flow spreads with a constant front. A radial, or 2D flow spreads in two directions, having an increasing front length. Spherical, or 3D flow is the flow in a well connected fracture system, or deforming fractures. Modified from Doe & Geier (1990).*
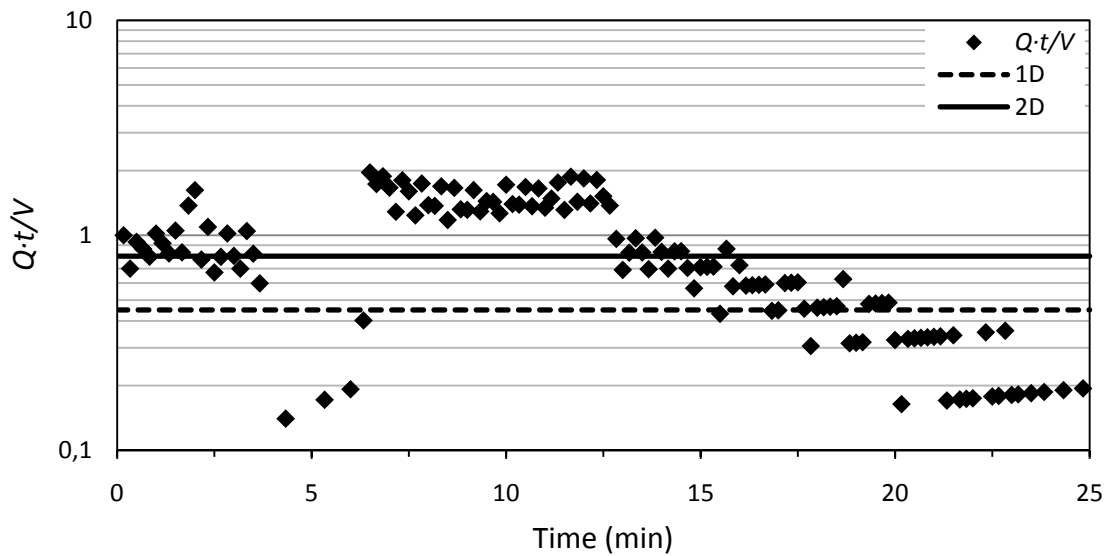
*Figure 2.6: Example of a flow dimensionality diagram, with data from a grouting session in Hallandsås. At 7-12 min there is a 3D-flow, 13-14 min a 2D-flow and 16-18 min a 1D-flow. See Appendix VI.*

$$\frac{d \cdot \log V}{d \cdot \log t} = \frac{Q \cdot t}{V}$$

Eq. 2.14

Fransson et al. (2010) describes that a 2D flow regime may indicate fractures with few contact points and low stiffness. Thus a flow going from 2D to 3D could be due to deformation. The application of flow dimensionality, in this thesis, is to see if it can be an indicator for deformation. A 3D flow can either be seen as flow in a well connected fracture network, deformation of fractures, or both.

## 2.1.5 Grouting

The purpose of grouting is to reduce the inflow of water into a tunnel. There is often a maximum allowed inflow rate that determines the grouting magnitude that is needed. There are two different options when a tunnel should be grouted, either during the excavation of the tunnel, pre-grouting, or after the excavation is done, post-grouting. The common concept is usually to pre-grout and if the inflow rate still is exceeded the affected sections is post-grouted. The work is done by making boreholes that forms a fan around the tunnel. A grouting agent is then pumped into the holes and spread out in the connecting fractures, causing an increased pore pressure. The parameters that determine the grout design is, according to Funehag (2007):

- Rock characteristics (transmissivity, fracture orientation, intensity, aperture and length)

- Grouting performance (overpressure and time)

- Material characteristics of the grout (yield strength, viscosity and hardening/gel induction time)

According to these aspects the rock mass needs to be well characterized and analyzed both as a desk study and in field, in order to design a successful grouting fan. The three main aspects, mentioned above, can be affected either directly or indirectly. A direct parameter is for example the pump overpressure that can be changed directly if needed, while an indirect parameter is the rock characteristics where the parameter itself cannot be changed and in order to make a change the borehole design must be redone. For the application relevant to this thesis the rock characteristics and grouting performance are of interest, and are further discussed below.

A rock mass consists of a large variation of fracture apertures, in a range from ten to a few hundred micrometers (Gothäll & Stille 2009). Because of this different grouting agents are needed in order to seal a sufficient amount of the fractures, sufficient enough to meet the maximum allowed inflow rate. There are two types of grouting agents, cementitious and non-cementitious, where the first is used for apertures larger than 100 μm (Gustafson 2009) since its granular composition won't allow it to penetrate smaller fractures. A non-cementitious agent is used for smaller apertures, where for example silica sol can penetrate fractures down to at least 14 μm (Funehag 2007).

Because of the different rheology of the grouting agents', the penetration length must be estimated with different methods whether it is a Bingham (cementitious) or Newtonian fluid (silica sol or water). Bingham fluids often have a higher viscosity than Newtonian fluids and may also have shear strength. According to this difference two different methods of estimate penetration length is needed. The viscosity is temperature dependent and is lowered with higher temperatures (Funehag, 2007).

The maximum penetration length for cementitous agents is dependent on the grouting over pressure, $\Delta p$, the yield stress of the grout, $\tau_0$, and the hydraulic aperture, $b_{hyd}$, and is described by Eq. 2.15 (Gustafson and Stille, 1996).

$$I_{max}^{cement} = \left(\frac{\Delta p}{2\tau_0}\right) \cdot b_{hyd} \qquad \text{Eq. 2.15}$$

Funehag (2007) has estimated the maximum penetration length for silica sol with the following equation:

$$I_{max}^{silica} = 0,45 \cdot b_{hyd} \cdot \sqrt{\frac{\Delta p \cdot t_G}{6\mu_0}} \qquad \text{Eq. 2.16}$$

Where $t_G$ is the gel induction time and $\mu_0$ is the initial viscosity. The gel induction time is the time it takes for the silica sol to double its initial viscosity. A radial flow is assumed in both Eq. 2.15 and Eq. 2.16. For cement grout the actual penetration length is approximately 30 % of the maximum length (Gustafson, 2009). An increased aperture, $b$, will lead to a larger maximum penetration length, which is equivalent to a higher velocity of the grout. Therefore a wider fracture is filled with grout faster than narrow

ones. The grout pump pressure will be constant in the grout hose and the borehole but will drop rapidly with increased distance in the fracture network (Gustafson and Stille, 2005).

## 2.1.6   Deformation modes

There are a number of different ways of describing deformation. The ones deemed most relevant for this thesis are presented below. The direction of deformation, i.e. normal deformation or shearing is described. Also the pressure conditions when the deformation occurs, i.e. before and after the normal stress is exceeded, is described. Gothäll (2009) denotes deformations that occur when the effective stress is zero as *jacking*. The measurement method used for this thesis work does not allow a qualitative assessment of the type of deformation. Therefore the general term *deformation,* is used throughout the thesis.

Normal deformation is a movement perpendicular to the fracture surfaces. This can be reversible; resilient, or irreversible; permanent. Shearing is a slip movement along the fracture surfaces, which can occur when a shear stress is applied on the fracture and the friction, i.e. asperities and roughness, of the fracture cannot resist the stress. An increased pore pressure, causing a reduction of the normal stress may stimulate shear deformation.

When the grout fills the fracture voids between the contact points it will carry a part of the normal load that lies upon the fracture. As the pressure induced by the grout increases, three stages of load conditions can be seen; in the first stage the grout pressure on the fracture sides is small compared to the normal load, the load is carried by the contact points. The second stage is called the critical stage, where the grout pressure, the stress in contact areas and normal pressure are fairly equal. The third stage is the post-critical stage, where the grout pressure is larger than the normal load, thus separating the contact points, and creating a larger load on the rock mass. The largest deformations occur in stage three (Gothäll 2009).
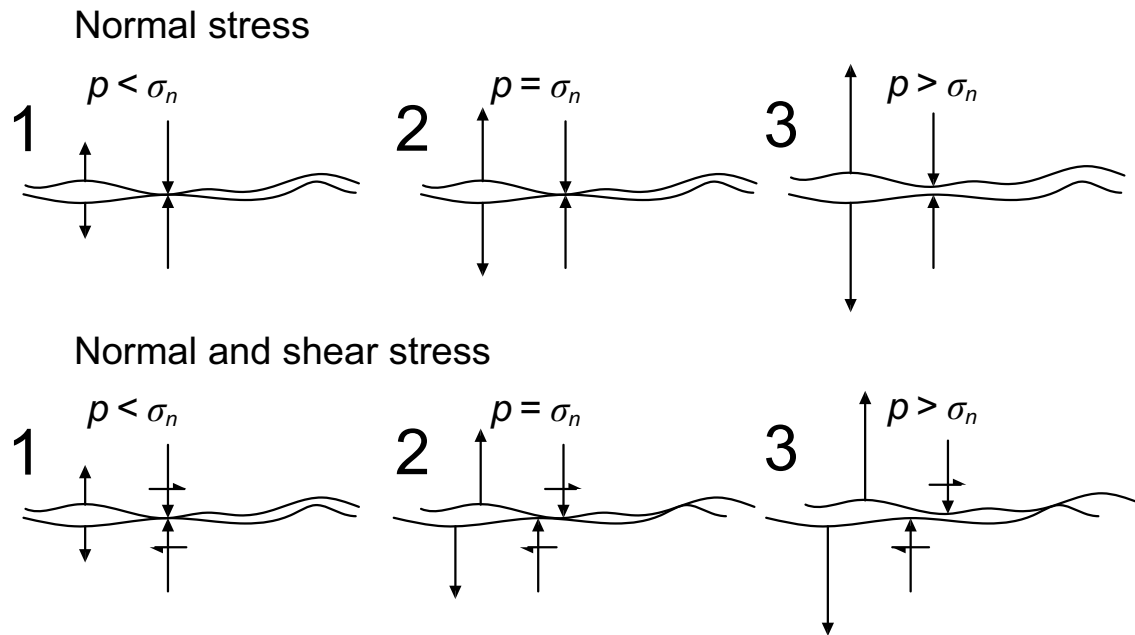
Normal stress



Normal and shear stress



*Figure 2.7: The three stages of fluid pressure loadings and their corresponding deformation. The top row presents deformation for fractures subject to normal stress. The bottom row presents deformation for fractures subject to normal and shear stress.*

If the fracture is subject to shear stresses when the contact points are separated, and the fracture loses its shear strength, these stresses need to redistribute, which may cause a movement along the fracture. This may occur in either stage 1 or stage 2, depending on the size of the shear stress. A deeper analysis of this failure mode might be possible to perform with the calculated stresses, and fracture characteristics, such as roughness and fillings, but such analysis is beyond the scope of this thesis.

Gothäll (2009) describes the total normal dilation when grouting a fracture as:

$$\Delta a_g = \Delta a_i + \Delta a_u + \Delta a_J \qquad \text{Eq. 2.17}$$

Where $\Delta a_i$ is the initial deformation that occurs when the pre-load is reduced; stage 1 in Figure 2.7. $\Delta a_u$ is deformation due to redistribution of stresses from other fractures, and corresponds to stage 2 in Figure 2.7. $\Delta a_J$ is jacking due to grouting in the post-critical stage; 3 in Figure 2.7. Each of these terms, $\Delta a_i$, $\Delta a_u$, $\Delta a_J$, are dominant for respective pressure stage, therefore the total deformation due to grouting in stage 3 is approximately equal to $\Delta a_J$ (Gothäll 2009).

## 2.1.7 Hydraulic testing

A number of different borehole tests can be performed in order to determine the hydraulic properties of a rock mass. Relevant for this thesis are water pressure tests, pressure build-up tests and natural inflow tests. Generally a short duration test provides information of the fracture system close to the borehole and long duration tests describe the conditions further away (Hernqvist 2009).

The theory behind, and the method used for conducting the tests performed in the boreholes is presented below. For each test a method for evaluating the transmissivity is suggested. With the transmissivity, $T$, known the cubic law can be used for calculating hydraulic aperture according to Eq. 2.7.

For the hydraulic tests packers has been mounted in the tested boreholes. The purpose of a packer is to make a watertight connection between the borehole and a tube that valves and various test equipment can be connected to. There are two general kinds of packers available; single and double, where a single packer is used for measuring from the bottom of the hole to the packer position. A double packer has two mounting points, and can measure the borehole between these points.

Water pressure tests (WPT) describe the fractures close to the tested borehole. A predefined overpressure above the groundwater pressure is pumped into the borehole and kept stable for a time interval. Pressure and flow data is used for estimating the transmissivity. The pumped flow, $Q$, and the difference in hydraulic head, $\Delta h$, can be used to assess the transmissivity, $T$, of the tested section of the borehole. If the length, $L$, of the tested section is much larger than the radius, $r_w$, of the borehole, Eq. 2.18 can be used.

$$T = \frac{Q}{2 \cdot \pi \Delta h} \cdot \ln\left(\frac{L}{r_w}\right)$$
Eq. 2.18

Natural inflow tests (NIT) describe the water conducting fractures close to the tested borehole. A natural inflow test is performed by measuring the steady free flow into a borehole. For evaluation of the transmissivity from NIT the pressure head, $\Delta h$ is needed. It can be obtained by measuring the pressure for 15 minutes in the borehole before the inflow measurement. For a short duration test where the radius of influence is limited, $T$ can, according to Fransson (2001) be approximated as Eq. 2.8 as a simplification of Thiem's equation (Gustafson 2009):

$$T = \frac{Q}{2 \cdot \pi \Delta h} \cdot \ln\left(\frac{R_0}{r_w}\right)$$
Eq. 2.19

Pressure build up tests (PBT) can describe the fractures at a larger distance, and larger structures, such as fracture zones. A pressure build-up test is performed in two steps: first a period of free flow from the borehole, followed by a period of recovery (Hernqvist 2009). A longer test describes a larger rock volume and a short test describes the local conditions close to the tested borehole. During the flow period, denoted $t_p$, the inflow, $Q$, is given time to stabilize, and is measured. At the end of the flow period the packer is closed and the pressure starts to rise. The pressure rise is logged and the build-up curve can be used for further analysis. The recovery period in the evaluation of the test must be equal or shorter than the flow period (Hernqvist 2009). The dimensionality of the flow can be assessed by plotting the pressure increase against the equivalent

recovery time, $t_e$, in a log-log chart, and compared to type-curves for 0, 1, 2 and 3D flow (Hernqvist 2009). $t_e$ is defined as:

$$t_e = \frac{t' \cdot t_p}{t' + t_p}$$

Eq. 2.20

The transmissivity for the fractures of the tested borehole can be estimated with the Jacob's method as (Gustafson 2009):

$$T = \frac{0.183 \cdot Q}{\Delta s}$$

Eq. 2.21

Where $Q$ is the measured flow before closing the borehole and $\Delta s$ is the pressure increase (in m) during one decade of time in a semi logarithmic plot obtained during the build-up, see Figure 2.8.

The Chalmers flow log (CFL) is a small section inflow measurement device, where inflow to the tested section can be measured with for example stopwatch and a sampling tube. The measured interval is 0.5 m, which is separated from the rest of the borehole by three rubber discs at each end. The small measurement interval enables measurement of individual fractures (Gustafson 2009) under the assumption that the measured interval is small in relation to the fracture intensity (Hernqvist 2009). The construction of the rubber discs does not allow pressurizing the measured interval; therefore the CFL can only be used for inflow measurements.

The testing with CFL is performed by pushing the CFL into the borehole by the tube that leads water from the tested interval. When in position it is pulled out a couple of centimetres, so the rubber discs turns and tightens to the borehole wall. The testing itself is a series of NITs, and the theory for NIT applies to CFL. Eq. 2.19 can be used for evaluation of the transmissivity (Gustafson 2009).
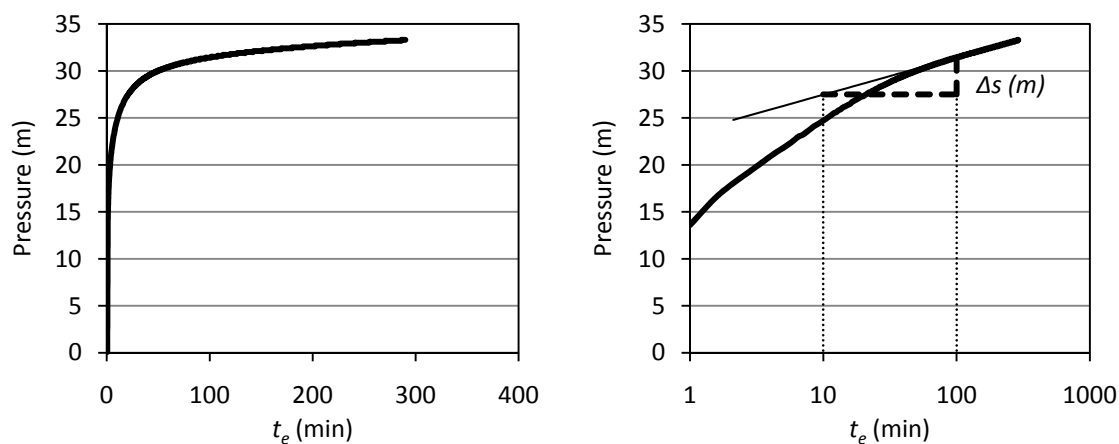


*Figure 2.8:Left: Example of pressure build-up curve obtained during the testing in the service tunnel. Right: The same data in a semi logarithmic plot, and the principles for evaluating Δs.*

## 2.2    Conceptual model

The conceptual model is based on the theory presented in Section 2.1. The purpose is to create a model that describes the deformation as a result of the reduced effective normal stress due to an increased pore pressure, e.g. water or grout pressure. The normal stress is described by means of two general concepts. The first is fracture stiffness, $k_n$, which is evaluated from borehole testing and grouting and is evaluated according to Eq. 2.9 and Eq. 2.13. The second concept is based on global rock stress estimations. The secondary stress redistributions around the tunnel are evaluated according to Kirsch (Eq. 2.4- Eq. 2.6) and Hoek (Examine2D). The local stresses are not known but as suggested in Fransson et al. (2010) low fracture stiffness can be used to indicate low effective stress.

The injection pressure, $p_g$ or $p_{WPT}$, in a fracture is assumed to drop linearly with distance, Figure 2.9 and Figure 2.10. At the grout spread front, the pressure is equal to the groundwater pressure, $p_w$. For stiffness calculations the change in effective stress is needed. This stress change is approximated as the average value of grout overpressure, under assumption that the pressure reduction with distance is linear. This is equal to $\Delta p/3$, see Fransson et al. (2010). Figure 2.9 shows the application of the water pressure testing, with corresponding deformation measurement. The overpressure is increased in steps. Figure 2.10 shows the grouting, with a constant overpressure over time, and corresponding principle for deformation.
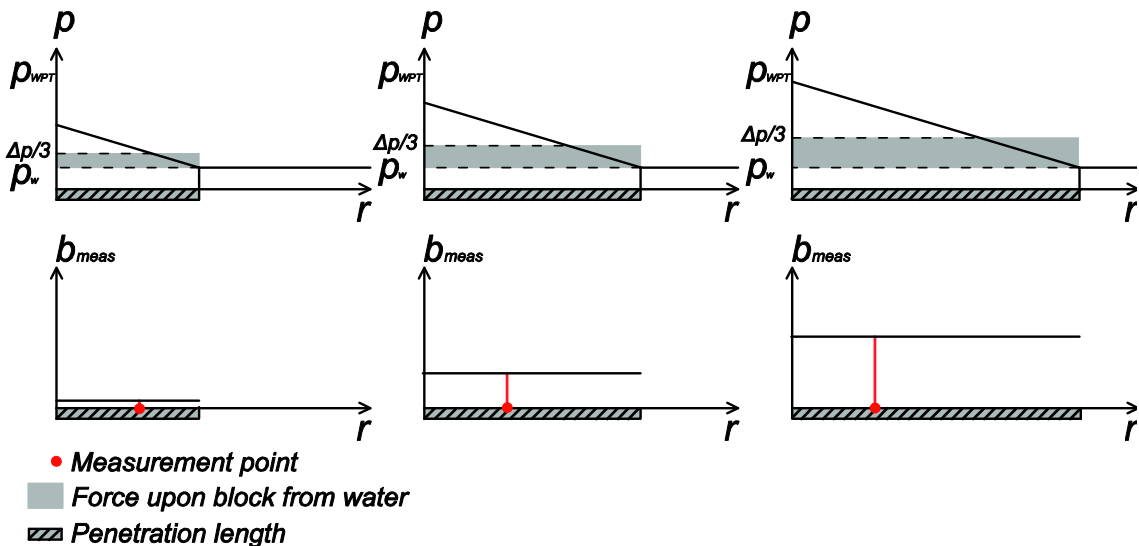


● *Measurement point*

▨ *Force upon block from water*

▨▨ *Penetration length*

*Figure 2.9: Shows the pressure reduction with the radius, r, from the borehole. The penetration of the grout is indicated with the grey bar below the x-axis. The force from the water to the rock blocks, marked with a grey box, is under the assumption that r<block size. The fluid pressure, Δp/3, will act uniformly on the fracture decreasing its effective stress and uniformly deforming the fracture.*
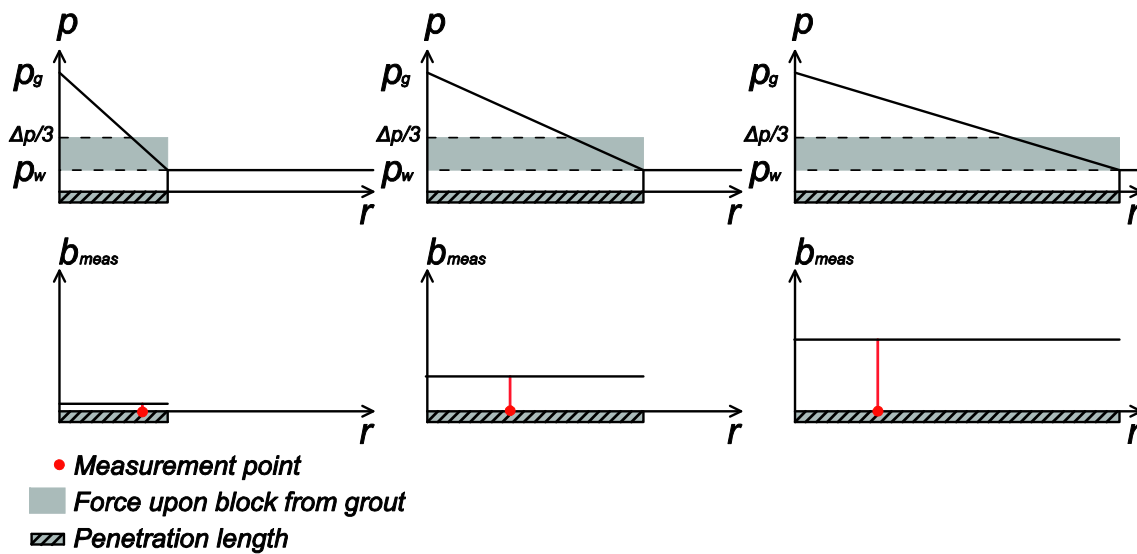
Figure 2.10: *Shows the concept of grout pressure profile and the corresponding deformation. The fluid pressure, Δp/3, will act uniformly on the fracture decreasing its effective stress and uniformly deforming the fracture. The force from the grout to the rock blocks, marked with a grey box, is under the assumption that r<block size.*

In Paragraph 2.1.3 the fracture stiffness is described in two ways. One way is to describe it as a change in effective normal stress divided by a change in aperture; a deformation (Eq. 2.9). Another way is to describe it proportional to the storativity, which can be calculated with an empirical relation to transmissivity (Eq. 2.13). Both methods are used where data is available. Deformation value in Eq. 2.9 can be either measured deformation, $\Delta b_{meas}$, or change in hydraulic aperture $\Delta b_{hyd}$.

With the primary and secondary stress situation in a tunnel wall conceptually described as in Paragraph 2.1.1, a fracture normal stress situation is introduced (Figure 2.11). This is an example of the behaviour of generalized fractures, onto which the stresses act. The description is performed in two dimensions, with an assumed fracture dip of 90°, which eliminates the influence of the vertical stress.

In Figure 2.11 the stress interaction upon a point on a fracture close to the wall is indicated with arrows; the largest principal stress, $\sigma_H$, here oriented parallel to the tunnel direction, acts at an angle, $\kappa$, upon the fracture planes. This stress is indicated in its effective components: normal and shear stress. The stress induced by the grout is perpendicular to the fracture plane. The smallest principal stress, $\sigma_h$, is zero at the tunnel wall, but increases with distance into the rock mass.

The normal stress, $\sigma_n$, is defined as the part of the horizontal stresses that is perpendicular to the fracture plane, and the shear stress, $\tau$, is the parallel part. They can be calculated with the following equations:

$$\sigma_n = \sigma_\parallel \cdot \sin(\kappa) + \sigma_\perp \cdot \cos(\kappa) \qquad \text{Eq. 2.22}$$

$$\tau = \sigma_\parallel \cdot \cos(\kappa) - \sigma_\perp \cdot \sin(\kappa) \qquad \text{Eq. 2.23}$$

Where $\sigma_{/\!/}$ and $\sigma_\perp$ is the principal stresses that are parallel and perpendicular to the tunnel and $\kappa$ is the angle between the tunnel wall and the fracture orientation.
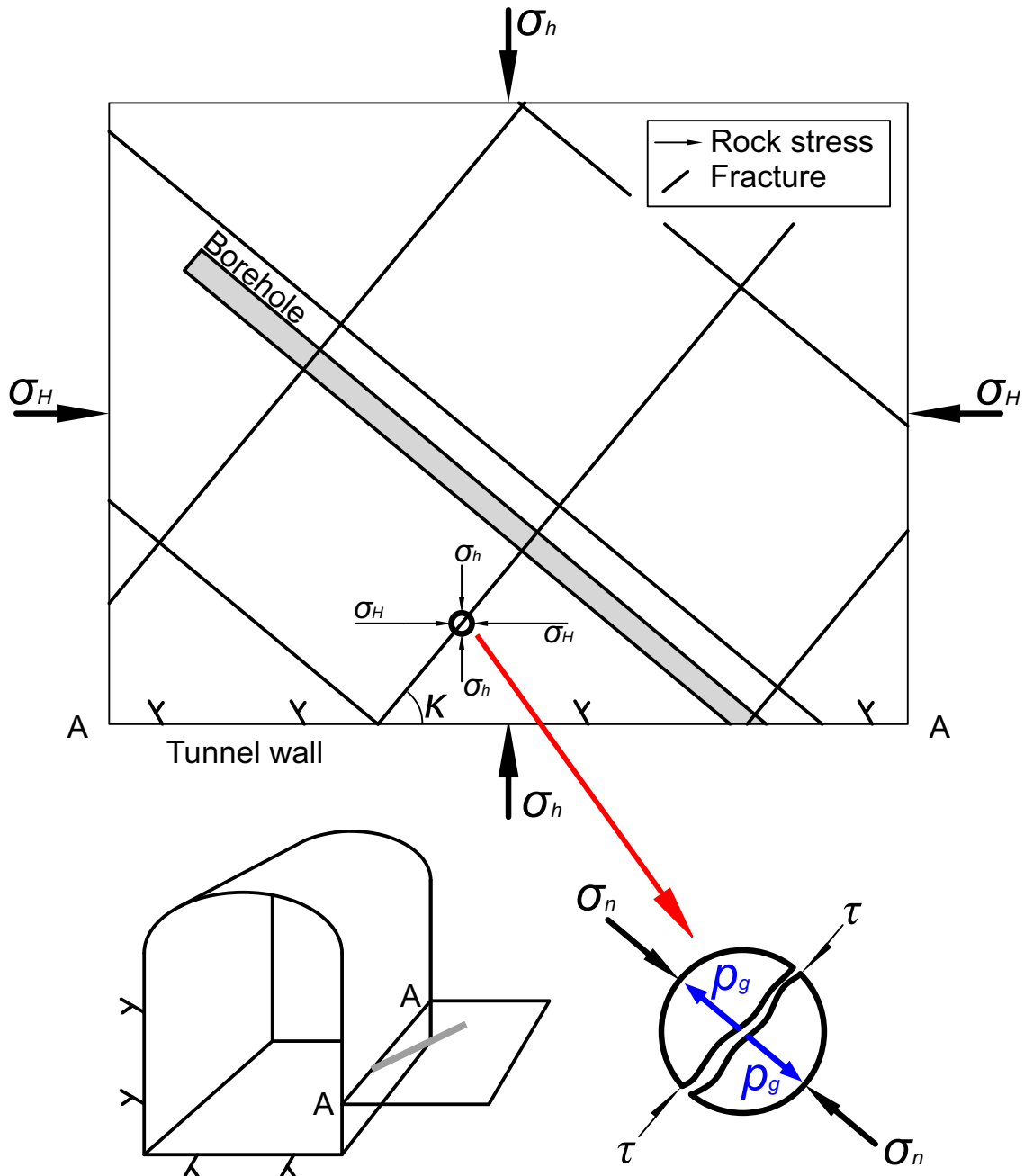


*Figure 2.11: Shows the stress interaction on a horizontal plane in a tunnel wall. The horizontal stresses $\sigma_H$ and $\sigma_h$ result in a normal and shear stress on a fracture, $\sigma_n$ and $\tau$. The blue represent the grouting pressure, which counteracts the normal stress.*

## 2.3    Deformation measurement equipment

First the principle of the equipment is described, followed by an account for all of the components. The analog and digital logging procedures are described, and an example of output data is presented.

Deformation is measured in a borehole close to the ordinary borehole in a grouting fan, see Figure 2.12. An anchor, fastened to a rod is inserted into the measured borehole. The anchor is mechanically expanded until it is firmly attached in the drilled hole. The rod extends out of the borehole. Teflon bushings acts as a suspension that centers the rod in the borehole, but does not obstruct any axial movements of the rod, see Figure 2.13. At the tunnel wall, close to the borehole with the rod, a steel frame is bolted. To this frame the sensors are attached, and set parallel with the rod, see Figure 2.12.
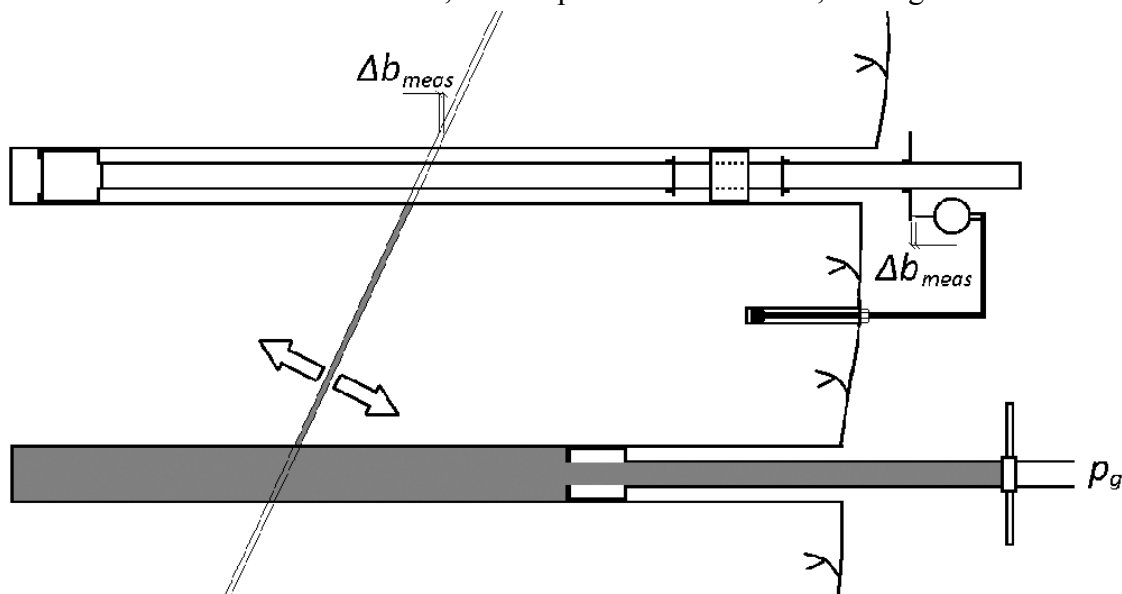


*Figure 2.12: The principle for deformation measurements. A packer is placed in the lower borehole, which is grouted. The grout pressure causes a fracture to deform. In the upper borehole a rod is fastened at the bottom of the hole with an anchor, the rod is suspended with Teflon bushings. A deformation sensor attached to the wall measures the relative movement between the wall and the rod, i.e. the total deformation along the borehole. It is favourable if the distance between the boreholes is smaller than the fracture intensity, i.e. the block size.*
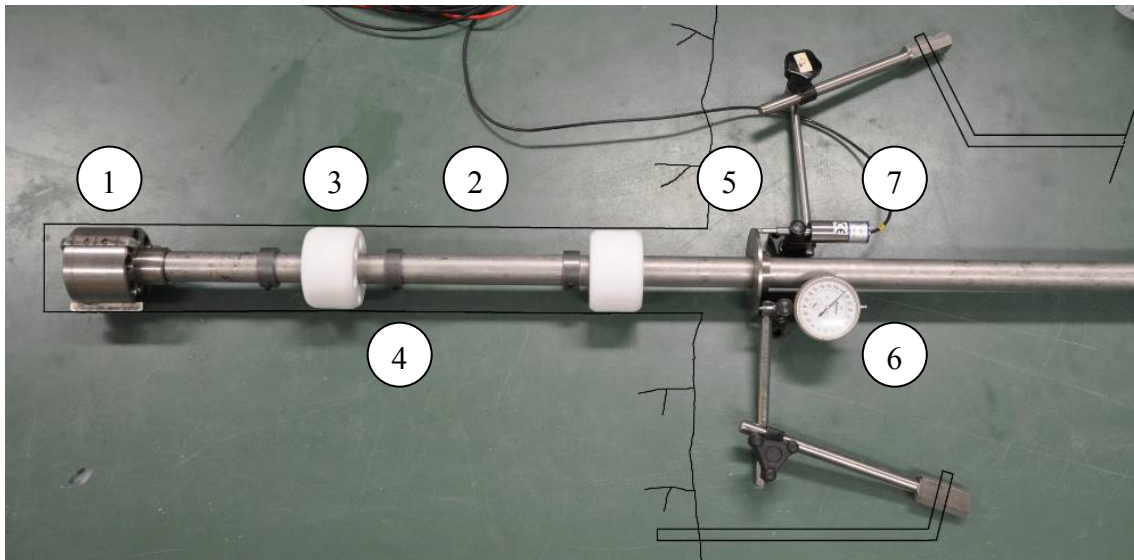
*Figure 2.13 The test set-up schematically arranged as meant to be used. The length of the part inserted in the rock has been reduced for visibility reasons.*

1. **Anchor:** The anchor consists of three wings that are forced out of the anchor house with a cone that can be screwed with a socket wrench through the rod. The anchor is 70 mm in diameter, and can be expanded to about 80 mm. A rubber o-ring helps the wings back when the anchor is released.
2. **Rod:** Stainless steel pipes, 2.5 m long, 30 mm in diameter, which can be joined to larger lengths. At the end the rod has an inner thread that fits the anchor.
3. **Teflon bushings:** 73 mm outer diameter with a center hole that fits the rod, and smaller holes that allow water and grout to pass the bushing.
4. **Stop rings:** Stop rings are attached to the rod, and the bushings can move between these.
5. **Reference plane:** A larger stop ring that is fastened to the rod outside the hole. It is used for the deformation sensors.
6. **Analog sensor:** The analog sensor has a resolution of 0.001 mm. The analog deformation data, measured during water pressure tests, was obtained by one person standing in a lift, watching the sensor, and noting the values and corresponding time. For deformation during grouting, the analog logging was performed with a camera on the ground.
7. **Digital sensor:** The digital sensor is an electronic LVDT sensor (RDP group D2 200A/256) connected to a logger that can be started and configured with a computer.

Analog and digital data can be seen for a WPT/deformation test performed at Hallandsås. The sensors correspond well if the sampling rate of the analog logging is sufficient, see Figure 2.14.
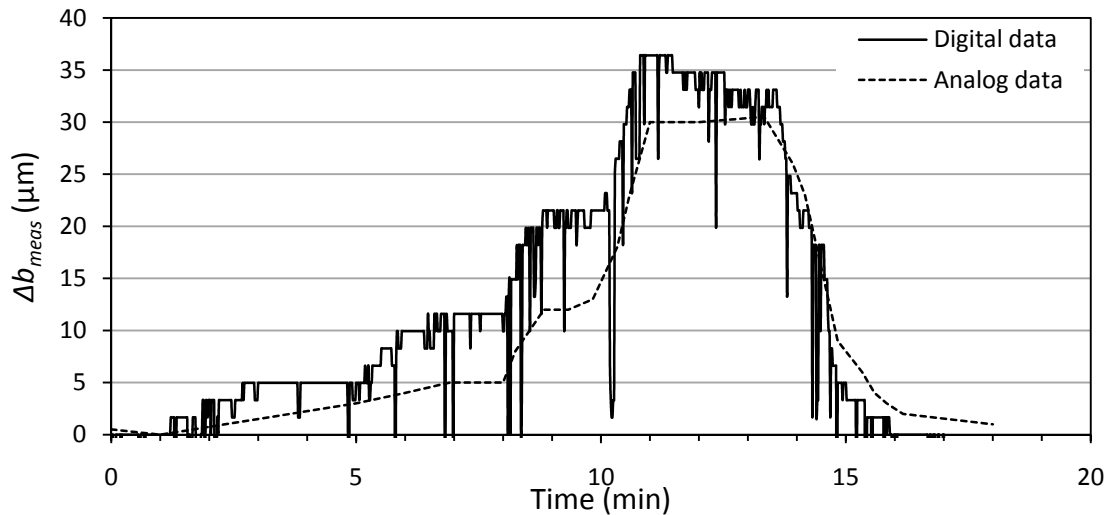
*Figure 2.14: Analog and digital deformation data from a WPT/deformation test performed at Hallandsås.*

## 2.4    Case study: Old service tunnel

The service tunnel is located under Gothenburg. The rock type in the area is a red granodiorite that is 2.5-1.0 billion years old. The fracture intensity in the drilled cored boreholes is 3 fractures per meter in KBH1, and 7 in KBH2. The cross section of the tunnel is small, only 12 m$^2$. The tunnel was excavated by drill-and-blast methodology from the north-west end, from lower to higher in the tunnel length scale (see Figure 2.15). The excavation of the studied tunnel part was performed in 1970-1972. The test site has a rock cover of 50 m, and the inclination of the tunnel is 4° (7 %) upwards in the tunnel length scale.

Pre-grouting was performed with cementitious grout but other grouting agents were tested, such as polyurethane and TACSS, none of these were used systematically (Riise 2007). The pre-grouting fans were oriented forward in the excavation direction. The 100 m section (2/990 – 3/090) where the test site is situated was pre grouted with 3585 kg of cement grout, distributed on 180 boreholes. Where needed post-grouting was conducted, a total of 9 post-grouting holes were grouted in the 100 m section, totalling 800 kg of cement. The walls and ceiling was shotcreted with unreinforced concrete, and where the grouting was insufficient additional shotcrete was applied. The total pre-grouting pressure was 1.5 MPa, and post-grouting pressure was 1.2 MPa. If a groundwater pressure of 0.3 MPa is assumed the resulting grouting overpressure is 1.2 and 0.9 MPa respectively.

In order to find fractures that may be prone to deform when grouting, a three-dimensional geometric model was built in AutoCAD. Simultaneously a hydraulic testing program was performed and data from these measurements were used in order to update the geometric model. The geometric model was updated two times, first with data from mapping of two cored boreholes (KBH1 and KBH2), secondly with mapping data from the third cored borehole, KBH3.
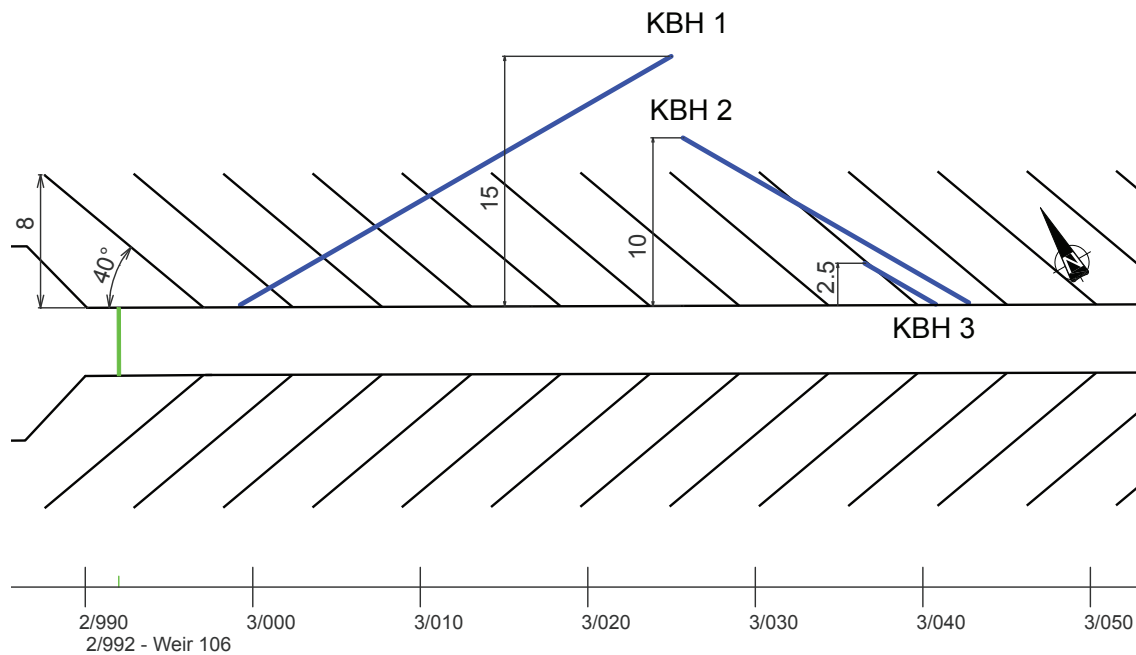
*Figure 2.15: The position and orientation of KBH1 and KBH2, and the 2010 post-grouting fans indicated. The pre-grouting was conducted in the opposite direction to the indicated fans.*

### 2.4.1 Rock stresses

The stress situation in the tunnel wall is described according to Figure 2.16 and Figure 2.17. The stresses in the service tunnel are estimated as described in
Table 2.1. Stress measurements has been performed in the Röda Sten Rock Laboratory, see He (1992) and in the Götatunnel by Sintef, 2001. The stress state used in the analysis is a generalisation of the values from the Götatunnel. The distance between the test site and the Götatunnel site is about 1 km.

*Table 2.1: The result of one theoretical stress estimate, as described in Eq. 2.1-2.3, and three sets of in situ stress measurements. The stress measurements from the Götatunnel are the ones closest to the old service tunnel. A generalization of these measurements has been used as stress values for the analysis.*

| Method (no.of samples) | $\sigma_1$ ($\sigma_H$) (MPa) | Strike/ dip | $\sigma_2$ ($\sigma_h$) (MPa) | Strike/ dip | $\sigma_3$ ($\sigma_v$) (MPa) | Strike/ dip |
|---|---|---|---|---|---|---|
| Eq. 2.1-Eq. 2.3 | 4.8 | x/0 | 3.4 | x/0 | 1.3 | x/90 |
| Götatunnel 1 (1) | 14.7±1.3 | 192/6 | 6.6±1.8 | 89/64 | 6.5±2.4 | 285/25 |
| Götatunnel 2 (1) | 7.9±0.8 | 197/13 | 5.0±0.6 | 299/45 | 4.0±1.1 | 96/43 |
| Röda Sten RL (7) | 7.2±2.0 | 102/7 | 3.4±1.3 | 194/9 | 2.0±1.0 | 335/78 |
| *Generalized stress situation used in analysis* | **10** | **210/0** | **7** | **300/0** | **5** | **x/90** |

Three generalized fracture sets has been drawn in Figure 2.16, their angles from the tunnel wall (20°, 45° and 80°) corresponds to the fracture sets described in Paragraph 2.4.3, the spacing of the fractures are set adequately for visibility, and is not the actual

spacing of the fractures. The normal and shear stresses ($\sigma_n$, $\tau$) resulting from $\sigma_H$ and $\sigma_h$ is illustrated for a point on one fracture. The secondary stresses from the tunnel do not affect $\sigma_h$, but have a large impact on $\sigma_H$, see Figure 2.17. $\sigma_H$ is equal to zero at the tunnel wall.

The normal stress upon the three fracture directions was estimated for stresses calculated with Kirsch equations, Eq 2.4-2.6, and Examine2D (see Figure 2.17). For the calculation according to Kirsch $\sigma_h$ is constant and $\sigma_H$ varies according to the equation describing $\sigma_r$ (Eq. 2.4). For the calculation with Examine2D the stresses from Table 2.1 are used as input.
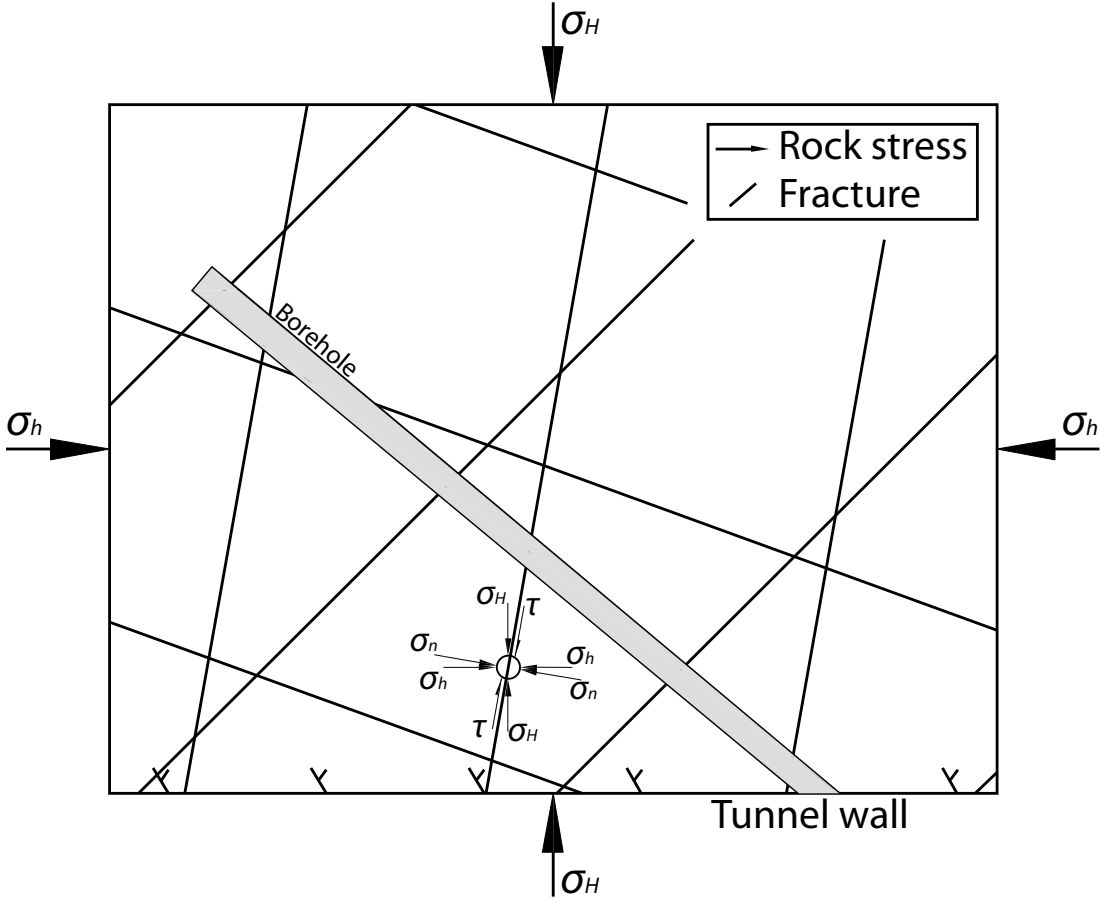


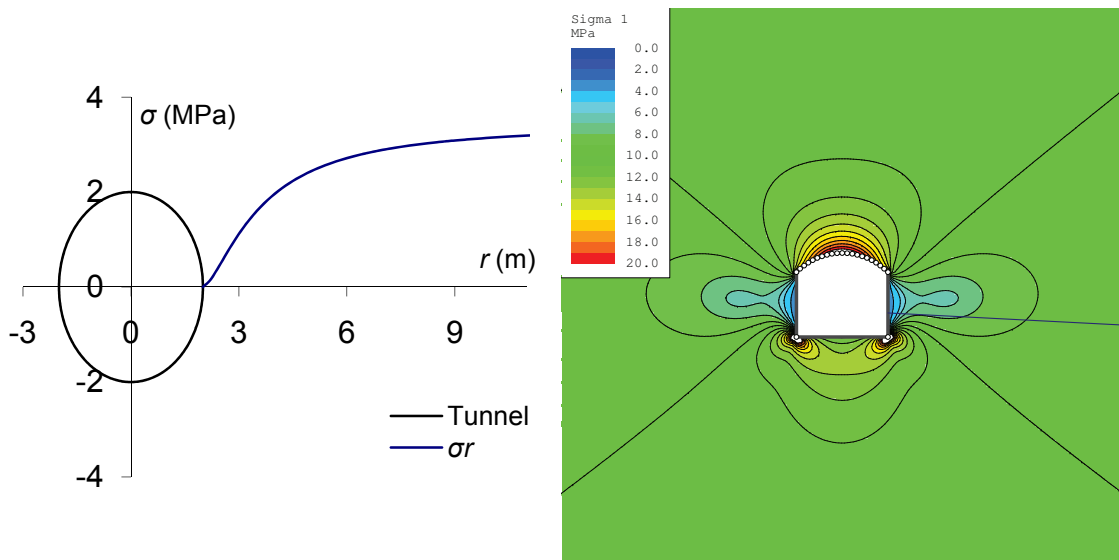*Figure 2.16: A conceptual rock stress model for the service tunnel.*

*Figure 2.17: Left: The radial stress from the Kirsch equations, $\sigma_r$, corresponds to $\sigma_h$ through the centre of the tunnel, and therefore leaves the rock mass close to the tunnel wall unloaded in that direction. Right: Theoretical rock stress calculated with Examine2D.*

### 2.4.2 Coredrilling and mapping

Each of the drill cores from KBH1, KBH2 and KBH3 were mapped by Christin Döse, geologist at Tyréns, see Table 2.2. The mapping was performed with regard to rock type, orientation and mineralogy of open fractures and prominent structures, for example breccias. Estimates of fracture aperture were done in classes; 0.2 mm for fractures where the core pieces fit well, and interlocks; 0.5 mm for small fractures where the core pieces do not interlock, or where channelling can be seen. Larger values were used for fractures with aperture greater than 0.5 mm. Fractures which are possibly hydraulically active are denoted as open, whereas those that are not are denoted closed. The orientation of the core was performed by markings made at the bottom of the borehole during drilling, ergo the end of the next core piece; however, there are too few markings for a completely reliable orientation. Intersection angle ($\alpha$-angle) and rotation along core axis ($\beta$-angle) relative to reference mark was measured on the core, and recalculated to strike and dip in situ. Possible errors that sum up to an uncertainty for the strike and dip of the mapped fractures consists of:

- Marking of the borehole
- Passages where the core is difficult to puzzle
- Roughness of measurement of $\alpha$ and $\beta$ angle

*Table 2.2: Mapped features in the drill cores.*

|                           | KBH1  | KBH2  | KBH3 |
|---------------------------|-------|-------|------|
| **Length of core (m)**    | 33.24 | 19.74 | 4.72 |
| **Number of mapped features** | 191 | 147 | 30 |
| **Open fractures**        | 110   | 140   | 21   |

### 2.4.3 Geometric modelling

The first geometric model, version 0, was based on a mapping of fractures in the tunnel walls and roof performed when the tunnel was excavated. Version 1 is an update of version 0, where data from mapping of two cored boreholes are inserted and, matched with the fractures from version 0. Version 1 was the base for placing one new cored borehole, KBH3, where a deformation was meant to be measured. When KBH3 was drilled, the fractures of the core were matched with version 1, and this update was called version 2. From version 2 the fracture matching of KBH2 and KBH3 was used for indicating fractures present in both boreholes. The mapping from the tunnel walls and roof, which served as a basis for version 0 (Figure 2.18), can be seen in Table 2.3. The inclination of the tunnel is 4°; 7 %, upwards in the tunnel length scale.

The work with the first version indicated that the third drilled borehole should be placed close to KBH2, which also had the largest inflow of water. Therefore the further analysis is focused in the vicinity of KBH2. This version is an update of the previous one, where the mapping of KBH2 is considered.

*Table 2.3: The fracture sets used in the further modelling.*

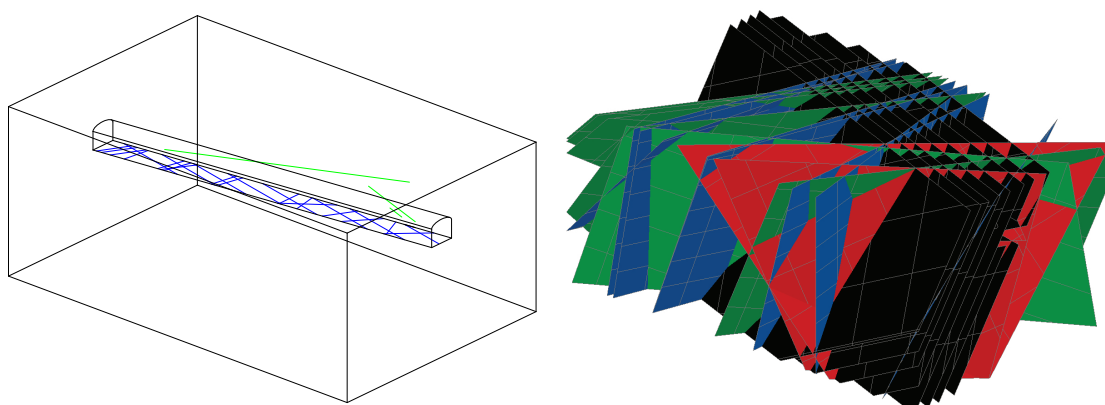| Fracture set | Colour code | Strike interval / dip interval |
|---|---|---|
| **1** | Black | 110 – 140 / 40 - 60 |
| **2** | Blue | 210 – 230 / 50 – 80 |
| **3** | Red | 60 – 90 / 50 - 90 |
| **4** | Green | 250 – 270 / 50 - 70 |
| **Remaining** | Magenta | Directions not included in set 1-4 |



*Figure 2.18: Left: The sketch of fractures mapped from the tunnel wall and roof (blue lines), the green lines represent drilled core holes. Right: The same model with the corresponding fracture surfaces, the different colours represent the fracture sets in Table 2.3.*
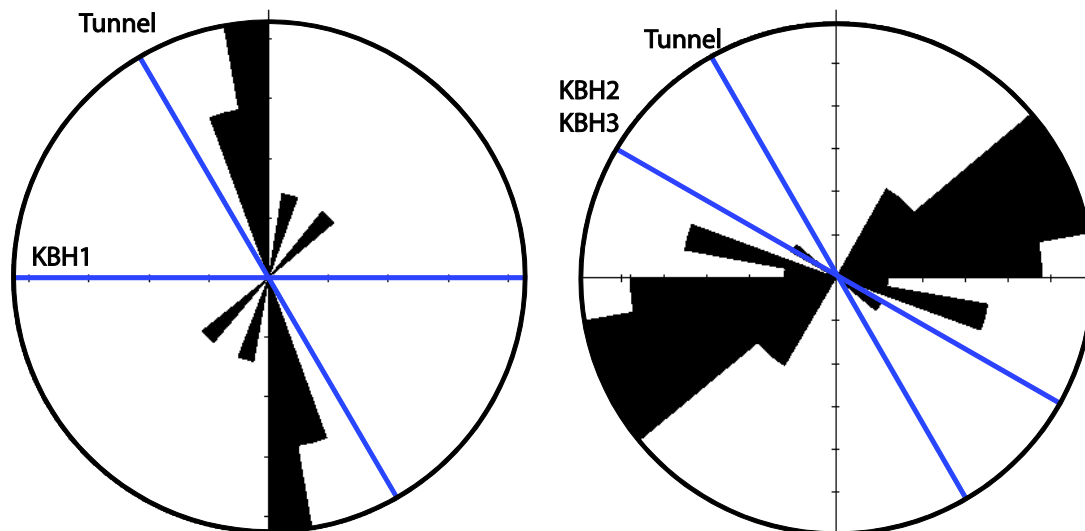
*Figure 2.19: Left: Directions of fractures that contain cement (8 data) mapped from KBH1. Right: Directions of fractures that contain cement (28 data) mapped from KBH2. No Terzhagi correction has been made.*

The fractures intersected by KBH1 and KBH2, that contain cement are located as seen in Figure 2.19. Conclusions drawn from the presence of cement is that both boreholes' data sets contain mostly fractures somewhat perpendicular to the borehole direction, since those are more probable to be intersected. The direction of the pre-grouting fans could explain the cement in KBH1. If post-grouting has been conducted in the area, this could explain the grouted fractures in KBH2.

Based upon version 1, KBH3 was placed 2 m from KBH2, at tunnel length 3/041.3, with the same bearing and inclination: 330° (30° from wall) and 10° downwards. No stress modelling had been performed at this stage. An assumption of a low fracture normal stress, if the fracture lies within 1.2 m of the tunnel wall, is applied. The placing of KBH3 was based on the following reasoning:

- Should be placed near KBH2 where the rock mass is better characterized and a larger inflow can be expected.
- KBH3 should intersect a fracture which was not sealed during the pre-grouting.
- KBH3 should intersect a fracture which has a hydraulic aperture.

A correlation between the fracture mapping from KBH2 and KBH3 were made. The mapped fractures were linearly extrapolated to find a coexisting fracture that stretches between the two cored boreholes, see Figure 2.20. Model 2 was used for designing a hydraulic testing program. This was used to decide whether it should be possible to perform a deformation measurement at this location.
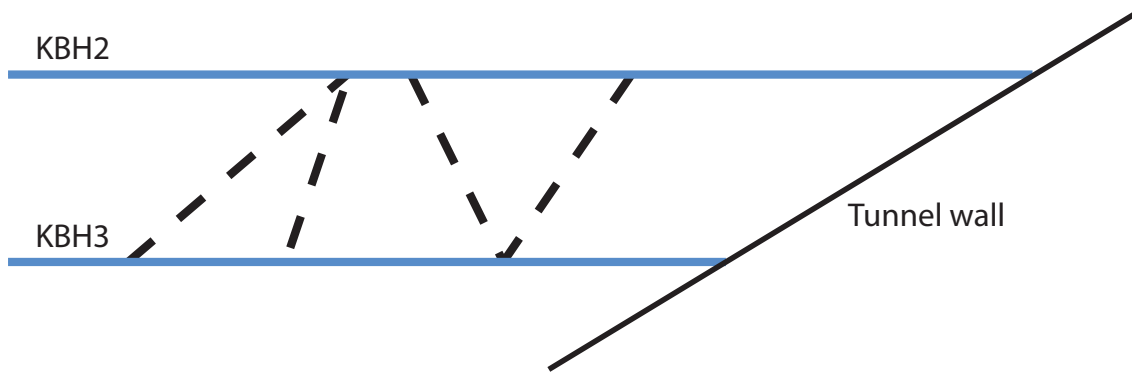
*Figure 2.20: The fractures of set 1, 2, 3 and 4 mapped in KBH2 and KBH3 where a fracture of the same direction is present in both KBH2 and KBH3, at corresponding depths. The black line represents the tunnel wall, the blue lines the boreholes, and the dashed lines the possibly connected fractures.*

### 2.4.4 Hydraulic testing programme

An account for the hydraulic testing programme conducted in the service tunnel is as follows. The first 63 mm-cored borehole, KBH1, was drilled, and every third meter the drilling was halted. At each such halt NIT and pressure measurement was conducted. Thereafter a WPT was performed. The overpressure was 0.3 or 0.5 MPa, this pressure was held for 5 minutes and then raised 0.2 MPa, which was held for another 5 min. At the 9 m test halt and after completion, 33 m, a longer pressure build up test (PBT) were performed. The hole was opened and kept open for a period of time, natural inflow were achieved and measured, and then the packer was closed and an electronic pressure logging was initiated. The same procedure was followed for the 20 m long KBH2.

When the location of KBH3 was decided a test programme for this hole was initiated. The hole was bored as 63 mm, and enlarged to 75 mm. At 3 m depth a NIT with pressure measurement was conducted, this was also done for the full hole, 4.7 m. A PBT was performed in KBH2, with KBH3 closed, and NIT and PBT in KBH3 with KBH2 closed.

In order to find out if there is any connecting fracture(s) between KBH2 and KBH3 a PBT logging of KBH3 was performed, see Figure 2.21. At the end of this test KBH2 was opened and the pressure in KBH3 instantaneously started to decrease; during the following hour the pressure was lowered 0.04 MPa.

Thereafter a couple of water pressure tests were performed in order to find a connection between KBH3 and the nearby KBH2. First a WPT with 1.05, 1.5 and 1.9 MPa pressure was performed in KBH2, with pressure logging in KBH3. Thereafter water pressure tests of 1.5 and 2 MPa was conducted in KBH3 with the pressure logger in KBH2. These indicated a too weak connection between the boreholes and no deformation measurements were conducted. However, data from hydraulic testing is analysed, see Chapter 4.
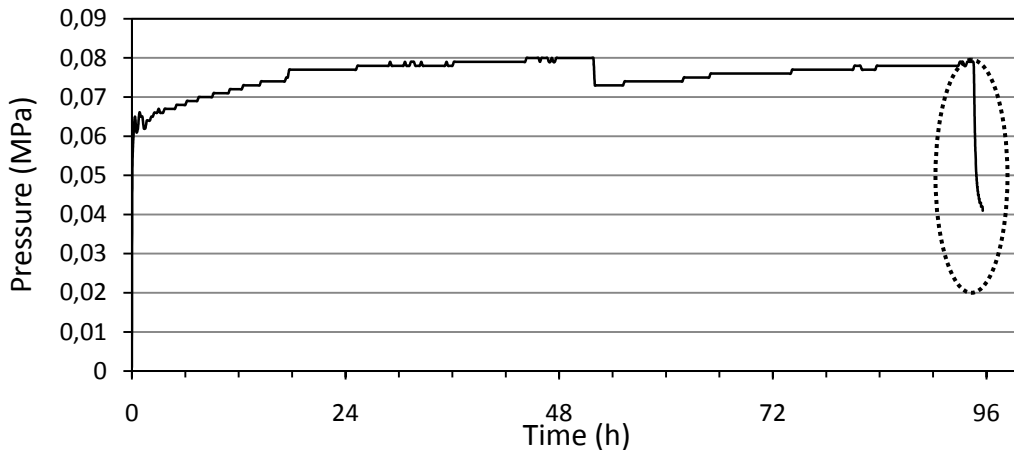
*Figure 2.21: Pressure buildup test in KBH3, packer inserted 1.6 m. The dotted ellipse shows the pressure drop when KBH2 is opened.*

## 2.5    Case study: Hallandsås

Hallandsås is a horst that was formed about 500 – 70 million years ago as an effect of Africa colliding with Europe. The formation has been subject to large movements, and contains a high frequency of fracture zones. In Mesozoic time, Sweden was situated close to the equator, and the hot humid climate caused deep weathering, which still is present in the fracture zones. The rock type most frequently occurring is gneiss, which has been subject to several regional metamorphoses. Amphibolite and diabase is common as dikes or smaller masses.

The tunnel is a railroad tunnel, 8.7 km long, and the studied section was excavated with drill and blast methodology. The site is situated in the west tunnel pipe at 190+903, in the tunnel length scale. The fracture intensity was analyzed at 191+780 at a bearing of 35° and was about 20 fractures/m (Funehag & Gustafson 2004). The studied section is reinforced with up to 0.5 m of shotcrete. Pre-grouting was conducted with both cementitious and non-cementitous grout agents.
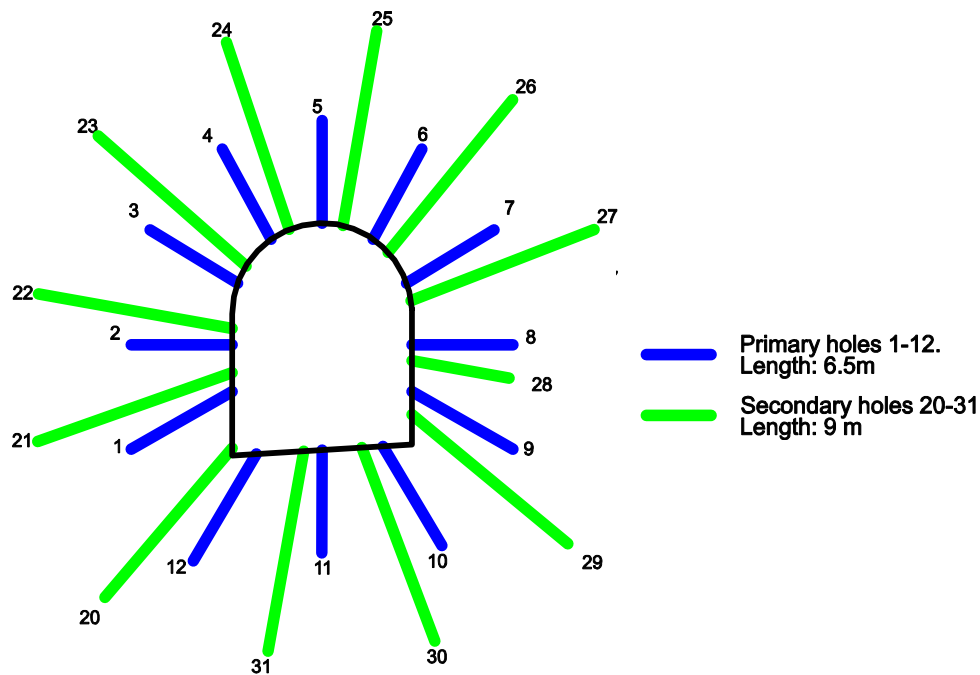
*Figure 2.22: The primary and secondary boreholes that were grouted in Hallandsås. The distance between BH8 and BH28 is one meter. The distance between BH8 and BH7 and BH9 respectively is four meters.*

### 2.5.1 Rock stresses

The primary stress situation in Hallandsås can be described as[1]:

$$\sigma_v = \rho \cdot g \cdot z$$
$$\sigma_h = \sigma_v$$
$$\sigma_H = 2 \cdot \sigma_v$$

Where $\sigma_v$ is vertical, $\sigma_H$ is parallel to the tunnel and $\sigma_h$ is perpendicular to the tunnel. The stress situation in the Hallandsås tunnel wall is described according to Figure 2.23 and Figure 2.24. In Figure 2.23 $\sigma_H$ is the largest horizontal principal stress. Two generalized fracture sets, strike 345° and 65°, has been added. Their angles from the tunnel wall correspond to the general fracture sets described by Funehag and Gustafson (2004). The normal- and shear stresses ($\sigma_n$, $\tau$) resulting from $\sigma_H$ and $\sigma_h$ is illustrated for a point (circle) on one fracture. The secondary stresses from the tunnel do not affect $\sigma_H$, but have a large impact on $\sigma_h$, see Figure 2.24.

The normal stress upon the two fracture directions was estimated for stresses calculated with Kirsch's equations (Eq. 2.4 - Eq. 2.6) and Examine2D. For the Kirsch solution $\sigma_H$ is constant and $\sigma_h$ varies according to the equation describing $\sigma_r$. For the Examine2D solution $\sigma_H$ is double $\sigma_V$ and $\sigma_h$ equal to $\sigma_V$ .

---

[1] Kenneth Rosell tunnelchef, Swedish transport administration, mail contact 2010-04-15.
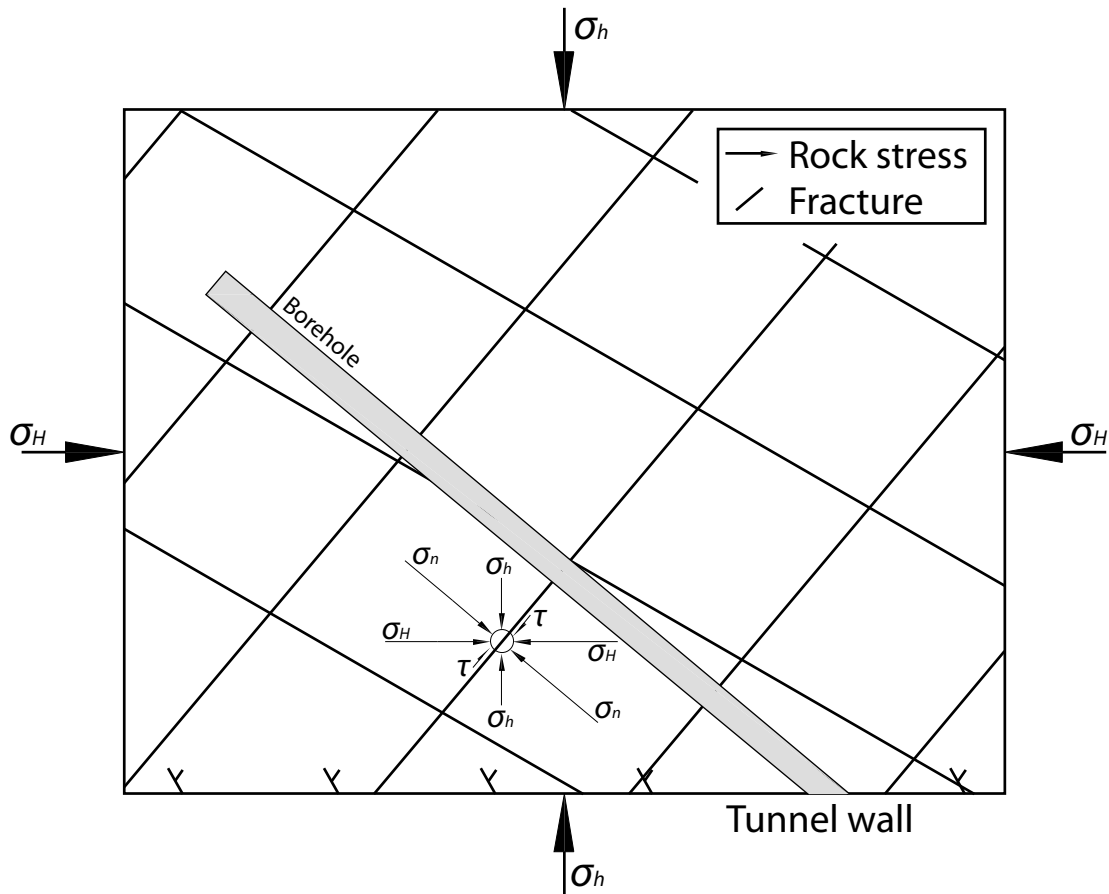
*Figure 2.23: A conceptual rock stress model for the Hallandsås tunnel. The two fracture sets has a strike of 345° and 65° respectively. The spacing of the fractures is set adequate for visibility, and is not the actual spacing.*
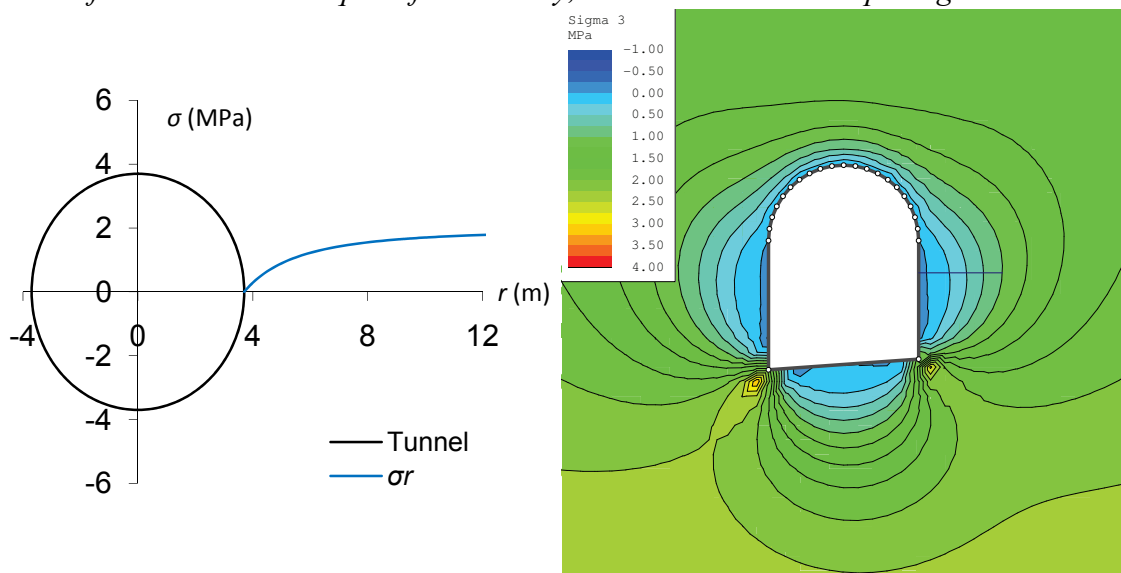


*Figure 2.24 Left: Kirsch solution to stress field in the tunnel wall of Hallandsås; with increasing distance from the tunnel, $\sigma_r$ goes towards $\sigma_h$. Right: Examine2D solution for the same principal stresses.*

## 2.5.2 Hydraulic testing programme

The deformation measurement and preceding hydraulic tests followed a test program which can be seen in its full extent in Appendix II, a summary of the program follows here. The testing was initiated when the primary grouting fan was drilled. Natural inflow to the holes in the walls and floor was measured, and the hole with the largest superficial inflow was chosen. Criteria for the selection were chosen as follows:

1. Wall-hole with $Q_{tot} \geq 5$ l/min, and $Q_{out} \geq 2$ l/min
2. Floor-hole with $Q_{tot} \geq 5$ l/min, and $Q_{out} \geq 2$ l/min
3. Wall-hole with $Q_{tot} \geq 5$ l/min
4. Floor-hole with $Q_{tot} \geq 5$ l/min
5. If none of 1-4 is fulfilled, use the hole with the largest total inflow, $Q_{tot}$

Where $Q_{tot}$ is the total flow from borehole and $Q_{out}$ is the flow from 0-3 m depth of the borehole.

According to Table 2.4 borehole 8 (BH8) in fan 1 was chosen, see Figure 2.22. BH8 in fan 2 was better according to the criterions but due to unsuccessful drilling it could not be used for testing. Therefore all references to borehole numbers in Hallandsås refer to fan 1. The next step was to drill a nearby hole from the secondary fan, BH28. In BH8 NIT, CFL and a 10 min PBT were performed at packer depth 1m. NIT and PBT were repeated for packer depth 3 m. BH28 were closed during this testing. The same tests were then performed in BH28 with BH8 closed.

The next step in the program was to determine if there was a hydraulic connection between the two boreholes. The pressure was logged in BH8 and a WPT was performed in BH28, starting with 0.5 MPa overpressure, followed by an incremental increase of pressure of 0.2 MPa for 2 minutes, repeated until a notable response was seen in BH8. Maximum allowed pressure was the grouting pressure; 2.0 MPa.

When a connection was found the packer with pressure logging in BH8 was replaced by the deformation anchor, rod and sensors. The anchor depth was 4.5 m. A new WPT was initiated with the same testing procedure as in pressure connection test. The initial pressure of 0.5 MPa was held for 5 minutes, and if no deformation was seen on the analog sensor, the pressure was increased by 0.2 MPa for 2 minutes until a deformation occurred. When the deformation occurred the pressure was released for 2 minutes, to see whether the deformation returned. Thereafter the pumping was resumed with the next pressure step. When maximum pressure was reached, the pump was disconnected from BH8, and deformation logging in BH28 was supposed to continue until BH8 and the nearby holes were grouted. The grouting was suffering some delays, and the actual deformation during grouting was conducted two weeks later.

*Table 2.4: The inflow to boreholes in fan 1 and 2 in Hallandsås. The values for 2010-03-15 are measured by the contractor before testing, all holes were 6 m deep. The values for 2010-03-30 are measured by the contractor when the boreholes were prolonged to 9 m. Hole 8 and 28 was not prolonged. Values within [brackets] are measured as a part of our testing programme.*

| Borehole | Fan 1 $Q$ 2010-03-15 (l/min) | Fan 1 $Q$ 2010-03-30 (l/min) | Fan 2 $Q$ 2010-03-15 (l/min) |
|---|---|---|---|
| **1** | 0 | 0 | Dry |
| **2** | 0 | 0 | Dripping |
| **3** | 0 | 0.3 | Dripping |
| **4** | Dripping | 0.2 | Dripping |
| **5** | 0.5 | 5 | Dripping |
| **6** | 0.5 | 6 | Dripping |
| **7** | 4.0 | 5 | Dripping |
| **8** | 4.0 [1.7] | 7 | 10 |
| **9** | 1.9 | 5 | 2.8 |
| **10** | 0 | 0.5 | Dry |
| **11** | 0 | 0 | Dry |
| **12** | 0 | 0 | Dry |
| **28** | [2] | [6] | - |

# 3 Results

In this chapter the results are presented. Calculated normal rock stresses upon fracture planes are presented for the old service tunnel. The results from hydraulic tests performed in the service tunnel are described up to the point where the plans for deformation measurements were abandoned. For Hallandsås tunnel the corresponding rock stress calculations and hydraulic test data are shown. The results of deformation measurements performed in Hallandsås conclude the chapter.

## 3.1 Rock stresses in old service tunnel

In Figure 2.16 $\sigma_H$ is the largest horizontal principal stress, which has been set to 10 MPa, $\sigma_h$ is the smallest horizontal principal stress, 7 MPa, $\sigma_v$, the vertical principal stress is set to 5 MPa. This data was used to model the Kirsch solution. The stresses have also been modelled in Examine2D, with the same input data. The resulting normal stress upon fracture planes at an angle of 20°, 45° and 80° to the tunnel wall can be seen in Figure 3.1. According to this estimation a grout pressure of 2.0 MPa would not exceed the normal stress, but, as described in Paragraph 2.1.6 a shear stress may cause a fracture to deform before the normal stress is exceeded. The shear stresses were calculated in the same way as the normal (Eq. 2.23), and found to be in the same order of magnitude (see Appendix III).
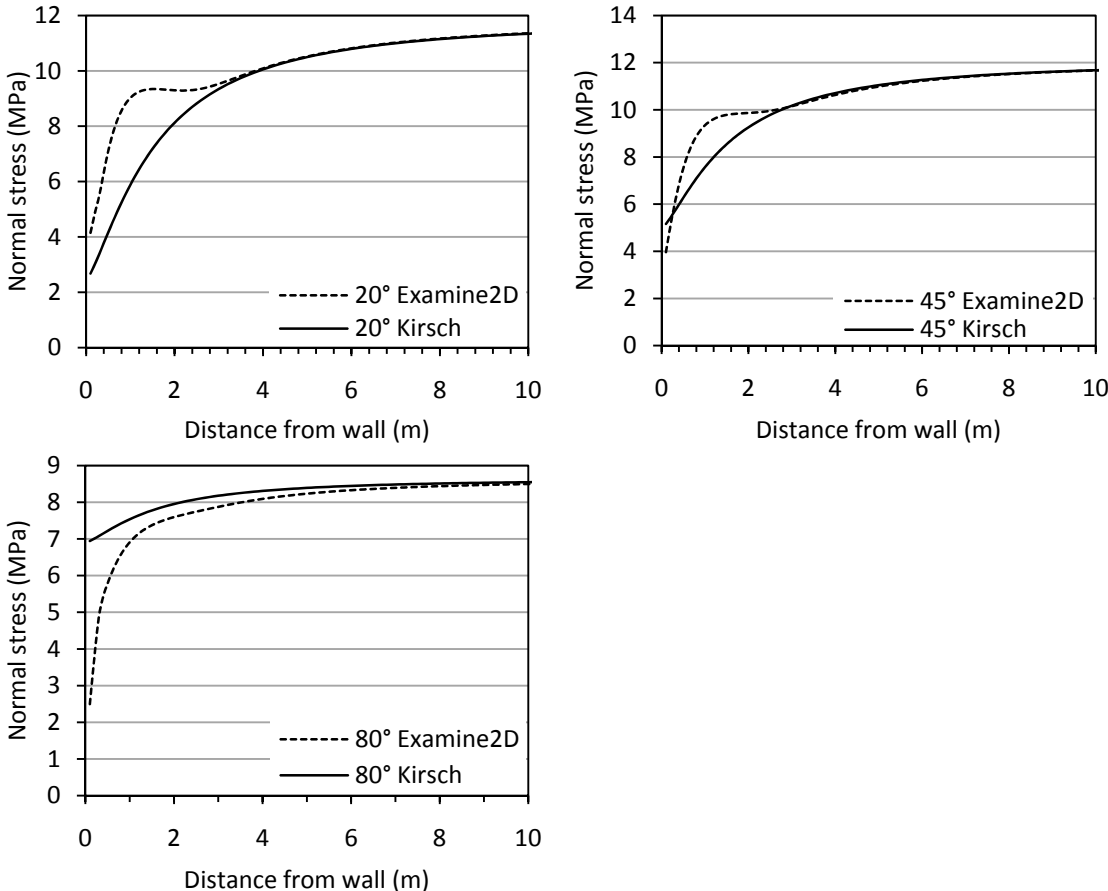


Figure 3.1: Normal stress on three fracture planes; 20°, 45° and 80° angle from tunnel wall, calculated with Kirsch equations and Examine2D

## 3.2 Hydraulic tests performed in old service tunnel

During drilling of KBH2 hydraulic tests was performed. From the tests a transmissivity is evaluated and the hydraulic aperture, $b_{hyd}$, is calculated according to Eq. 2.8, see Table 3.1. Note the increase in hydraulic aperture between 11.8 and 14.5 meters.

*Table 3.1: Transmissivity and estimation of hydraulic aperture from cubic-law, Eq. 2.7. The total pressure is stated after the water pressure tests.*

| Borehole | Section | WPT (0.6 MPa) | | WPT (0.8 MPa) | |
|----------|---------|---------------|---------------|---------------|---------------|
| | | $T$ (m²/s) | $b_{hyd}$ (μm) | $T$ (m²/s) | $b_{hyd}$ (μm) |
| **KBH2** | **1.5-2.75** | 0 | 0 | 0 | 0 |
| | **1.5-6** | $1.79 \cdot 10^{-8}$ | 31 | $1.60 \cdot 10^{-8}$ | 29 |
| | **1.5-9** | $5.56 \cdot 10^{-8}$ | 45 | $4.86 \cdot 10^{-8}$ | 43 |
| | **1.5-11.8** | $3.61 \cdot 10^{-8}$ | 39 | $3.33 \cdot 10^{-8}$ | 38 |
| | **1.5-14.5** | $8.33 \cdot 10^{-7}$ | 110 | $6.33 \cdot 10^{-7}$ | 100 |
| | **1.5-18** | $2.01 \cdot 10^{-6}$ | 147 | $1.72 \cdot 10^{-6}$ | 140 |
| | **1.5-20** | $1.99 \cdot 10^{-6}$ | 147 | $1.82 \cdot 10^{-6}$ | 142 |

*Table 3.2: Full hole WPT from KBH2 to KBH3. First the system stabilized for 3h with both holes closed, and then KBH3 were pressurized with 1.05, 1.3 and 1.9 MPa.*

| $p$ KBH2 (MPa) | $Q$ KBH2 (l/min) | $b$ (μm) | $p$ KBH3 (MPa) | $\Delta p$ KBH3 (MPa) | Test duration (h) |
|----------------|------------------|----------|----------------|----------------------|-------------------|
| **0.35** | 0 | 117 | 0.094 | 0 | 3 |
| **1.05** | 6.6 | 139 | 0.156 | 0.062 | 0.5 |
| **1.3** | 6.7 | 127 | 0.197 | 0.041 | 0.5 |
| **1.9** | 11.1 | 124 | 0.282 | 0.084 | 0.5 |

*Table 3.3: Full hole WPT from KBH3 to KBH2. First the system stabilized for 24h with both holes closed, and then KBH3 were pressurized with 1.5 and 2.0 MPa.*

| $p$ KBH3 (MPa) | $Q$ KBH3 (l/min) | $b$ (μm) | $p$ KBH2 (MPa) | $\Delta p$ KBH2 (MPa) | Test duration (h) |
|----------------|------------------|----------|----------------|----------------------|-------------------|
| **0.1** | 0 | | 0.36 | 0 | 24 |
| **1.5** | 0.0025 | 8 | 0.36 | 0 | 0.16 |
| **2.0** | 0.2 | 31 | 0.361 | 0.001 | 0.5 |

After KBH2 and KBH3 were drilled two test series of water pressure tests was performed. This was done in order to verify the connection between KBH2 and KBH3 that is shown in Figure 2.21. In the first series a PBT was performed in KBH3 and then KBH2 was pressurized with 1.05, 1.3 and 1.9 MPa, with no interruption between the pressure increases. During the test the pressure was logged in KBH3 and the result can be seen in Table 3.2. The same procedure was done in the second test series, but KBH3 was pressurized with 1.5 and 2.0 MPa. The pressure was logged in KBH2 and the result can be seen in Table 3.3.

At this stage, when it was clearly indicated (Table 3.1 and Table 3.3) that the aperture is small in the first meters of rock mass in both KBH2 and KBH3, no deformation was deemed likely to occur. Due to this fact and large delays in the grouting progress, it was decided not to measure deformation when grouting. The work was focused on measurements in Hallandsås instead.

## 3.3    Rock stresses in Hallandsås

The largest horizontal principal stress, $\sigma_H$, has been calculated to 4 MPa and the smallest to 2 MPa (Paragraph 2.5.1). The stress field was evaluated, according to Paragraph 2.1.1.2, and the results are presented below. According to this estimation a grout pressure of 2.0 MPa would exceed the normal stress upon a fracture at 30° angle to the tunnel wall within 0.15 m for the Kirsch solution and 0.7 m for the Examine2D solution if only normal stresses are regarded. For a 50° fracture the stress is always larger than 2 MPa. The shear stresses along the fractures was calculated in the same way, and found to be at the same magnitude as the normal stresses.
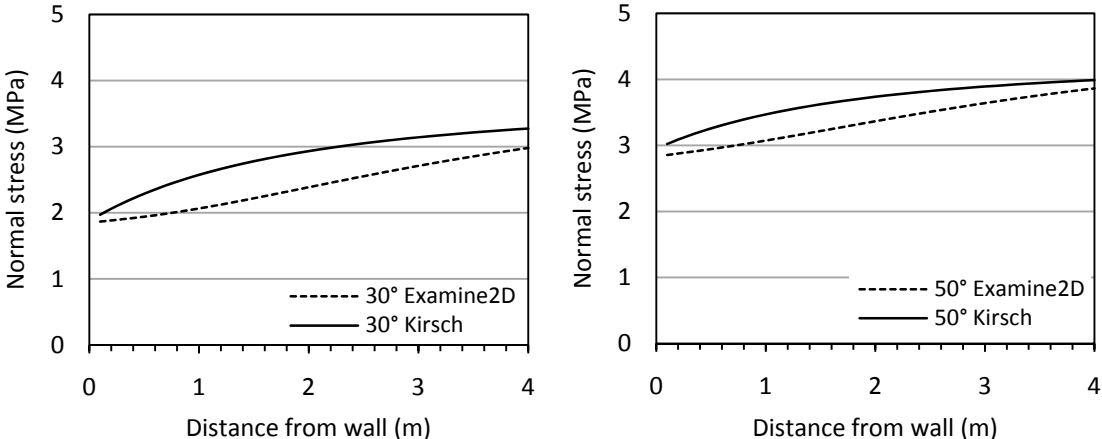


*Figure 3.2: Normal stress on two fracture planes; 30° and 50° from tunnel wall, calculated with Kirsch equations and Examine2D.*

## 3.4 Hydraulic tests performed in Hallandsås

The hydraulic tests were performed March 16 and March 31. Water pressure deformation measurements were performed after the hydraulic tests the 16th. Deformation measurements during grouting were performed after the hydraulic tests the 31st. The data are presented in Table 3.4. On the 16th March prior to the deformation measurement a pressure connection test was made. This test is similar to the deformation measurement, but the pressure is logged instead of the deformation.

The pump pressure in Figure 3.3 represents a generalization of the pressure data. The pumping equipment was not sophisticated enough to keep constant pressures, and it was difficult to manually keep constant pressures. The actual pressure deviations are generally ± 0.1 MPa. A connection was achieved at about 1.4 MPa, as the pressure in BH8 increased 0.386 MPa in 1 minute, until the pump was shut down and the pressure in BH8 started to drop again. The flow was running with pressure and flow from the supply hose for another 80 seconds, until closed. Thereafter the pressure dropped to 0.065 MPa, 95 % of this drop occurred in 86 seconds.

*Table 3.4: Inflow, pressure measurements and corresponding hydraulic aperture carried out at two occasions.*

|  | Distance to BH28 (m) | Q (l/min) | p (MPa) | b (μm) | Q (l/min) | p (MPa) | b (μm) |
|---|---|---|---|---|---|---|---|
|  |  | **16/3-2010** |  |  | **31/3-2010** |  |  |
| **BH28** | 0 | 0.7 | 0.13 | 109 | 6 | 0.2 | 317 |
| **BH8** | 1 | 1.7 | 0.3 | 115 | 7 | 0.2 | 210 |
| **BH7** | 3.8 | 4 | 0.3 | 152 | 5 | 0.5 | 138 |
| **BH9** | 4 | 1.9 | 0.3 | 119 | 5 | 0.2 | 188 |



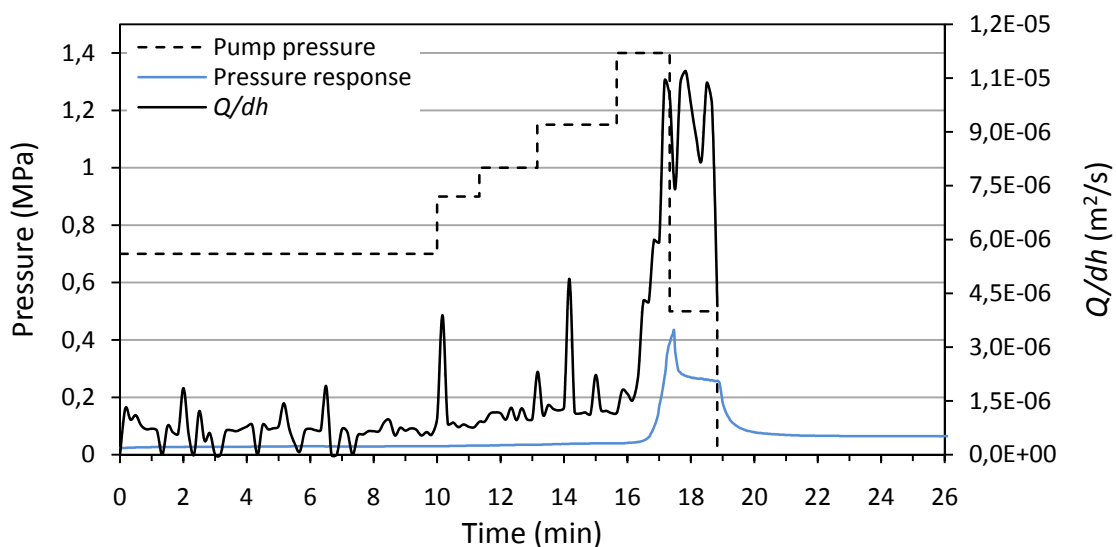*Figure 3.3: The pressure response test performed in Hallandsås. "Pump pressure" is the pressure pumped into BH28, "Q/dh" is the specific flow from the pump, and "Pressure response" is the measured pressure in BH8.*

## 3.5 Deformation measurements in Hallandsås

In this section the measured deformations from Hallandsås are presented. All of these measurements were performed in BH8. Four deformation tests were performed during water pressure tests, and are presented first. Thereafter deformation was logged during the grouting session of the three boreholes closest to BH8; BH9, BH28 and BH7, see Figure 2.22 for distance relation. The anchor of the deformation rod was placed at a depth of 4.5 m in all tests except the fourth water injection test, where the anchor was placed at a depth of 1.9 m. The deformation data are shown in Figure 3.4 - Figure 3.10, where also the applied pressure is plotted.

For the deformation during water pressure test the correlation between the sensors is good and the difference is within an error margin of 10 μm (see Appendix V). Therefore further analysis use only the analog data, since the data set is smaller, and does not contain noise. The correlation between the sensors was not as good for the grouting measurements, and the analog curve is not used for all cases (comparison graphs are presented in Appendix V). No digital data were obtained from the grouting of borehole 9 (see Figure 3.9), and therefore the analog data are used for this borehole. The boreholes were grouted in the order BH9, BH28 and BH7, and they are presented in that order.

The first test was performed 2010-03-17 20:50 and consists of two parts. In the first part the pressure was increased from 0 to 1.2 MPa during 11 minutes, see dotted line in Figure 3.4. The pressure was then set to 0 MPa and a 2 minute recovery was made in order to see if deformation is resilient. In the second part at t=13 min the pressure was supposed to be increased to 1.4 MPa but the equipment could only deliver 1.0 MPa. This part was performed during 3 min and the pressure was then set to 0 MPa and the recovery was logged.
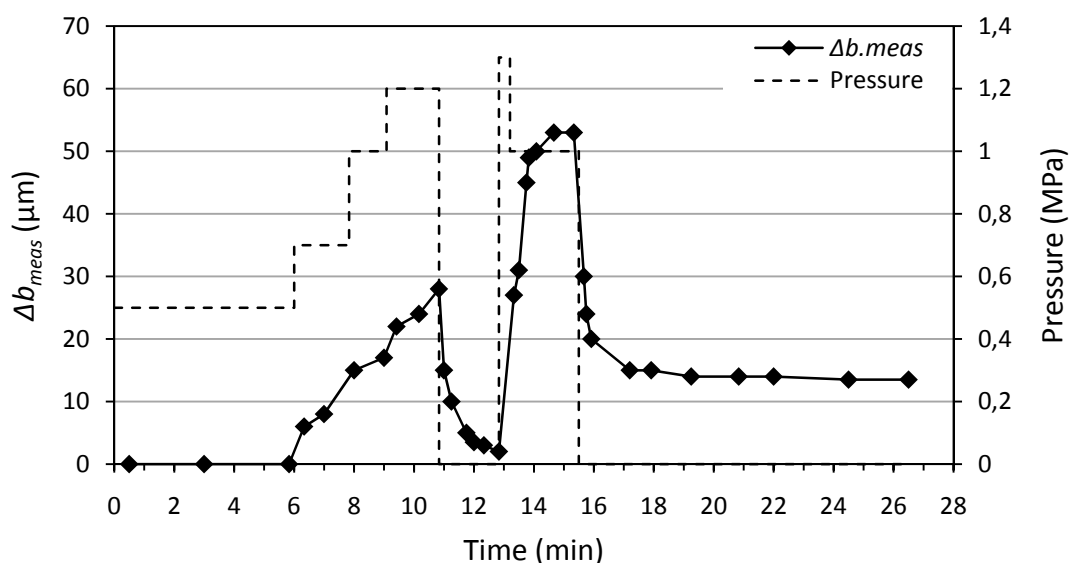


*Figure 3.4: Shows the deformation (analog) during the first water pressure test logged with an analog sensor. The pressure level is plotted on the secondary y-axis axis. The test was performed 2010-03-17 20:50.*

The second test starts directly after test one, though the deformation is normalized to zero, i.e. t= 0 min in test two is t= 26,5 min in test one, and deformation 13 μm in test 1 is deformation 0 μm in test 2. The pressure is increased from 0 to 1.0 MPa with the pressure steps that can be seen in Figure 3.5. When the test had run for 10 minutes the pressure was supposed to be set to 1.2 MPa, but the equipment could only deliver 1.0 MPa due to the increased flow.
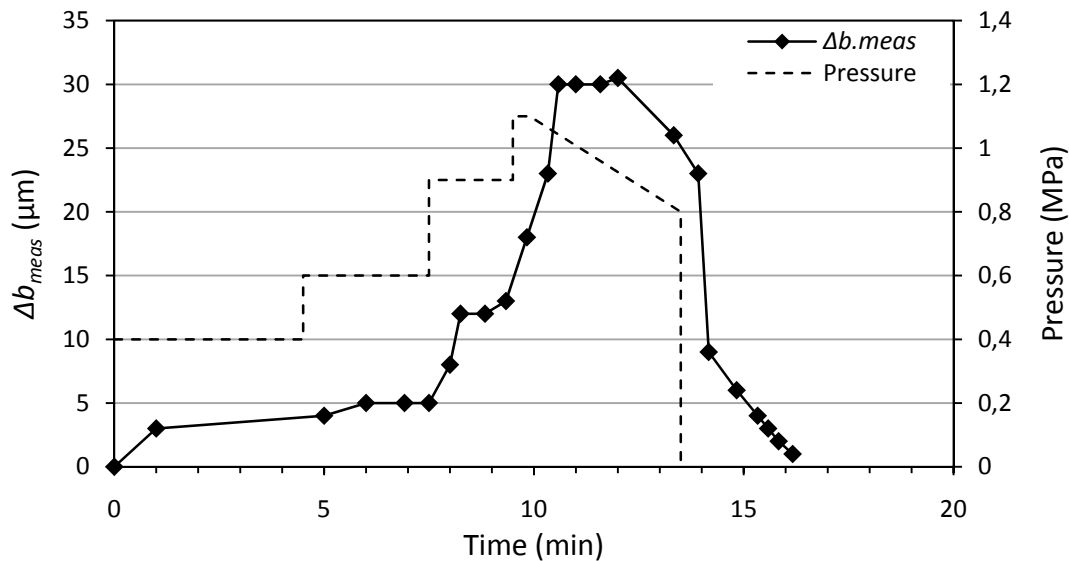


*Figure 3.5: Shows the deformation (analog) during the second water pressure test logged with an analog sensor. The pressure level is plotted on the secondary y-axis. The test was performed 2010-03-17 21:20.*

Test three and four was performed 2010-03-18 and is shown in Figure 3.6 and Figure 3.7. They are similar to test one and two and the deviation between the analog and digital sensor is less than 10 μm. Test four is performed at an anchor depth of 2 m, just outside a large fracture, and the inflow of this section (2.0-2.5 m) were 1.1 l/min, compared to the full hole inflow of 1.7 l/min. Measurement during the grouting two weeks later showed an increased full hole inflow; 6 l/min.
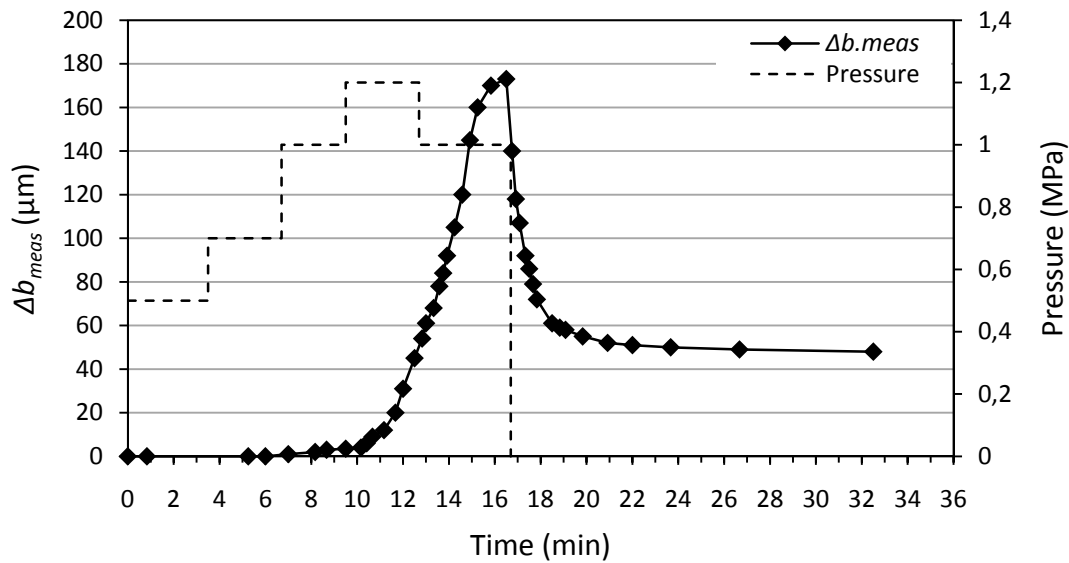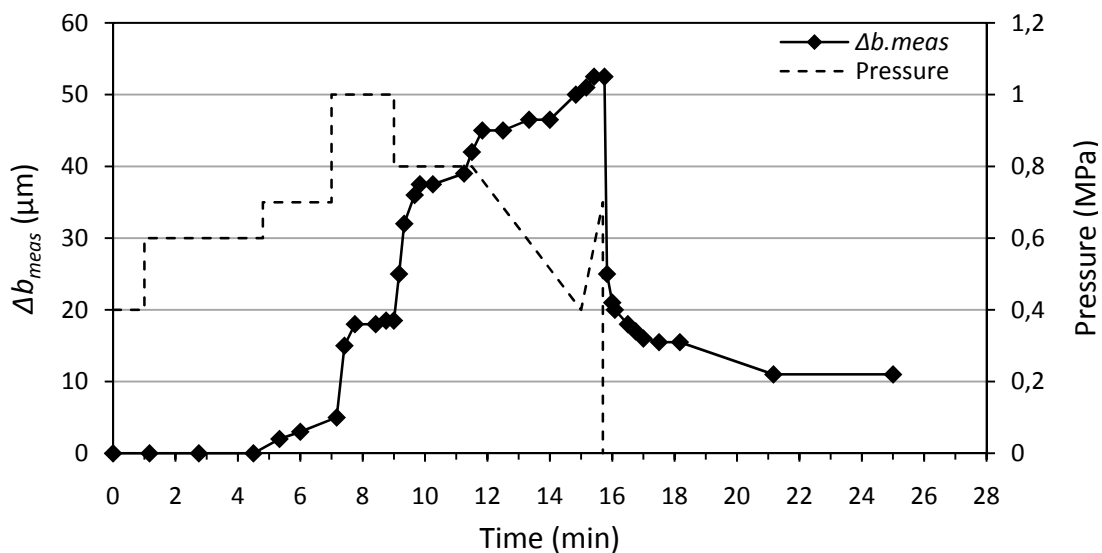
*Figure 3.6: Shows the deformation (analog) during the third water pressure test logged with an analog sensor. The pressure level is plotted on the secondary y-axis. The test was performed 2010-03-18 10:20.*



*Figure 3.7: Shows the deformation (analog) during the fourth water pressure test logged with an analog sensor. The pressure level is plotted on the secondary y-axis. The test was performed 2010-03-18 12:20.*

Deformation measurements was conducted during the grouting of BH9, BH28 and BH7. The reason for BH28 being grouted and deformations measured in BH8 is that packers were easier to get tight in BH28, and therefore it seemed more appropriate for grouting. BH9, situated about 4 m below BH8 was gruted with about 800 l of silica sol, divided into 4 batches. Between each batch there was a pause for mixing (see pressure profile in Figure 3.8). At the end of the grouting the sol is gelling causing more resistanse in the fracture network, therefore the desired pressure of 2.0 MPa was achieved. A total deformation of 36 μm was measured.
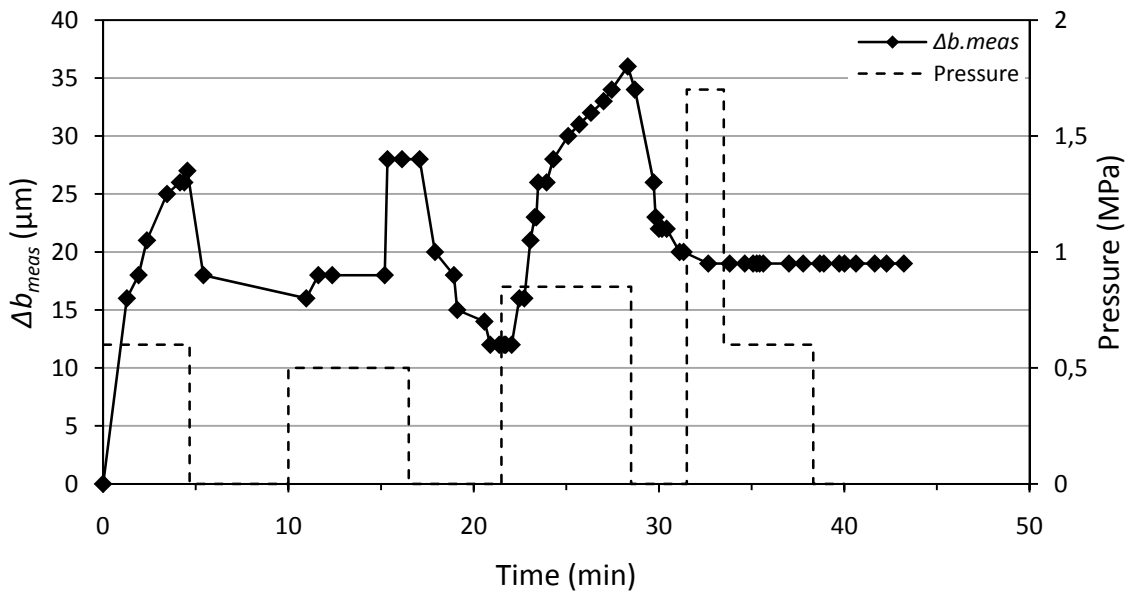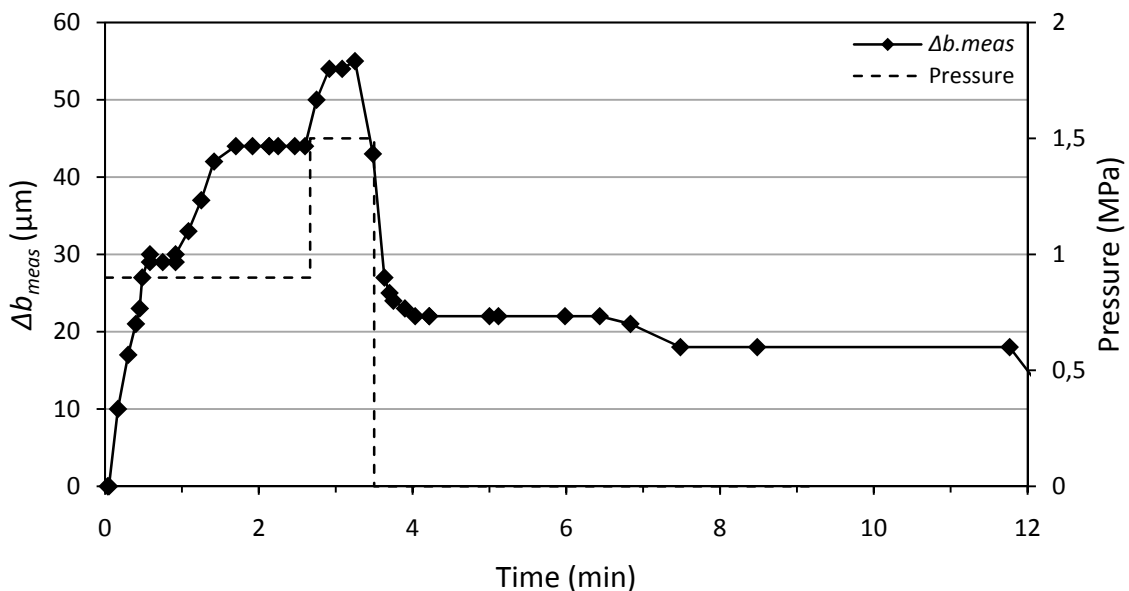
*Figure 3.8: Deformation (analog) measured during the grouting of BH9 (4 m below test borehole). The applied grout pressure is plotted on the right y-axis. The grouting started 2010-03-31 16:50.*

For the grouting of BH28, see Figure 3.9, a total quantity of about 100 l of silica sol was grouted. The gel time was 5 minutes long and the flow was reduced to almost zero after about three minutes. The deformation started to regress at this point also. Total deformation achieved was about 60 µm (analog and digital data differs a couple of µm).



*Figure 3.9: Deformation (analog) measured during the grouting of BH28 (1 m below test borehole). The applied grout pressure is plotted on the right y-axis. The grouting started 2010-03-31 21:40.*

The grouting of BH7 was conducted with one batch of silica sol, see Figure 3.10. About 100 l was grouted. 3.5 minutes after the grouting was initiated, sol was leaking out of the borehole, and the grouting paused until the packer was refastened. Thereafter the pressure was quite steady, and a deformation of 25 μm was measured.
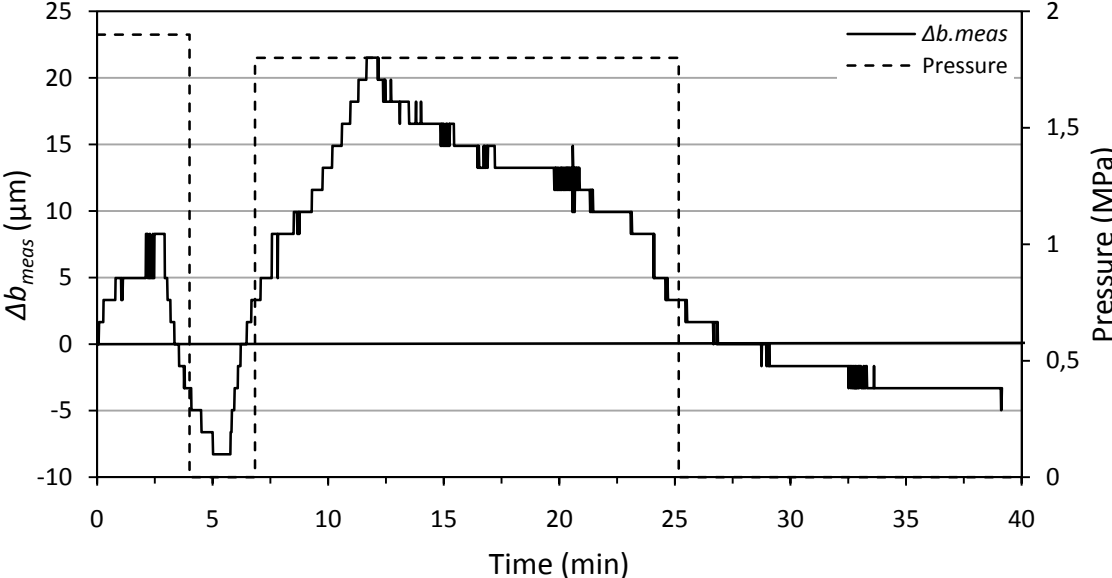


*Figure 3.10: Deformation (digital) measured during the grouting of BH7 (4 m above test borehole). The applied grout pressure is plotted on the right y-axis. The grouting started 2010-03-31 22:30.*

# 4    Analysis

The analysis of data focus on the deformation measurements during tests in BH28 conducted in Hallandsås. Data from BH7 and 9 is used as a complement to assess type of deformation and distance dependency. When the deformation measurement during the water pressure tests was conducted a large leakage was observed from the borehole, probably resulting in errors in flow dimension and underestimating the stiffness (see Appendix VI and Appendix IV). There was no deformation measurements performed in the old service tunnel.

Since the anchor for deformation measurements was not moved between the grouting of the different boreholes, deformation logging could proceed between the sessions. Each of the graphs presented in Section 3.5 (page 37) are normalised for a deformation of zero when the grouting started. However, the grouting of BH28 started at a deformation of 7 µm, when counting from the start of the logging, and for BH7 the corresponding value is 35 µm. For the deformation during the water pressure tests, the anchor was moved between test 2, 3 and 4, and therefore a value for the non-normalised initial deformation can only be obtained for test 2; 14 µm. When regarding the end of the deformation graphs for all tests, the rate of deformation recovery is very low, therefore the graph is assumed to fully describe the deformation recovery. In the cases where the ending value is larger than the initial value, this is seen as a permanent deformation.

In summary, permanent deformation is regarded as the difference between test start and end deformation. Resilient deformation is the difference between the highest and the lowest value during test minus the permanent deformation, see Figure 4.1 and the results is presented in Table 4.1. The resilient part of the deformation is larger than the permanent for all tests except for grouting of BH9.
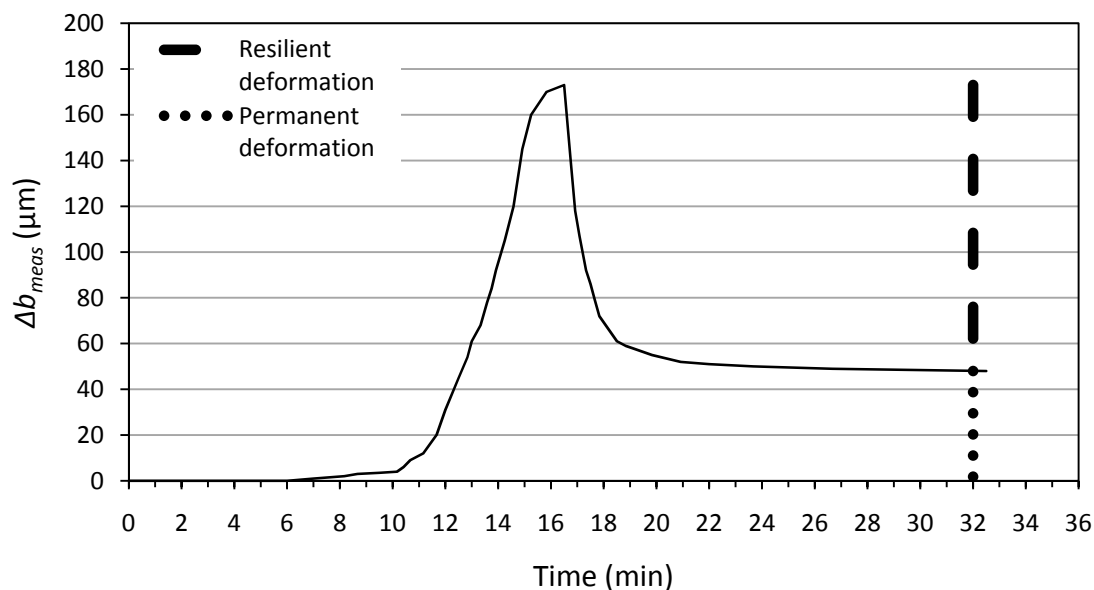


*Figure 4.1: Shows the concept of how resilient and permanent deformation is evaluated*

*Table 4.1: The remaining deformation after each test is described as permanent deformation. The regressive deformation, the difference between maximum and initial logger values minus the permanent deformation, is described as resilient deformation. G means test during a grouting session.*

| Test | WPT1 | WPT2 | WPT3 | WPT4 | G-BH9 | G-BH28 | G-BH7 |
|---|---|---|---|---|---|---|---|
| **Distance to BH8 (m)** | 1 | 1 | 1 | 1 | 4 | 1 | 4 |
| **Permanent (µm)** | 14 | 0 | 48 | 11 | 19 | 18 | 0 |
| **Resilient (µm)** | 39 | 31 | 125 | 42 | 17 | 37 | 30 |
| **Total (µm)** | 53 | 31 | 173 | 53 | 36 | 55 | 30 |

The theory from Paragraph 2.1.3 has been applied on in situ measurements to calculate the fracture normal stiffness. In Figure 4.2 two different stages, A and B, are presented. The stages correspond to an initial stage with a higher fracture normal stiffness, stage A, and a subsequent stage, B, with a lower stiffness. Intervals are chosen for stable deformation rates according to Appendix IV. The stiffness has been calculated with Eq. 2.9. The denominator in Eq. 2.9, $\Delta u_n$, is a change in aperture which has been assessed in two ways, measured deformation and a change in hydraulic aperture. The numerator in Eq. 2.9, $\Delta\sigma'_n$, is the change in effective stress, and set to the average grouting overpressure, $\Delta p/3$. The change in deformation and hydraulic aperture is evaluated as seen in Figure 4.3 and Appendix IV, where an interval is chosen for stage A and B. In this interval a difference between the maximum and minimum value for the measured deformation and hydraulic aperture is achieved.
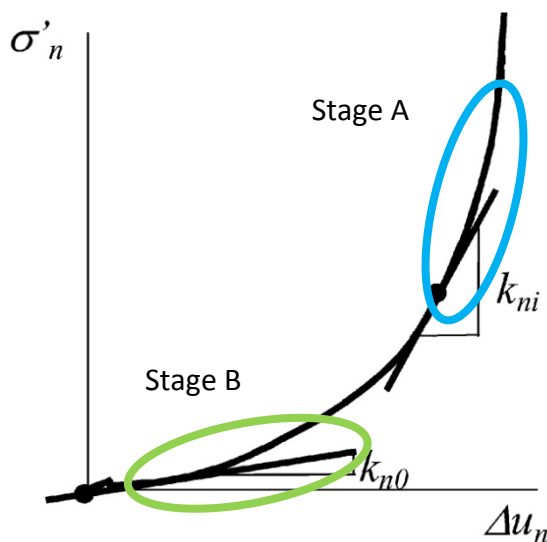


*Figure 4.2: Shows the deformation plotted with the effective stress. The blue ellipse represents an initial stage with a high fracture normal stiffness, Stage A. In this stage a large decrease of the effective stress results in a relatively small deformation of the fracture. The green ellipse shows a stage with lower fracture normal stiffness resulting in large deformation with a small decrease of the effective stress, Stage B. Modified from Rutqvist (1995).*
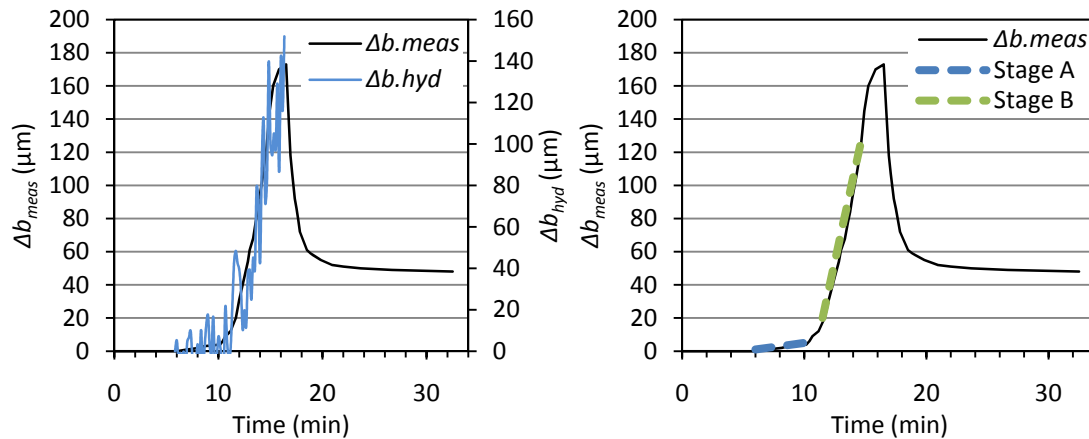
*Figure 4.3: Left: The measured deformation, $\Delta b_{meas}$, plotted together with the corresponding change of hydraulic aperture, $\Delta b_{hyd}$. Right: The measured deformation for the same test and the intervals where stiffness stage A and B are chosen. The data is for the third WPT performed with pumping in BH28 and measurement in BH8*

The stiffness has also been calculated according to Eq. 2.13, where the stiffness is described with a relation to the storativity, Eq. 2.12, (Fransson 2009). An empirical relation between the transmissivity and the storativity has been used as an estimate for the storativity, Eq. 2.11, (Rhén et al. 2008). The transmissivity used in this expression is evaluated according to Eq. 2.8 and corresponds to the start value of the stiffness interval, represented by the start of the blue and green lines in Figure 4.3. In Table 4.2 the fracture normal stiffness is presented for the deformation measurements and the initial testing to determine a pressure connection (see Paragraph 2.5.2).

*Table 4.2: Fracture normal stiffness for water pressure test and grouting estimated in three ways. Stiffness based on hydraulic aperture, $k_n^{hyd}$, and measured deformation, $k_n^{meas}$, is calculated according to Eq. 2.9. Stiffness based on an empirical relation between transmissivity and storativity, $k_n^S$, is calculated according to Eq. 2.13. Stage A and B is described in Figure 4.2. All stiffness values are expressed in GPa/m.*

| BH | Test | Date Time | Stage A | | | Stage B | | |
| | | | $k_n^{hyd}$ | $k_n^{meas}$ | $k_n^S$ | $k_n^{hyd}$ | $k_n^{meas}$ | $k_n^S$ |
|---|---|---|---|---|---|---|---|---|
| 28 | WPT | 03-17 15:30 | 17 | - | 20 | 4 | - | 11 |
| 28 | WPT | 03-17 20:50 | 7 | 10 | 4 | 7 | 7 | 3 |
| 28 | WPT | 03-17 21:20 | 4 | 23 | 3 | 14 | 11 | 2 |
| 28 | WPT | 03-18 10:20 | 1 | 79 | 2 | 4 | 3 | 5 |
| 28 | WPT | 03-18 12:20 | 52 | 37 | 4 | 3 | 9 | 4 |
| 9 | Grouting | 03-31 16:50 | - | - | - | (-3) | 5 | 3 |
| 28 | Grouting | 03-31 21:40 | - | - | - | 9 | 7 | 7 |
| 7 | Grouting | 03-31 22:30 | - | - | - | 7 | 19 | 289 |

Results from the deformation measurement and the flow dimension analysis in BH8 are presented in Figure 4.4 and Appendix VI. The pressure steps plotted is the total pressure, i.e. the pump pressure. As stated in Paragraph 2.1.4, a *Q·t/V*-value larger than 1.0 indicates a 3D flow, which could be either flow in a well connected 3D fracture network, deformation of fractures, or both. The general feature is that the flow dimension is at 3D when an increasing deformation is registered and 2D or lower when a regression is registered. Because of difficulties with the packer in BH28 during the water pressure tests, a leakage from this hole was observed. This might be the reason for the high values in the dimension analysis. Although the trend is that when a deformation occur the flow dimension is increased.

An estimation of the normal stress, in Hallandsås, has been performed in order to make a comparison with the conceptual rock stress model (results presented in Table 4.3). The measured deformation is plotted with the corresponding pump pressure, to assess which pressure that gave the majority of the deformation. The result presented in Figure 4.5 indicates that a large part of the deformation occur at 1.0-1.4 MPa pump pressure. Therefore the normal stress upon the deformed fracture is probably between 0.3-0.5 MPa, under the assumption that $\Delta p/3$ is the average pressure across the fracture that deforms .
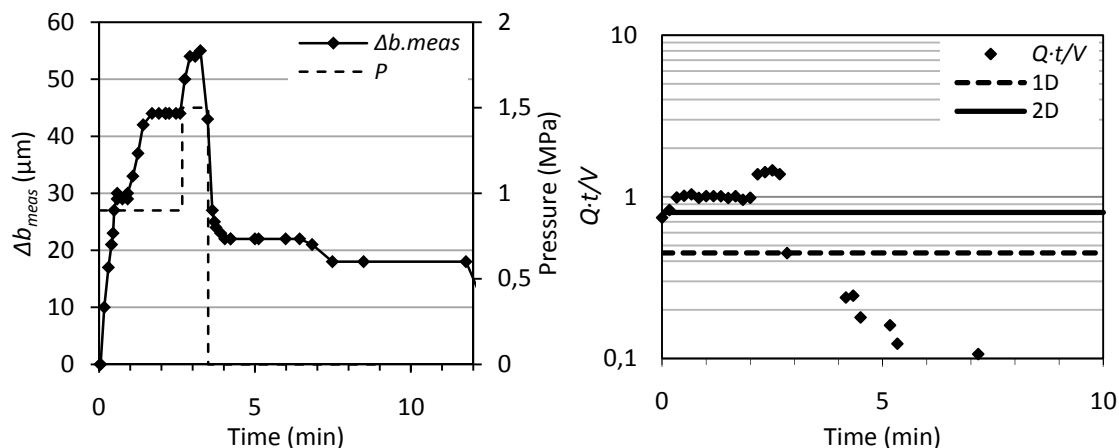


*Figure 4.4: Left: Deformation measured during the grouting of BH28. Right: The dimensionality analysis for the grout flow. The Q·t/V-value is above 0.8 when deformation occurs, which indicates 3D-flow.The gel time for this grout batch was 7 min, which might be the reason for the reduced flow after 3.5 min.*
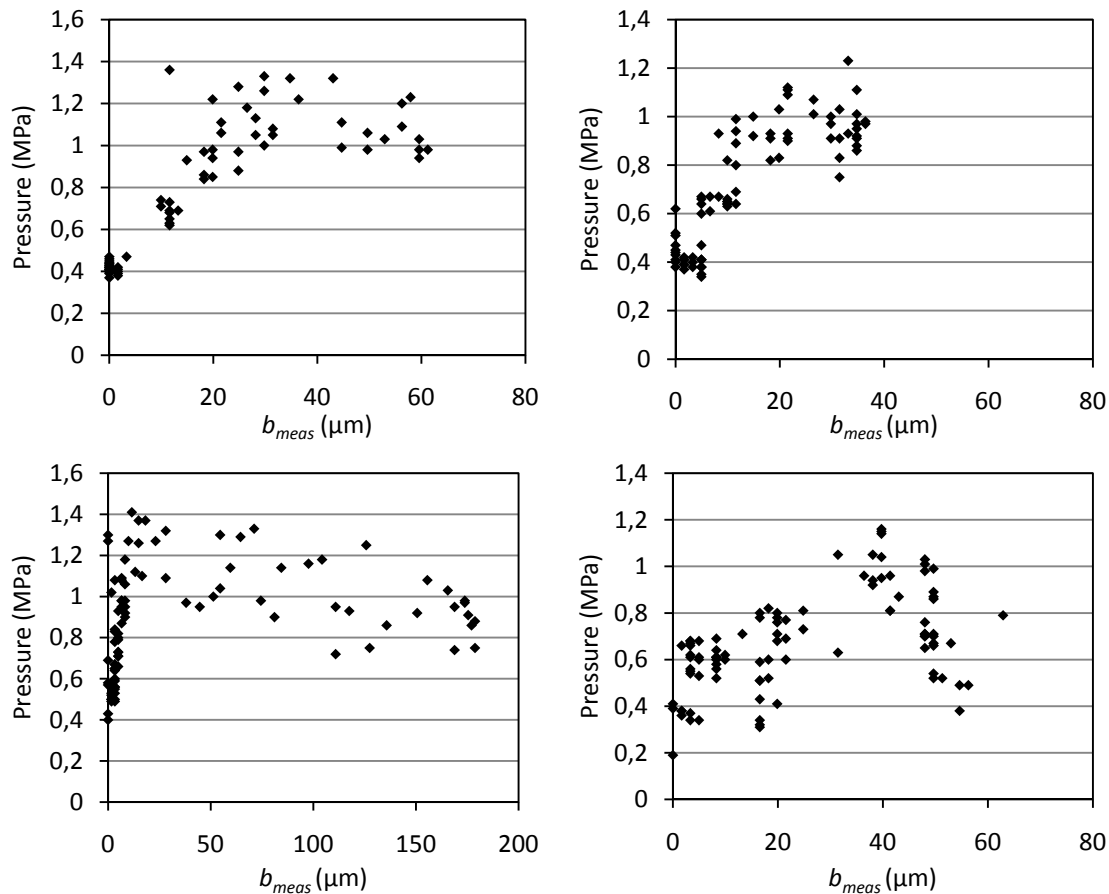
*Figure 4.5: Analysis of water pressure test and deformation data. Total pump pressure is plotted with measured deformation. The upper two figures were performed in day 1 and the bottom two day 2. The deformation rod was placed at 4 meter in test 1-3 and in the last test in day 2 it was moved to 1.9 meter, bottom right. The top left figure correspond to 12 min of pumping, top right; 14 min, bottom left; 17 min, bottom right; 16 min.*

If the deformation is assumed to occur in the fracture at 2 m depth in the borehole; just inside of the packer depth, the distance from the wall is 1.3 m. The normal stress at that distance, evaluated according to the Kirsch equations and Examine2D, can be seen in Table 4.3. The fracture seen at 2 m depth is probably oriented about 30 – 50°, but the calculated normal stresses for these directions does not match the 0.3-0.5 MPa that deformed the rock, see Figure 4.5.

*Table 4.3: The normal stress situation 1.3 m from the wall in the Hallandsås tunnel.*

|  | Kirsch Equations | Examine2D |
|---|---|---|
| Orientation | $\sigma_n$ (MPa) | $\sigma_n$ (MPa) |
| 30° | 2.2 | 2.8 |
| 50° | 3.2 | 3.6 |

Fracture stiffness was evaluated for KBH2 and KBH3 in the service tunnel, see Table 4.4. For KBH3 this was conducted as a full hole test of the 5 m long borehole, for KBH2 the presented stiffness originates from the testing during drilling when the borehole was 6 m deep.

Table 4.4: Calculated fracture normal stiffness, GPa/m, for service tunnel under Gothenburg. Stiffness based on hydraulic aperture, $k_n^{hyd}$ is calculated according to Eq. 2.9. Stiffness based on an empirical relation between transmissivity and storativity, $k_n^S$, is calculated according to Eq. 2.13.

| Borehole | Test | Date | $k_n^{hyd}$ | $k_n^S$ |
|----------|------|------|-------------|---------|
| **KBH2** | WPT | 09-11-13 | 45 | 121 |
| **KBH3** | WPT | 10-03-03 | 51 | 135 |

# 5    Discussion and conclusions

Zangerl et al. (2008) has compared the results of 115 in situ and laboratory normal closure experiments performed on granitic rock. The result was a substantial scatter even for well-defined laboratory tests. The authors point out that the stiffness depends on some factors that interact in extremely complex ways. Such factors are for example fracture surface geometry, asperity deformability, fracture interlocking and testing conditions.

Barton (2004ab) points out benefits of high pressure pre-grouting. But for a post grouting scenario, a high pressure may cause stability problems and ineffective grouting performance. Such pressures might create new flow paths. A way to eliminate the risk for such deformations is to set the pressure sufficiently low. Fransson et al. (2010) suggest that a low fracture stiffness can be used to indicate low effective stress and to evaluate a favourable grout pressure.

The objective of this thesis was to measure fracture deformation and evaluate it by means of comparing the measured deformation with estimated fracture stiffness and rock stress. The deformation measurements were successful in the Hallandsås tunnel. No measurements were performed in the service tunnel due to both a high rock stress and a low connectivity between the two tested boreholes.

The measurement method is deemed robust and accurate. The sensors correlate well, and the anchor could be firmly attached, even with the fractured rock in Hallandsås. The digital sensor was accurate, and correlated well with the analog logging, for the cases where the analog sampling rate was sufficient. Data from these measurements and flow data from the water pressure tests and grouting were used to evaluate fracture stiffness.

The fracture stiffness $k_n^{meas}$ and $k_n^{hyd}$ presented in Table 4.2 and Table 4.4 are evaluated as a difference between start and end of evaluation interval. $k_n^S$ is evaluated with the transmissivity (Eq. 2.8) value from the start of the evaluation interval. $k_n^{meas}$ depend on the measured deformation and $k_n^{hyd}$ and $k_n^S$ both depend on transmissivity in two different ways. The three sets of stiffness estimated for both tunnels are plotted in Figure 5.1 and Figure 5.2. More measurements are required in the service tunnel for a more detailed description of the stiffness variation.

Fransson (2009) has compiled stiffness against hydraulic aperture for measurements performed in granitic rock in various locations. The stiffness values of our measurements show some scatter but match the data set fairly well, see Figure 5.1.
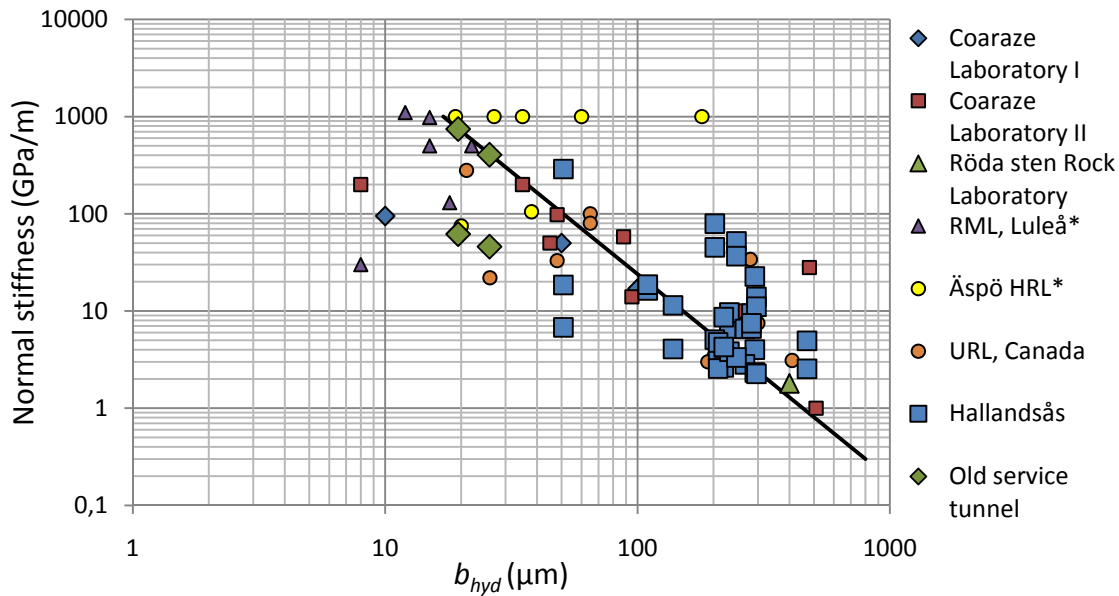
*Figure 5.1: Compilation of stiffness data, in a logarithmic plot, with our measurements included. Modified from Fransson (2009).*
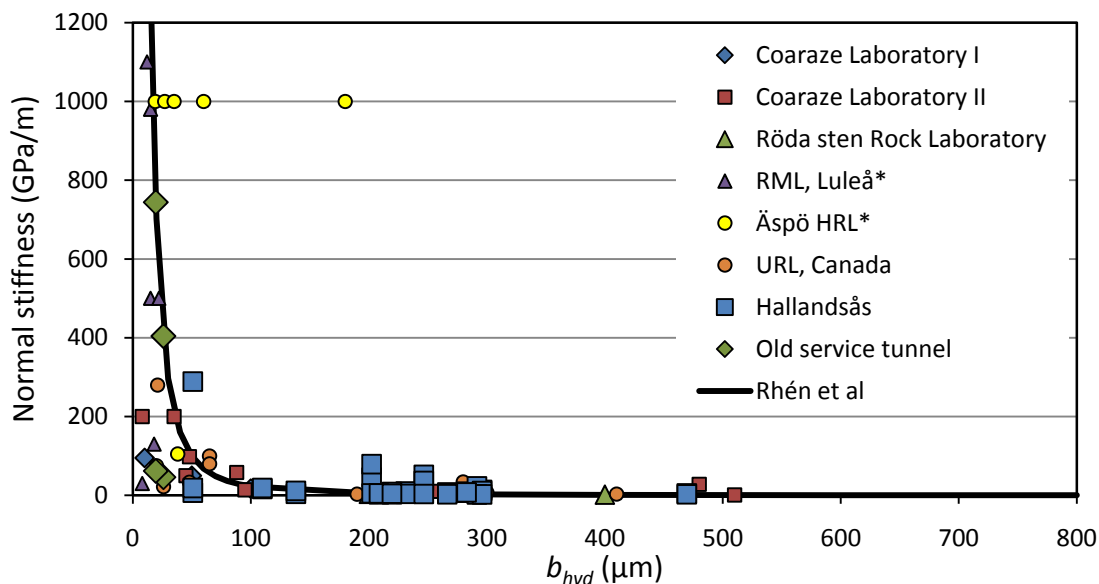


*Figure 5.2: Compilation of stiffness data with our measurements included, modified from Fransson (2009).*

The stiffness parameters $k_n^S$ and $k_n^{hyd}$ are subject to errors, as they are evaluated from water pressure tests where the transmissivity and hydraulic aperture most likely are overestimated due to a substantial leakage during these tests; too large $b_{hyd}$-values, and too low stiffness in Figure 5.1. The grouting sessions were more controlled, but the gelled silica sol from the first grouting test (BH9) may disturb the results of the second (BH28) and third (BH7) grouting test. Data points are added at a $b_{hyd}$ corresponding to the initial part of the evaluated stiffness interval i.e. our data could be plotted at somewhat larger $b_{hyd}$-values, however, this effect is smaller than the leakage. The stiffness estimates are based on the assumption that one third of the grouting overpressure describes the pressure situation along the deforming fracture. The assumption of a linearly declining pressure from the borehole to the grout spread front

(see Figure 2.10) may be a source of errors. The use of an average pressure gives an accurate assessment if the block size is larger than the distance between the injected and the measured borehole.

The pressure-volume-time data achieved from the grouting allowed an analysis of the flow dimensionality. The deformation seems to appear when a radial two dimensional flow becomes a three dimensional flow. This is caused by a pressure larger than the normal stress (fracture normal stiffness) and the result is an increase of the physical aperture, which means that the flow during the deformation is three dimensional, see Figure 5.3 and Fransson et al. (2010).

The reasoning above is under the assumption that the deformation is only normal deformations. The effect of shear stresses is likely to cause a shear slip along the deforming fracture, as described in Figure 2.7. Shear deformations might have been the permanent component of the measured deformations and the resilient deformations might have been a normal deformation.

The measured deformation of a fracture subject to normal deformation is an overestimation if the fracture is not perpendicular to the measurement borehole (see Figure 5.4). The measured deformations most likely overestimate the real normal deformation. A shearing of the fracture may increase this overestimation, since there are more movements in the direction that cannot be measured. If multiple fractures are present in the measurement interval, the measured value will be the sum of all deformations. The conceptual model shall be valid for this case also.

The rock stress calculations conducted with Kirsch equations (Eq. 2.4- Eq. 2.6) and Examine2D indicated a higher stress rate for the service tunnel than for Hallandsås. This was also indicated by the stiffness estimates. However the data set from the service tunnel is too small for reliable conclusions. The high fracture intensity in Hallandsås may facilitate stress redistributions, which allows deformations at lower stress levels than the ones estimated. As seen in Figure 4.5 most of the deformation occurs at a total injection pressure of 1.0 – 1.4 MPa, which result in an average pressure of 0.3-0.5 MPa in the injected fractures. Both the average and the maximum injection pressure is smaller than the calculated rock stress.
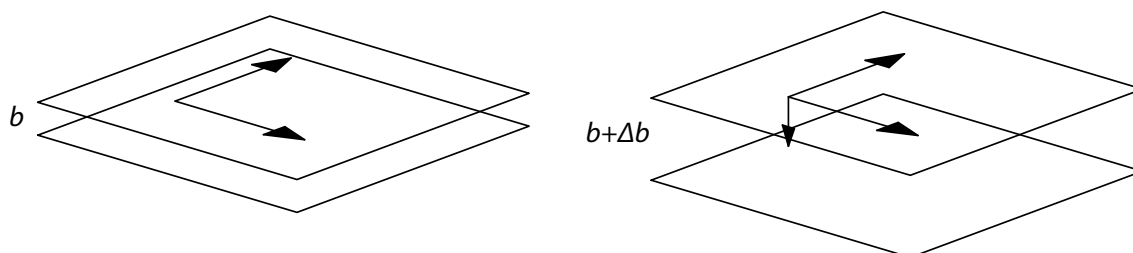


*Figure 5.3: Left: Radial flow; 2D flow. Right: A third flow dimension is introduced as the fracture surfaces are separated; 3D flow.*

Global stresses modelled under the assumption that the rock mass is homogenous and linearly elastic fails to model local variations in geometry, rock mechanical properties and fractures. These are features that might be needed to describe the stresses upon a fracture plane in a satisfactory way. More advanced modelling might be able to deal with these weaknesses, but that is beyond the scope of this thesis.

The mapped strikes and dips of fractures in the drill cores from the old service tunnel could substantially deviate from the true values if the insufficient core orientation markings are not in the bottom of the core, as intended. If this coincides with the roughness of the mapping method, a correct value could differ even more from the ones presented in this thesis. Even though core drilling could aid the grouting design, it is not deemed an efficient way of modelling fracture systems in order to find fractures that might deform. However, the suggestion is that an approach with more advanced stress modelling and stress measurements, coupled with well oriented drill cores and reliable mapping of fractures in the tunnel circumference shall be tested.

Measurements could have been performed in the old service tunnel in order to verify the statement that deformations were unlikely. But the project was delayed, so the grouting front did not advance to the cored boreholes within the spring when the work was carried out.
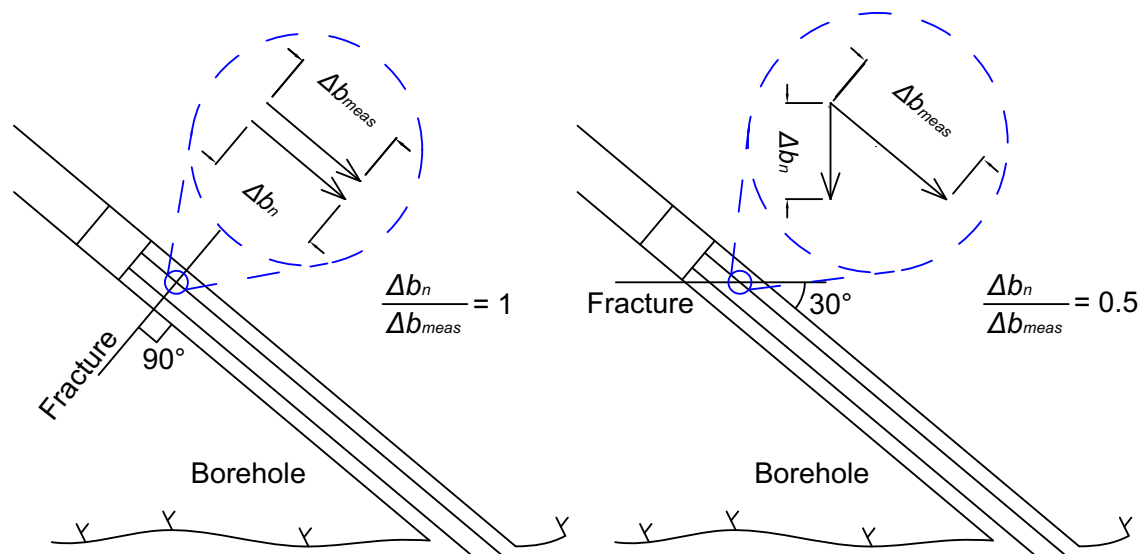


*Figure 5.4: Left: Deformation measurement across a fracture perpendicular to the borehole results in a correct value. Right: Measurements across fractures of other directions will cause an overestimation of the deformation.*

## 5.1   Conclusions

- The test setup presented in this thesis can effectively measure deformations across at least five meters of borehole.

- Fracture stiffness evaluated from deformation measurements and hydraulic testing correlates fairly well with stiffness data found in literature.

- The global rock stress approach gives a first estimate of the fracture stress situation.

- The grout flow domain when deformation occurred was generally 3D.

- The general feature is that the fractures have larger aperture and have lower stiffness in Hallandsås than in the service tunnel.

## 5.2   Further work

It is suggested that the qualitative approach with geometric modelling in order to find specific fractures prone to deformation shall be further tested. This approach can prove useful, if it is possible to determine in advance which fracture that might deform. The deformation modes and the interaction between them should be further coupled to the measured deformations in order to better describe the deformations that occur.

# References

Almén, K-E., Andersson, J-E., Carlsson, L., Hansson, K. & Larsson, N-Å., 1986: *Hydraulic testing in crystalline rock. A comperative study of single hole test methods*. SKB, Technical report 86-27. Stockholm

Amadei, B., & Stephansson, O. (1997): *Rock stress and its measurement.* Chapman & Hall, London 1997.

Barton, N. (2004a): The theory behind high pressure grouting- part 1. *Tunnels and Tunnelling International*. September 2004, pp. 28-30.

Barton, N. (2004b): The theory behind high pressure grouting- part 2. *Tunnels and Tunnelling International*. October 2004, pp. 33-35.

Butron, C., Gustafson, G., Fransson, Å., Funehag, J. (2010): Drip sealing of tunnels in hard rock: a new concept for the design and evaluation of permeation grouting. *Tunnelling and Underground Space Technology*. Vol 25, 2010 pp. 114-121.

Cornet, F.H., Li, L., Hulin, J.-P., Ippolito, I., Kurowski, P. (2003): The hydromechanical behavior of a fracture: an in situ experimental case study. *International journal of rock mechanics & mining sciences*. Vol. 40, 2003 pp. 1257-1270.

Doe, T., Geier, J., 1990. *Interpretations of fracture system geometry using well test data*. SKB Stripa Project TR 91-03, Svensk Kärnbränslehantering AB.

Eriksson, M., Stille, H. (2005): *Cementinjektering i hårt berg*. SveBeFo report K22. Stockholm 2005.

Fransson, Å. (1999): *Grouting predictions based on hydraulic tests of short duration: analytical, numerical and experimental approaches*. Licentiate Thesis. Department of Geology, Chalmers University of Technology, Göteborg, Sweden, 1999.

Fransson, Å. (2001): *Characterisation of fractured rock for grouting using hydrological methods*. Ph.D. Thesis. Department of Geology, Chalmers University of Technology, Gothenburg, Sweden, 2001.

Fransson, Å. (2009): *Literature survey: Relations between stress change, deformation and transmissivity for fractures and deformation zones based on in situ investigations*. SKB R-09-13. 2009.

Fransson, Å., Tsang, C.-F., Rutqvist, J., Gustafsson, G., (2010): Estimation of deformation and stiffness of fractures close to tunnels using data from single-hole hydraulic testing and grouting. *International Journal of Rock Mechanics and Mining Sciences*. 2010.

Funehag, J., Gustafson, G. (2004): *Injekteringsförsök med Cembinder® U22 i Hallandsås*. Department of GeoEngineering, Chalmers University of Technology, Gothenburg, Sweden, 2004:1.

Funehag, J. (2007): *Grouting of fractured rock with silica sol – grouting design based on penetration length.* Ph.D. Thesis. Department of Civil and Environmental Engineering, Chalmers University of Technology, Gothenburg, Sweden, 2007.

Gothäll R. Stille H (2009): Fracture dilation during grouting. *Tunneling and underground Space Technology.* Vol. 24, 2009 pp. 126-135.

Gothäll R. (2009): *Behaviour of Rock Fractures under Grout Pressure Loadings.* Ph.D. Thesis. Division of soil and Rock Mechanics, Royal Institute of Technology, Stockholm, Sweden, 2009.

Gustafson, G. (2009): *Hydrogeologi för bergbyggare.* Forskningsrådet Formas, Stockholm 2009.

Gustafson, G., Stille, H. 1996: Prediction of Groutability from Grout Properties and Hydrogeological Data. *Tunneling and Underground Space Technology.* Vol. 11 No. 3, 1996, pp 325-332

Gustafson, G., Stille, H. 2005: Stop Criteria for Cement Grouting. *Felsbau* vol 23 No. 3

Hakami, E. (1995): *Aperture distribution of rock fractures.* Ph.D. Thesis. Department of Civil and Environmental Engineering, Royal Institute of Technology, Stockholm, Sweden, 1995.

He, J. (1992): *Lined underground openings – Rock mechanical effects of high internal pressure.* Ph.D. Thesis. Chalmers University of Technology, Gothenburg 1992.

Hernqvist, L. (2009): *Characterization of the fracture system in hard rock for tunnel grouting.* Licentiate Thesis. Department of Civil and Environmental Engineering, Chalmers University of Technology, Gothenburg, Sweden, 2009.

Hoek, E. (2006): *Practical Rock Engineering -In situ and induced stresses* Available: http://www.rocscience.com/hoek/PracticalRockEngineering.asp

Jansson, T. (1998): *Calculation models for estimation of grout take in hard jointed rock.* Ph.D. Thesis. Department of Civil and Environmental Engineering, Royal Institute of Technology, Stockholm, Sweden, 1998.

Kirsch, E.G. (1898). Die Theorie der Elastizität und die Bedürfnisse der Festigkeitslehre. *Zeitschrift des Vereines deutscher Ingenieure*, Vol. 42, 1898, pp. 797–807.

Lindblom, U. (2001): *Bergbyggnadsteknik.* Kompendium för fortsättnings-kursen i teknisk geologi vid Chalmers tekniska högskola, Göteborg, 2001.

Rhén, I., Forsmark, T., Hartley, L., Jackson, P., Roberts, D., Swan, D., Gylling, B., (2008): *Hydrogeological conceptualisation and parameterisation, Site descriptive modelling SDM–Site Laxemar*, SKB R-08-78. 2008.

Riise, P. (2007): *Teletunnlar i Göteborg – Lite historik kring utbyggnaden.* Internal report WSP Printed 2007-02-08.

Rutqvist, J. (1995): *Coupled stress-flow properties of rock joints from hydraulic field testing*. Ph.D. Thesis. Department of Civil and Environmental Engineering, Royal Institute of Technology, Stockholm, Sweden, 1995.

Stephansson, O., Ljunggren, C., and Jing, L. (1991): Stress measurements and tectonic implications for Fennoscandia. *Tectonophysics* Vol. 189, No.1-4, 1991, pp. 317-322.

SGU. " *Bergkvalitetskarta över Göteborgs kommun*", 1:50 000. Serie *Ba 59 Bk*. LiberKartor, Stockholm.

Snow, D.T. (1968) Rock fracture spacings, openings and porosities. *Proc. Amer. Soc. Civil Engineers*, Vol.94, pp. 73–79.

Vermilye, J., Scholz, C. (1995). Relation between vein length and aperture. *Journal of Structural Geology*. Vol. 17, No. 3, 1995, pp. 423-434.

Witherspoon, P A, Wang, J S Y, Iwai, K, Gale, J E, (1980). Validity of the cubic law for fluid flow in a deformable fracture. *Water Resources Research*, Vol. 16, No. 6, 1980, pp. 1016-1024.

Zangerl, C., Evans, K.F., Eberhardt, E., Loew, S., (2008). Normal stiffness of fractures in granitic rock: A compilation of laboratory and in-situ experiments. *International Journal of Rock Mechanics & Mining Sciences*. Vol. 45, 2008, pp. 1500-1507.

# List of Appendices

# Appendix I

## Test programme old service tunnel

Below, the sequence of testing performed in the old service tunnel under Gothenburg is presented.

1. Drilling KBH2 and KBH3 with 3 m sections, diameter 63 mm.

2. NIT and pressure measurement.

3. WPT with Geosigma test set up.

4. 1-3 was repeated until required depth was achieved. Total length for KBH1 is 33 m and 20 m for KBH2.

5. PBT was tested at 9 m depth and full hole depth, 20 m respectively 33 m.

6. Determine location of KBH3 based on core mapping from KBH2.

7. NIT was performed in KBH2 before drilling of KBH3 was initiated.

8. Drilling KBH3 with 3 m sections, diameter 63 mm.

9. NIT and pressure measurement.

10. WPT with hand pump.

11. 8-10 was repeated until required depth was achieved. Total length for KBH3 is 4,7 m.

12. Reaming to 76mm

13. PBT was performed in KBH2 wh.ile KBH3 was closed.

14. NIT was performed in KBH3 while KBH2 was closed.

15. PBT was performed in KBH3 while KBH2 was closed.

16. Pressure connection tests. WPT was performed in KBH2 and pressure was logged in KBH3.

17. Pressure connection tests. WPT was performed in KBH3 and pressure was logged in KBH2.

# Appendix II

# Test programme Hallandsås

In this appendix the test programme for testing in Hallandsås is presented.

| Activity | Purpose | Equipment Chalmers | Equipment Skanska/BV | Estimated time |
|---|---|---|---|---|
| **INFLOW TEST (NIT)**<br><br>Measure the natural inflow in all holes that can be reached from the floor (5)<br>&bull; Place packer at 0.5-1 m depth<br>&bull; Measure full-hole flow, $Q_{tot}$, for 1 min<br>&bull; If the hole flows more than 5 l/min, place packer at 3 m depth<br>&bull; Measure superficial flow, $Q_{out}$<br>&bull; Measure inner flow, $Q_{inner}$<br>&bull; Use appropriate container (40 ml, 100 ml, 1 l, 2 l, 10 l)<br><br>Chose hole for further testing with the following criterions:<br>1. Wall-hole with $Q_{tot} \geq 5$ l/min, and $Q_{out} \geq 2$ l/min<br>2. Floor-hole with $Q_{tot} \geq 5$ l/min, and $Q_{out} \geq 2$ l/min<br>3. Wall-hole with $Q_{tot} \geq 5$ l/min<br>4. Floor-hole with $Q_{tot} \geq 5$ l/min<br>5. If none of 1-4 is fulfilled, use the hole with the largest inflow | To determine which hole that shall be evaluated, according to the flow criterions. | &bull; Stopwatch<br>&bull; Liquid container (40 ml, 100 ml, 1 l, 2 l, 10 l)<br>&bull; Funnel<br>&bull; Protocol | &bull; Packer, length 4 m, $\phi$ 63 mm | 30 min<br><br>**Start Tuesday 16/3** |

*Continued on next page.*

| Activity | Purpose | Equipment Chalmers | Equipment Skanska/BV | Estimated time |
|---|---|---|---|---|
| **DRILLING**<br><br>The chosen hole is enlarged to ▯ 75 mm (henceforth called BHX)<br><br>The adjacent hole in the secondary or tertiary fan is drilled to 6 m depth, $\phi$ 75 mm (henceforth called BHY) | | | Drill rig | |
| **TEST-ASSEMBLE DEFORMATION EQUIPMENT**<br><br>Assemble and disassemble deformation rod | Is it possible to perform the testing in poor rock? Yes/No<br><br>If No: Stop testing, go home, cry<br><br>If Yes: Continue, smile | • Deformation rod | | 10 min<br><br>**16/3** |
| **PRESSURE BUILD UP TEST (PBT) NIT, CHALMERS FLOW LOGGER (CFL)**<br>**Place packer at 0,5-1 m depth in BHX and BHY**<br>Close BHY<br>  1. NIT: Measure natural inflow in BHX<br>     • Measure full hole flow, $Q_{tot,}$ for 1 min<br>  2. CFL: Measure natural inflow in BHX , start at bottom of hole<br>     • Measure inflow in BHX in 0,5 m sections, BHY closed<br>  3. NIT: Measure natural inflow in BHX after CFL-test | To determine full hole and inner pressure and flow for both boreholes in order to evaluate transmissivity and hydraulic aperture.<br><br><br>Determine the depth of large inflows | • Packer, length 4 m, $\phi$ 75 mm<br>• Packer, length 2 m, $\phi$ 75 mm<br>• CFL-equipment<br>• Stopwatch<br>• Liquid container (40 ml, 100 ml, 1 l, 2 l, 10 l)<br>• Funnel<br>• Logger-equipment (pressure) | • Electricity | 120 min<br><br>**Shall be finished 16/3** |

- Measure full hole flow, $Q_{tot,}$ for 1 min
4. PBT: Measure pressure for 10 min in BHX
    - Packer position 0,5-1 m
    - Close packer
    - Start logger (interval 2 s)
    - Measure for 10 min

**Place packer at 3 m depth**

Redo paragraph 1 and 4 for this depth

Redo entire sequence for BHY (with reverse order of the packer depths) with BHX closed.

Close both boreholes

Calculate transmissivity and hydraulic aperture

Calculate flow time between BHX and BHY

| | | - Computer <br> - Protocol | | |
|---|---|---|---|---|
| **PRESSURE CONNECTION TEST** <br><br> WPT in BHX <br> - Pressure logging continues since previous test <br> - Connect grouting pump to BHX <br> - Start test, $\Delta P$= 5 bar, overpressure for 15 min <br> - Note if flow changes from grouting pump <br> - Note if pressure in BHY changes | To see pressure changes in BHY = Is there a connection? <br> **Yes/No** | - 2 packers, length 2 m, $\phi$ 75 mm <br> - Logger-equipment (pressure) <br> - Stopwatch <br> - Protocol | - Pump for WPT <br> - Hiltihammer <br> - Expander bolts | 30 min <br><br> **17/3** |
| **No** <br> - Increase pressure of th WPT with 2 bar at a time, 2 minutes each until a connection can be seen. Maximum 20 bar <br> - Note if flow is changed from grouting pump <br> - Note if pressure in BHY changes | To see pressure changes in BHY = Is there a connection? <br> **Yes** | | - Grouting pump with logac | 30 min <br><br> **17/3** |

| Activity | Purpose | Equipment Chalmers | Equipment Skanska/BV | Estimated time |
|---|---|---|---|---|
| **DEFORMATION MEASUREMENT WHEN PERFORMING WPT**<br><br>**Yes**<br><br>Perform deformation measurements during WPT<br>  &bull;  Remove packer from BHY<br>  &bull;  Assemble deformation rod at depth 4,5 m<br>  &bull;  Fasten wall reference plane<br>  &bull;  Assemble deformation loggers at reference plane<br>  &bull;  Note the appearance of the wall<br>  &bull;  Start deformation logging, wait 10 minutes<br>  &bull;  Pump BHX with the smallest pressure that gave a connection<br>  &bull;  Any response on anlog deformation logger? Yes/No<br>  &bull;  Note the appearance of the wall<br>  &bull;  If No: increase pressure with 2 bar at a time, 5 minutes each until deformation can be seen<br>  &bull;  If yes: smile, reduce pressure and note if deformation returns<br>  &bull;  Increase pressure with 2 bar and note deformation, repeat 3-4 times<br>      &bull;  Is the deformation linear?<br>  &bull;  Let deformation logger continue, stop WPT | Stimulate a deformation.<br><br><br>Is our theory about deformation correct?<br><br><br>Is it possible to log with the accurancy needed?<br><br><br><br>Find the pressure that causes a deformation<br><br><br>Is the deformation elastic and/or linear? | &bull; Packer, length 2 m, ⌀ 75 mm<br>&bull; Deformation rod<br>&bull; Wall reference plane<br>&bull; Deformation loggers<br>&bull; Stopwatch<br>&bull; Protocol | &bull; Grouting pump with logac<br>&bull; Hiltibore<br>&bull; Expanderbolts | 90 min<br><br>**17/3**<br><br><br><br><br><br><br><br><br><br><br><br><br><br><br><br><br>**18/3** |

*Continued on next page.*

| DEFORMATION MEASUREMENT WHEN GROUTING | Measure deformation | | | Grouting |
|---|---|---|---|---|
| **DEFORMATION MEASUREMENT WHEN GROUTING**<br><br>Deformation logging continues when the crouting starts<br>&bull; BHY untoched since last test, logging continues<br>&bull; Note time for grouting of different boreholes, when the holes are filled | Measure deformation<br><br>Correlate deformation logging results with grouting of different holes in fan | | | Grouting |

Effective test time:

 Max 3 working days

## Summary

- NIT
    - o Hole chosen according to criteria
- DRILLING
    - o Drill a hole in secondary or tertiary fan
- CHOSEN HOLES ENLARGED TO 75 MM
- PBT, NIT AND CFL 0,5 m SECTIONS
    - o Full and half depth in both holes
    - o For both holes; find position of large inflows with CFL
- PRESSURE CONNECTION TEST
    - o WPT in one hole, pressure logging in the other, to find a connection
- DEFORMATION MEASSUREMENT WHEN PERFORMING WPT
    - o Pressure intervals of 2 bar maximum to 20 bar
    - o At deformation; reduce pressure and measure deformation
    - o Continue WPT with a higher pressure
    - o Measure deformation, reduce pressure start over with higher pressure
    - o When results achieved:
- DEFORMATION MEASUREMENT WHEN GROUTING
    - o Log deformation when grouting

# Appendix III

## Rock stress calculations

The rock stresses around the studied tunnels has been calculated in two ways, which are described in this appendix. The software Examine2D, is a freeware, downloadable from http://www.rocscience.com/products/Examine2D.asp. The other way of assessing rock stresses is by the Kirsch (1898) equations, presented in the report.

First, Examine2D and Kirsch calculations are presented for the Hallandsås tunnel, thereafter the same for the old service tunnel. The calculated stresses upon fractures of different orientations are shown for both cases. Graphs of comparison between the two estimation methods for both tunnels conclude this appendix.

The normal and shear stresses upon fracture planes in the two tunnels are calculated according to the following equations:

$$\sigma_n = \sigma_\parallel \cdot \sin(\kappa) + \sigma_\perp \cdot \cos(\kappa)$$

$$\tau = \sigma_\parallel \cdot \cos(\kappa) - \sigma_\perp \cdot \sin(\kappa)$$

Where $\sigma_\parallel$ is parallel to the tunnel, $\sigma_\perp$ is perpendicular to the tunnel, and $\kappa$ is the angle between tunnel wall and fracture strike.

The Kirsch calculations have been made with the following equation:

$$\sigma_r = \frac{1}{2}\sigma_z\left((1+k)\left(1 - \frac{a^2}{r^2}\right) + (1-k)\left(1 - 4\frac{a^2}{r^2} + 3\frac{a^4}{r^4}\right) \cdot \cos 2\theta\right)$$

Where $\sigma_r$ is the radial stress, $k$ is the ratio $\sigma_h/\sigma_v$, $a$ is the tunnel radius, $r$ is the radius to the calculated point and $\theta$ is the angle between the vertical centreline and the calculated point.

## Examine2D Hallandsås

The input data used is the stress relation that $\sigma_v$ is equal to the weight of the overburden (75 m, 0.0268 MN/m$^3$), and $\sigma_H$ is parallel to the tunnel, and equal to $2 \cdot \sigma_v$. The minor horizontal stress, $\sigma_h$, is perpendicular to the tunnel, and equal to $\sigma_v$. The output is a graphical presentation, see Figure A.III-1, and a data table, *Table A.III-1*.
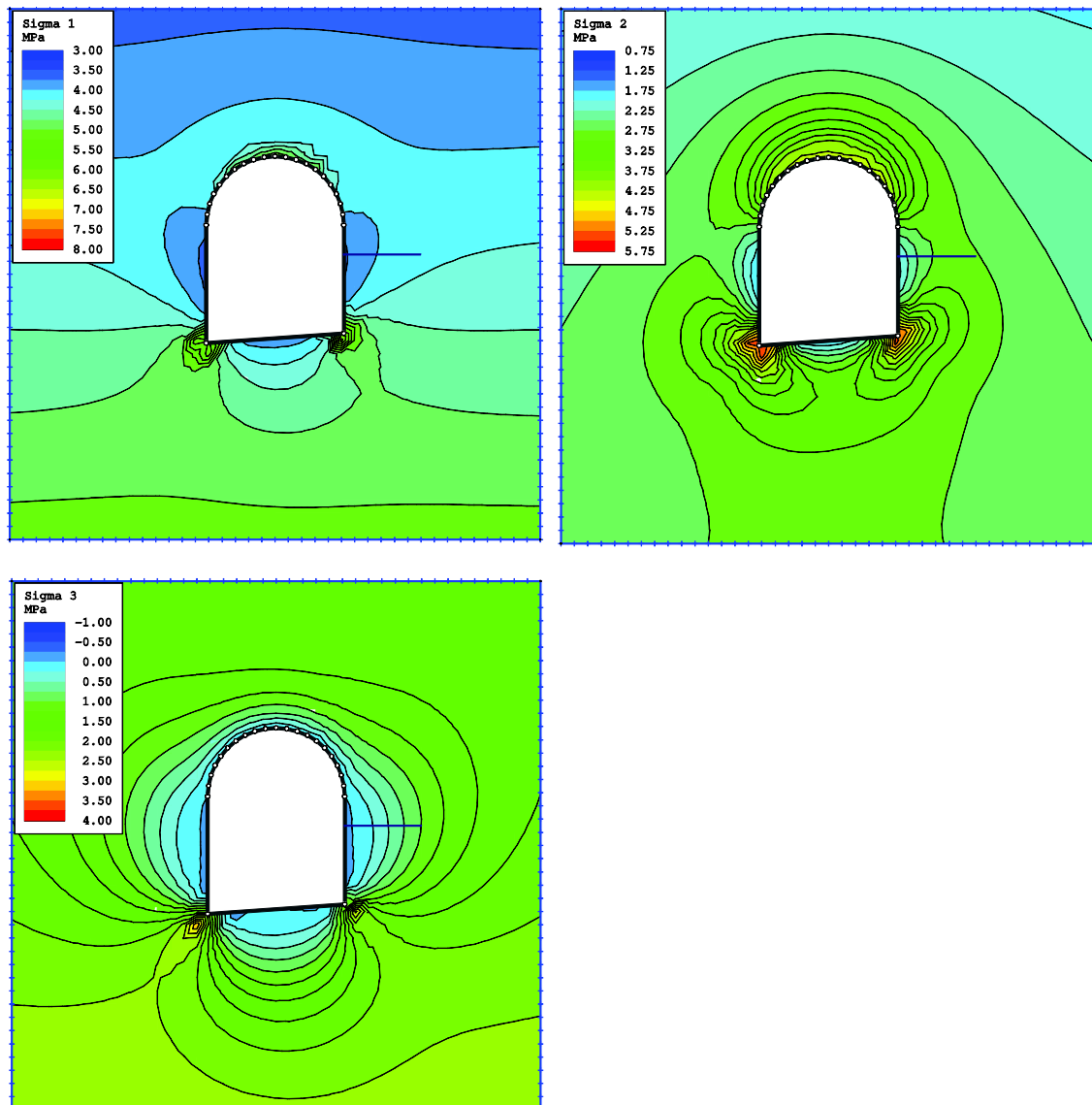


*Figure A.III-1: The three principal stresses in Hallandsås modelled in Examine2D.*

Table A.III-1: *Output data table from Examine2D, and calculated normal and shear stresses upon fractures at 30° and 50° angle to the tunnel wall. The x-length scale is along the measurement borehole, which is indicated by a line in the wall in Figure A.III-1.*

| $x$ (m) | $\sigma_H$ (MPa) | $\sigma_v$ (MPa) | $\sigma_h$ (MPa) | $\sigma_N$ 30° (MPa) | $\sigma_N$ 50° (MPa) | $\tau$ 30° (MPa) | $\tau$ 50° (MPa) |
|---|---|---|---|---|---|---|---|
| **0.2** | 3.75 | 2.03 | 0.01 | 1.88 | 2.88 | 3.24 | 2.40 |
| **0.4** | 3.79 | 2.19 | 0.03 | 1.92 | 2.92 | 3.27 | 2.42 |
| **0.6** | 3.83 | 2.33 | 0.05 | 1.96 | 2.97 | 3.29 | 2.42 |
| **0.8** | 3.87 | 2.45 | 0.09 | 2.01 | 3.02 | 3.31 | 2.42 |
| **1** | 3.90 | 2.55 | 0.13 | 2.06 | 3.07 | 3.32 | 2.41 |
| **1.2** | 3.94 | 2.63 | 0.18 | 2.12 | 3.13 | 3.32 | 2.39 |
| **1.4** | 3.97 | 2.69 | 0.23 | 2.19 | 3.19 | 3.32 | 2.37 |
| **1.6** | 3.99 | 2.74 | 0.29 | 2.25 | 3.25 | 3.31 | 2.34 |
| **1.8** | 4.02 | 2.77 | 0.36 | 2.32 | 3.31 | 3.30 | 2.31 |
| **2** | 4.04 | 2.80 | 0.42 | 2.39 | 3.37 | 3.29 | 2.27 |
| **2.2** | 4.06 | 2.82 | 0.49 | 2.45 | 3.42 | 3.27 | 2.24 |
| **2.4** | 4.08 | 2.83 | 0.55 | 2.52 | 3.48 | 3.26 | 2.20 |
| **2.6** | 4.10 | 2.83 | 0.62 | 2.58 | 3.54 | 3.24 | 2.16 |
| **2.8** | 4.11 | 2.83 | 0.68 | 2.65 | 3.59 | 3.22 | 2.12 |
| **3** | 4.13 | 2.82 | 0.75 | 2.71 | 3.64 | 3.20 | 2.08 |
| **3.2** | 4.14 | 2.81 | 0.81 | 2.77 | 3.69 | 3.18 | 2.04 |
| **3.4** | 4.15 | 2.80 | 0.86 | 2.83 | 3.74 | 3.16 | 2.01 |
| **3.6** | 4.16 | 2.79 | 0.92 | 2.88 | 3.78 | 3.15 | 1.97 |
| **3.8** | 4.17 | 2.78 | 0.98 | 2.93 | 3.82 | 3.13 | 1.94 |
| **4** | 4.18 | 2.76 | 1.03 | 2.98 | 3.86 | 3.11 | 1.90 |

## Kirsch Hallandsås

The input data for the Kirsch calculation was as presented in *Table A.III-2* and the results as presented in Table A.III-3.

*Table A.III-2: The input data for Kirsch calculation for Hallandsås tunnel.*

| | | |
|---|---|---|
| $z$ | 75 | m |
| $\sigma_z$ | 1.97 | MPa |
| $\sigma_x$ | 1.97 | MPa |
| $\sigma_y$ | 3.94 | MPa |
| $k$ | 1 | - |
| $a$ | 3.7 | m |
| $\theta$ | 1.57 | rad |

*Table A.III-3: The calculated radial stress, and the corresponding normal and shear stresses for fractures at 30° and 50° angle to the tunnel wall.*

| $x$ (m) | $\sigma_r$ (MPa) | $\sigma_N$ 30° (MPa) | $\sigma_N$ 50° (MPa) | $\tau$ 30° (MPa) | $\tau$ 50° (MPa) |
|---|---|---|---|---|---|
| 0.2 | 0.10 | 2.06 | 3.09 | 3.36 | 2.46 |
| 0.4 | 0.28 | 2.22 | 3.20 | 3.27 | 2.32 |
| 0.6 | 0.44 | 2.35 | 3.30 | 3.19 | 2.20 |
| 0.8 | 0.58 | 2.47 | 3.39 | 3.13 | 2.09 |
| 1.0 | 0.70 | 2.57 | 3.47 | 3.07 | 2.00 |
| 1.2 | 0.80 | 2.66 | 3.54 | 3.02 | 1.92 |
| 1.4 | 0.89 | 2.74 | 3.59 | 2.97 | 1.85 |
| 1.6 | 0.97 | 2.81 | 3.65 | 2.93 | 1.79 |
| 1.8 | 1.05 | 2.88 | 3.69 | 2.89 | 1.73 |
| 2.0 | 1.11 | 2.93 | 3.74 | 2.86 | 1.68 |
| 2.2 | 1.17 | 2.98 | 3.77 | 2.83 | 1.64 |
| 2.4 | 1.22 | 3.03 | 3.81 | 2.80 | 1.60 |
| 2.6 | 1.27 | 3.07 | 3.84 | 2.78 | 1.56 |
| 2.8 | 1.31 | 3.11 | 3.86 | 2.76 | 1.53 |
| 3.0 | 1.35 | 3.14 | 3.89 | 2.74 | 1.50 |
| 3.2 | 1.39 | 3.17 | 3.91 | 2.72 | 1.47 |
| 3.4 | 1.42 | 3.20 | 3.93 | 2.70 | 1.45 |
| 3.6 | 1.45 | 3.23 | 3.95 | 2.69 | 1.42 |
| 3.8 | 1.48 | 3.25 | 3.97 | 2.68 | 1.40 |
| 4.0 | 1.50 | 3.27 | 3.99 | 2.66 | 1.38 |

## Examine2D Service tunnel

The input data used is the stress relation that $\sigma_v$ is equal to 5 MPa, $\sigma_h$ is parallel to the tunnel, and equal to 7 MPa. The major horizontal stress, $\sigma_H$, is perpendicular to the tunnel, and equal to 10 MPa. These values were chosen as a generalised "mean" of the stress measurements conducted in the Götatunnel, 1 km away. The output is a graphical presentation; see Figure A.III-2, and a data table, *Table A.III-1*.
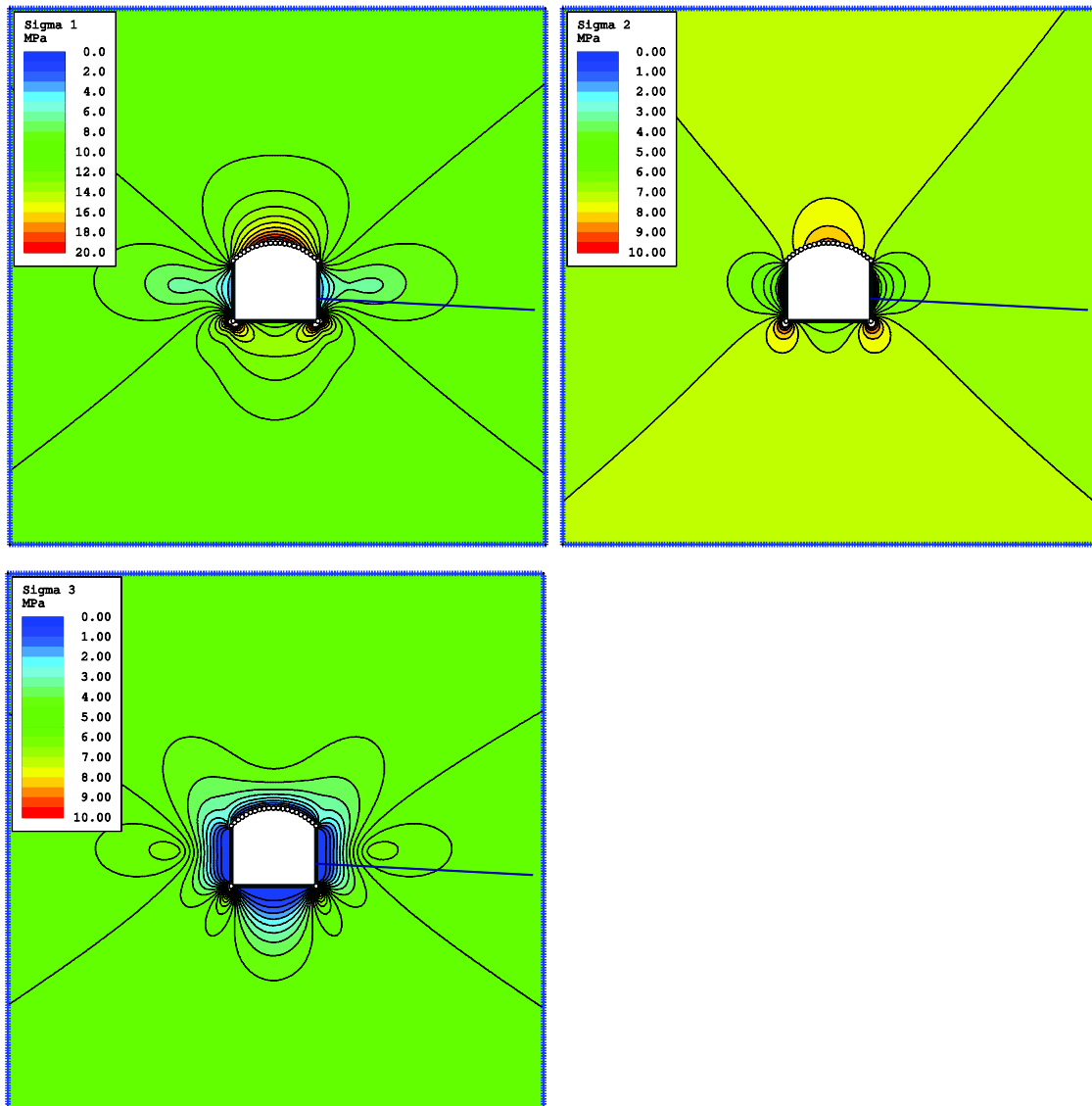


*Figure A.III-2: The three principal stresses in the service tunnel modelled in Examine2D.*

*Table A.III-4: Output data table from Examine2D, and calculated normal and shear stresses upon fractures at 20°, 45° and 80° angle to the tunnel wall. The x-length scale is along the measurement borehole, which is indicated by a line in the wall in Figure A.III-1.*

| x (m) | $\sigma_H$ (MPa) | $\sigma_h$ (MPa) | $\sigma_v$ (MPa) | $\sigma_N$ 20° (MPa) | $\sigma_N$ 45° (MPa) | $\sigma_N$ 80° (MPa) | $\tau$ 20° (MPa) | $\tau$ 45° (MPa) | $\tau$ 80° (MPa) |
|---|---|---|---|---|---|---|---|---|---|
| 0.2 | 4.05 | 3.09 | 0.12 | 4.87 | 5.05 | 3.75 | 4.29 | 5.05 | 4.53 |
| 0.4 | 5.05 | 4.61 | 0.40 | 6.32 | 6.83 | 5.42 | 6.06 | 6.83 | 5.77 |
| 0.6 | 6.36 | 5.07 | 0.90 | 7.71 | 8.08 | 6.09 | 6.94 | 8.08 | 7.15 |
| 0.8 | 7.13 | 5.42 | 1.54 | 8.56 | 8.88 | 6.57 | 7.53 | 8.88 | 7.97 |
| 1.0 | 7.53 | 5.69 | 2.22 | 9.02 | 9.35 | 6.91 | 7.92 | 9.35 | 8.40 |
| 1.2 | 7.69 | 5.90 | 2.90 | 9.24 | 9.61 | 7.14 | 8.17 | 9.61 | 8.60 |
| 1.4 | 7.72 | 6.06 | 3.52 | 9.33 | 9.75 | 7.31 | 8.34 | 9.75 | 8.66 |
| 1.6 | 7.69 | 6.19 | 4.07 | 9.34 | 9.81 | 7.43 | 8.45 | 9.81 | 8.65 |
| 1.8 | 7.63 | 6.29 | 4.55 | 9.32 | 9.84 | 7.52 | 8.52 | 9.84 | 8.61 |
| 2.0 | 7.57 | 6.38 | 4.94 | 9.30 | 9.86 | 7.60 | 8.58 | 9.86 | 8.56 |
| 2.2 | 7.54 | 6.45 | 5.26 | 9.29 | 9.89 | 7.66 | 8.64 | 9.89 | 8.54 |
| 2.4 | 7.53 | 6.51 | 5.49 | 9.30 | 9.93 | 7.72 | 8.69 | 9.93 | 8.55 |
| 2.6 | 7.57 | 6.56 | 5.66 | 9.35 | 9.99 | 7.77 | 8.75 | 9.99 | 8.59 |
| 2.8 | 7.63 | 6.60 | 5.76 | 9.43 | 10.06 | 7.82 | 8.81 | 10.06 | 8.66 |
| 3.0 | 7.72 | 6.63 | 5.82 | 9.53 | 10.15 | 7.88 | 8.88 | 10.15 | 8.76 |
| 3.2 | 7.83 | 6.67 | 5.83 | 9.64 | 10.25 | 7.93 | 8.94 | 10.25 | 8.87 |
| 3.4 | 7.94 | 6.69 | 5.83 | 9.76 | 10.35 | 7.97 | 9.01 | 10.35 | 8.99 |
| 3.6 | 8.06 | 6.72 | 5.81 | 9.87 | 10.45 | 8.02 | 9.07 | 10.45 | 9.10 |
| 3.8 | 8.17 | 6.74 | 5.79 | 9.98 | 10.54 | 8.06 | 9.13 | 10.54 | 9.22 |
| 4.0 | 8.28 | 6.76 | 5.76 | 10.09 | 10.63 | 8.09 | 9.18 | 10.63 | 9.32 |
| 4.5 | 8.51 | 6.80 | 5.68 | 10.32 | 10.82 | 8.17 | 9.30 | 10.82 | 9.56 |
| 5.0 | 8.71 | 6.83 | 5.60 | 10.52 | 10.99 | 8.24 | 9.39 | 10.99 | 9.76 |
| 5.5 | 8.87 | 6.85 | 5.54 | 10.68 | 11.12 | 8.29 | 9.47 | 11.12 | 9.93 |
| 6.0 | 9.01 | 6.87 | 5.48 | 10.81 | 11.23 | 8.33 | 9.54 | 11.23 | 10.06 |
| 6.5 | 9.12 | 6.89 | 5.43 | 10.92 | 11.32 | 8.36 | 9.59 | 11.32 | 10.18 |
| 7.0 | 9.21 | 6.90 | 5.38 | 11.02 | 11.39 | 8.39 | 9.63 | 11.39 | 10.27 |
| 7.5 | 9.29 | 6.91 | 5.35 | 11.10 | 11.46 | 8.42 | 9.67 | 11.46 | 10.35 |
| 8.0 | 9.36 | 6.92 | 5.31 | 11.17 | 11.51 | 8.44 | 9.70 | 11.51 | 10.42 |
| 8.5 | 9.42 | 6.93 | 5.28 | 11.22 | 11.56 | 8.46 | 9.73 | 11.56 | 10.48 |
| 9.0 | 9.47 | 6.93 | 5.26 | 11.27 | 11.60 | 8.47 | 9.76 | 11.60 | 10.53 |
| 9.5 | 9.52 | 6.94 | 5.24 | 11.32 | 11.64 | 8.49 | 9.78 | 11.64 | 10.58 |
| 10.0 | 9.56 | 6.94 | 5.22 | 11.36 | 11.67 | 8.50 | 9.79 | 11.67 | 10.62 |
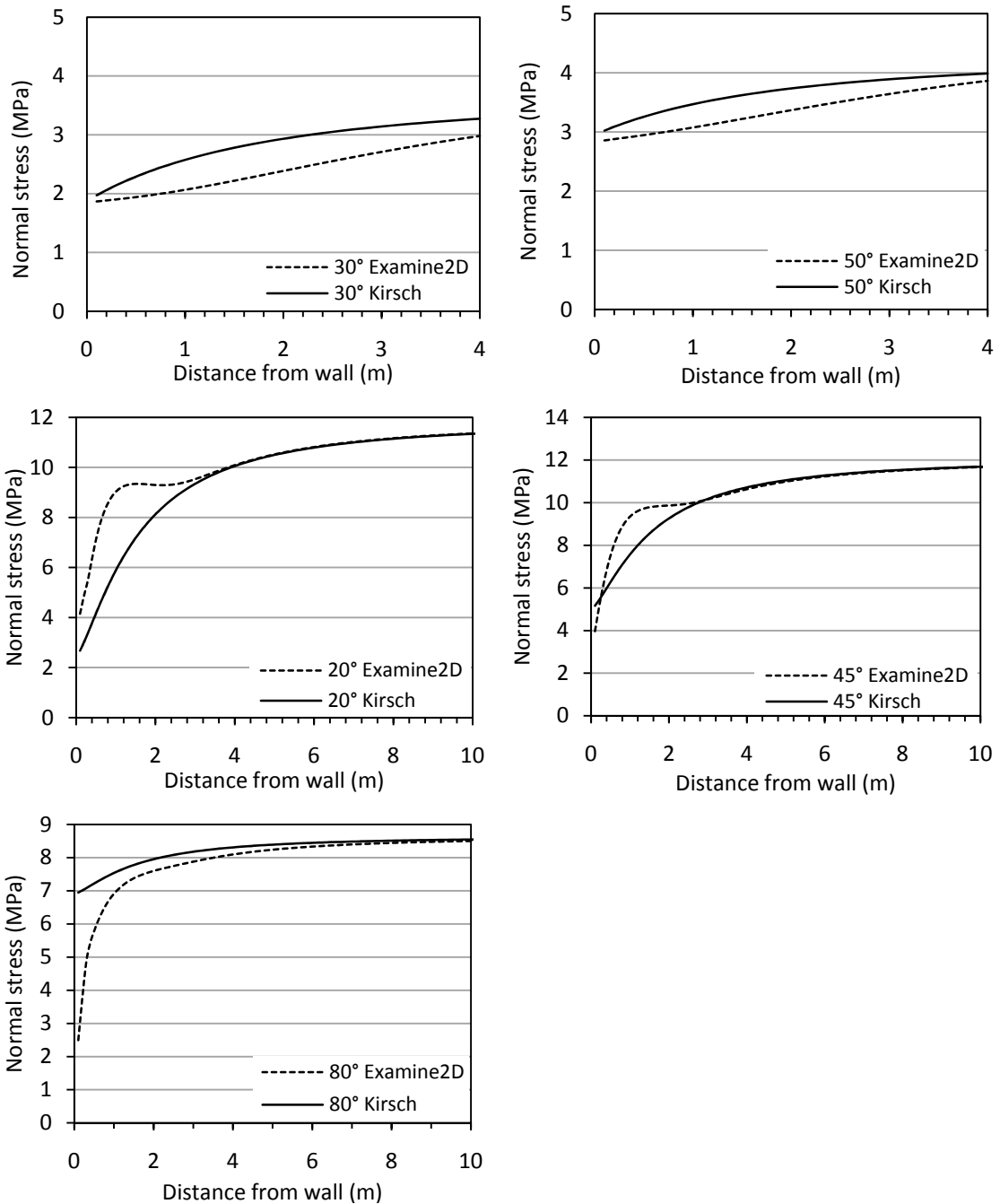
*Figure A.III-3: The normal stress upon fractures at Hallandsås, 30° and 50° to the wall, and service tunnel in Gothenburg, 20°, 45° and 80°. Each graph contain the estimate with Examine2D and the Kirsch equations.*

**CHALMERS**, *Civil and Environmental Engineering*, Master's Thesis 2010:87

# Appendix IV

## Stiffness calculations

### Hallandsås tunnel

First a table of all input and output data for Hallandsås is presented. Thereafter the diagrams and principles for evaluating the stiffness stages from deformation curves are presented. The MathCad-code for calculating the stiffness is presented for one Hallandsås test and stiffness estimates for the service tunnel under Gothenburg concludes this appendix.

*Table A.IV-1: Input data for stiffness calculations for Hallandsås tunnel.*

| BH | Test | Date Time | Stage | $\Delta p$ (MPa) | $T_1$ (m²/s) | $T_2$ (m²/s) | $b_{hyd,1}$ (µm) | $b_{hyd,2}$ (µm) | $b_{meas}$ (µm) |
|---|---|---|---|---|---|---|---|---|---|
| 28 | WPT | 03-17 | A | 0.91 | $8.31·10^{-7}$ | $1.33·10^{-6}$ | 110 | 130 | - |
|    |     | 15:30 | B | 1.19 | $1.66·10^{-6}$ | $8.25·10^{-6}$ | 140 | 240 | - |
| 28 | WPT | 03-17 | A | 0.81 | $7.78·10^{-6}$ | $1.27·10^{-5}$ | 230 | 270 | 28 |
|    |     | 20:50 | B | 1.04 | $1.19·10^{-5}$ | $2.01·10^{-5}$ | 270 | 320 | 53 |
| 28 | WPT | 03-17 | A | 0.34 | $1.56·10^{-5}$ | $2.06·10^{-5}$ | 290 | 320 | 5 |
|    |     | 21:20 | B | 0.83 | $1.63·10^{-5}$ | $1.98·10^{-5}$ | 300 | 320 | 25 |
| 28 | WPT | 03-18 | A | 0.95 | $5.21·10^{-6}$ | $5.77·10^{-6}$ | 200 | 210 | 4 |
|    |     | 10:20 | B | 0.96 | $5.71·10^{-6}$ | $1.56·10^{-5}$ | 210 | 290 | 125 |
| 28 | WPT | 03-18 | A | 0.55 | $9.43·10^{-6}$ | $9.84·10^{-6}$ | 250 | 250 | 5 |
|    |     | 12:20 | B | 0.83 | $6.66·10^{-6}$ | $2.16·10^{-5}$ | 220 | 330 | 32 |
| 9 | Grouting | 03-31 | A | - | - | - | - | - | - |
|   |          | 16:50 | B | 0.40 | $(2.0·10^{-5})$ | $(1.4·10^{-5})$ | 470 | 420 | 27 |
| 28 | Grouting | 03-31 | A | - | - | - | - | - | - |
|    |          | 21:40 | B | 0.89 | $4.37·10^{-6}$ | $6.00·10^{-6}$ | 280 | 310 | 45 |
| 7 | Grouting | 03-31 | A | - | - | - | - | - | - |
|   |          | 22:30 | B | 1.39 | $2.54·10^{-8}$ | $3.27·10^{-7}$ | 50 | 120 | 25 |

*Table A.IV-2: Fracture normal stiffness for water pressure tests and grouting in Hallandsås, estimated in three ways. All stiffness values are expressed in GPa/m.*

| | | | Stage A | | | Stage B | | |
|---|---|---|---|---|---|---|---|---|
| BH | Test | Date Time | $k_n^{hyd}$ | $k_n^{meas}$ | $k_n^S$ | $k_n^{hyd}$ | $k_n^{meas}$ | $k_n^S$ |
| **28** | WPT | 03-17 15:30 | 16 | - | 19 | 4 | - | 11 |
| **28** | WPT | 03-17 20:50 | 7 | 10 | 4 | 7 | 7 | 3 |
| **28** | WPT | 03-17 21:20 | 4 | 23 | 2 | 14 | 11 | 2 |
| **28** | WPT | 03-18 10:20 | 45 | 79 | 5 | 4 | 3 | 5 |
| **28** | WPT | 03-18 12:20 | 52 | 37 | 3 | 3 | 9 | 4 |
| **9** | Grouting | 03-31 16:50 | - | - | - | -3 | 5 | 3 |
| **28** | Grouting | 03-31 21:40 | - | - | - | 9 | 7 | 7 |
| **7** | Grouting | 03-31 22:30 | - | - | - | 7 | 19 | 289 |

For the water pressure tests there was a substantial leakage out of the borehole. This leakage may cause too high values of transmissivity, and affect the $k_n^{hyd}$ and $k_n^S$.

Figures A.IV-1 through A.IV-8 presents data from Hallandsås, all figures have the following layout: In the left figure the measured deformation and the change in hydraulic aperture from pump data is presented. In the right figure stiffness stage A and B is evaluated from the transmissivity from pump data.
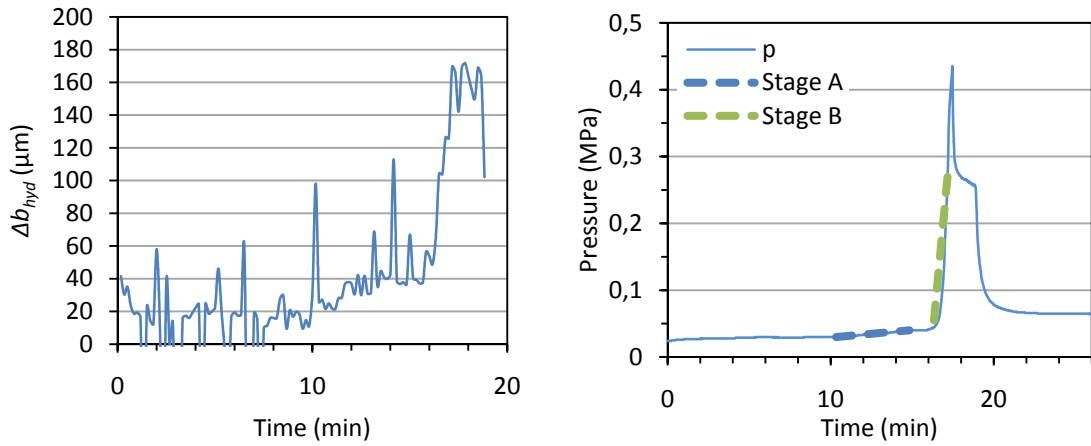


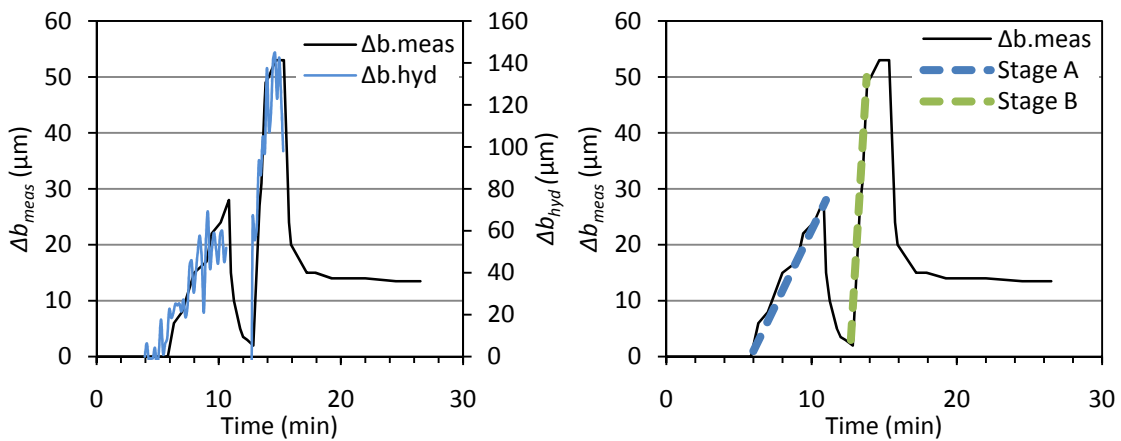*Figure A.IV-1: Pressure connection test, performed on 2010-03-17 at 15:30*



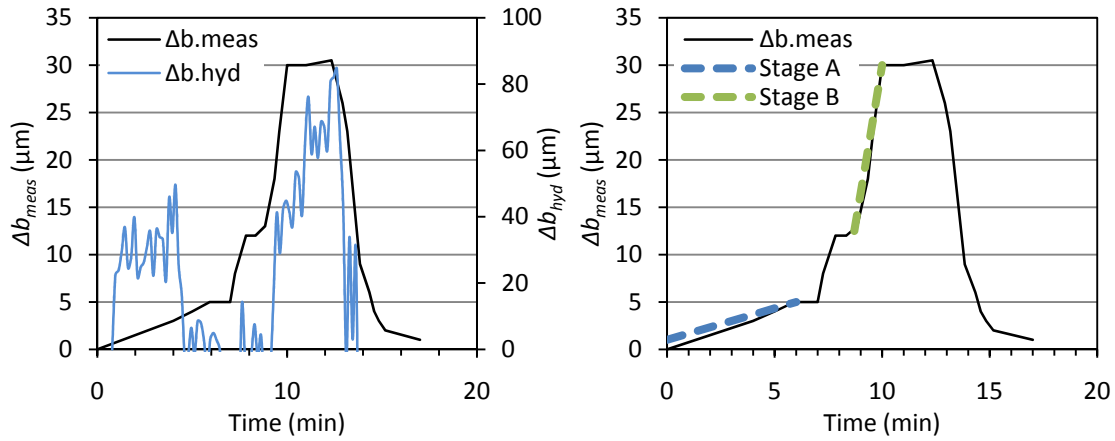*Figure A.IV-2: WPT, performed on 2010-03-17 at 20:50*
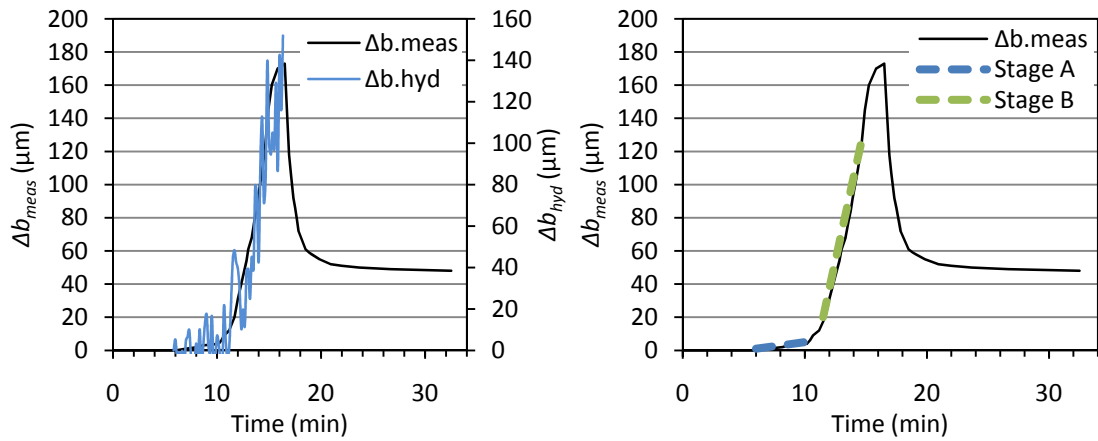
*Figure A.IV-3: WPT, performed on 2010-03-17 at 21:20*



*Figure A.IV-4: WPT, performed on 2010-03-18 at 10:20*
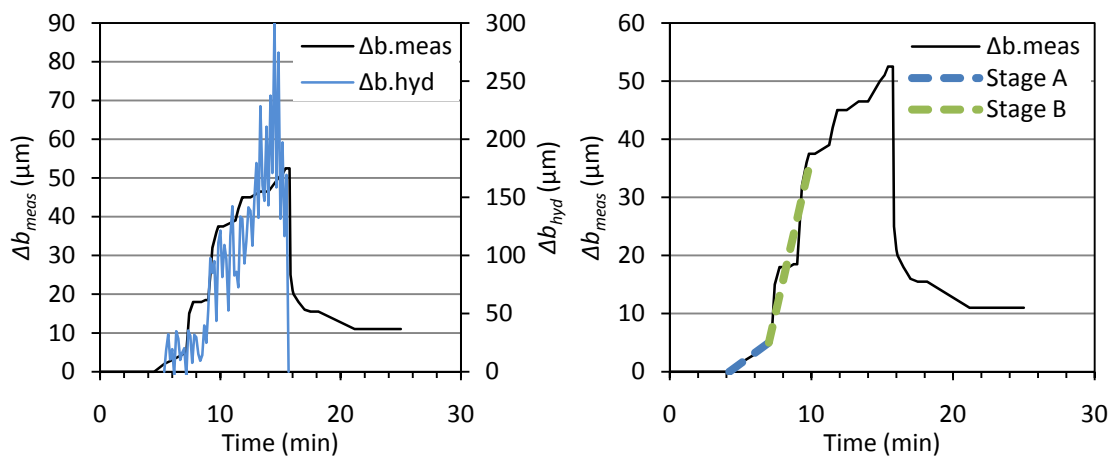


*Figure A.IV-5: WPT, performed on 2010-03-18 at 12:20*
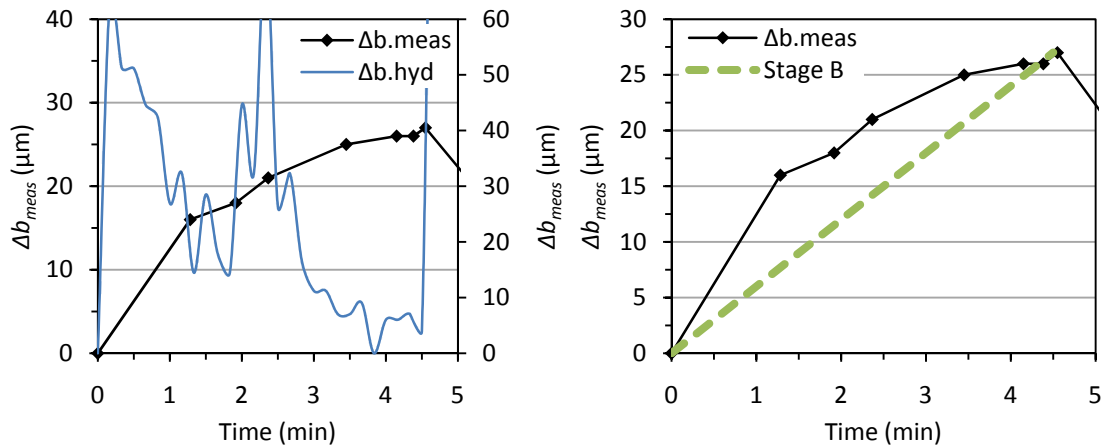
*Figure A.IV-6: Grouting BH9, performed on 2010-03-31 at 16:50*
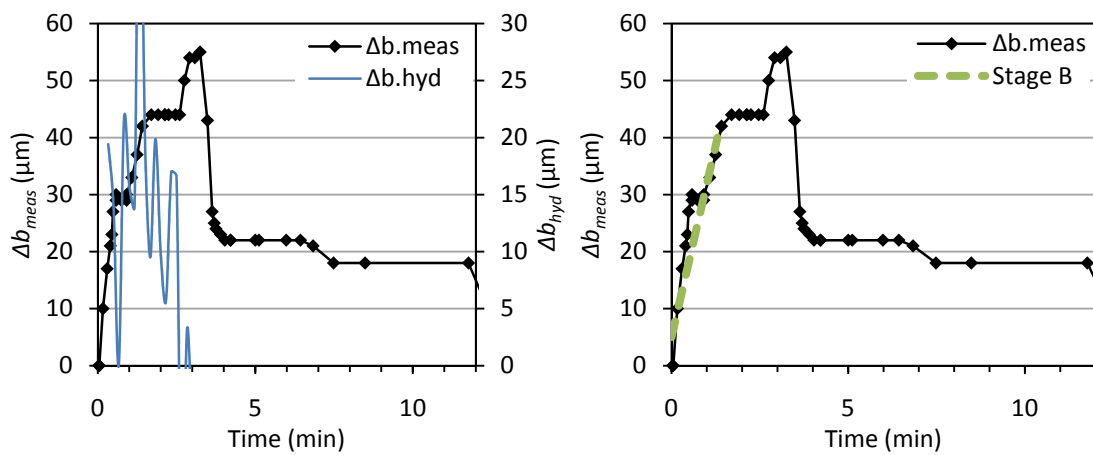


*Figure A.IV-7: Grouting BH28 performed on 2010-03-31 at 21:40*
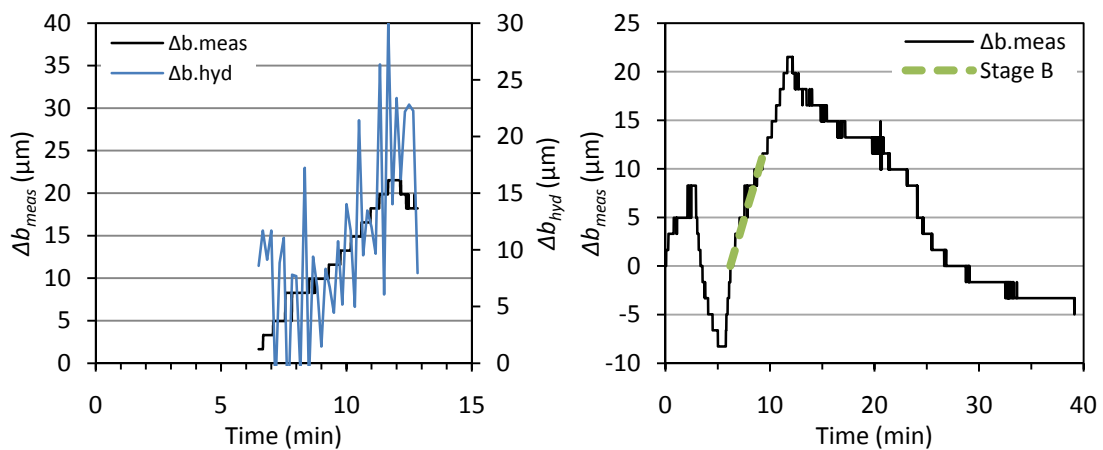


*Figure A.IV-8: Grouting BH7, performed on 2010-03-31 at 22:30*

Stiffness calculations

Input

$Holedepth := 6 \cdot m$

Index NIT and WPT is valid for calculation of stiffness Stage A for WPTs. For stage B, the NIT index means "Initial" and the WPT index means "After"
Index g means grout

$\Delta P := 0.55 \cdot MPa$

$\rho_w := 1000 \dfrac{kg}{m^3}$ $\qquad \rho_g := 1300 \dfrac{kg}{m^3}$

$\mu_w := 0.0013 \, Pa \cdot s$ $\qquad \mu_g := 0.0055 \, Pa \cdot s$

$b_{meas} := 5 \cdot 10^{-6} \cdot m$

$T_1 := 9.43 \cdot 10^{-6} \cdot \dfrac{m^2}{s}$

$x := 1 \cdot \left[ \left( \dfrac{m^2}{s} \right)^{0.71} \right]^{-1}$

$T_2 := 9.84 \cdot 10^{-6} \cdot \dfrac{m^2}{s}$

Help unit for $k_{nS}$

Calculations

$\Delta P_{mean} := \dfrac{\Delta P}{3} = 0.183 \, MPa$

$b_1 := \sqrt[3]{\dfrac{(12 \cdot \mu_g \cdot T_1)}{g \cdot \rho_g}} = 3.655 \times 10^{-4} \, m$ $\qquad b_{1my} := b_1 \cdot 1000000 = 365.48 \, m$

$b_2 := \sqrt[3]{\dfrac{(12 \cdot \mu_g \cdot T_2)}{g \cdot \rho_g}} = 3.707 \times 10^{-4} \, m$ $\qquad b_{2my} := b_2 \cdot 1000000 = 370.702 \, m$

Stiffness from hydraulic testing

$k_n := \dfrac{\Delta P_{mean}}{(b_2 - b_1)} = 35.109 \dfrac{GPa}{m}$

Stiffness from deformation measurements

$k_{n.meas} := \dfrac{\Delta P_{mean}}{(b_{meas})} = 36.667 \dfrac{GPa}{m}$

Stiffness from empiricism

$k_{n.S} := \dfrac{(\rho_g \cdot g)}{x \cdot 0.0109 \left[ \dfrac{(T_1)}{2} \right]^{0.71}} = 7.077 \cdot \dfrac{GPa}{m}$

*Table A.IV-3: Input data for stiffness calculations for service tunnel under Gothenburg.*

| Borehole | Test | Date | $\Delta p$ (Mpa) | $T_1$ (m$^2$/s) | $T_2$ (m$^2$/s) | $b_{hyd,1}$ (μm) | $b_{hyd,2}$ (μm) |
|----------|------|------|------------------|-----------------|-----------------|------------------|------------------|
| **KBH2** | WPT | 2009-11-16 | 0.48 | $1.09 \cdot 10^{-8}$ | $1.60 \cdot 10^{-8}$ | 26 | 29 |
| **KBH3** | WPT | 2010-03-03 | 1.96 | $4.63 \cdot 10^{-9}$ | $1.70 \cdot 10^{-8}$ | 19 | 30 |

*Table A.IV-4: Calculated stiffness, GPa/m for service tunnel under Gothenburg.*

| Borehole | Test | Date | $k_n^{hyd}$ | $k_n^S$ |
|----------|------|------|-------------|---------|
| **KBH2** | WPT | 2009-11-16 | 46 | 404 |
| **KBH3** | WPT | 2010-03-03 | 62 | 744 |

Figure A.V-9 shows the hydraulic aperture change in KBH3 during a water pressure test and the corresponding stiffness evaluation interval.
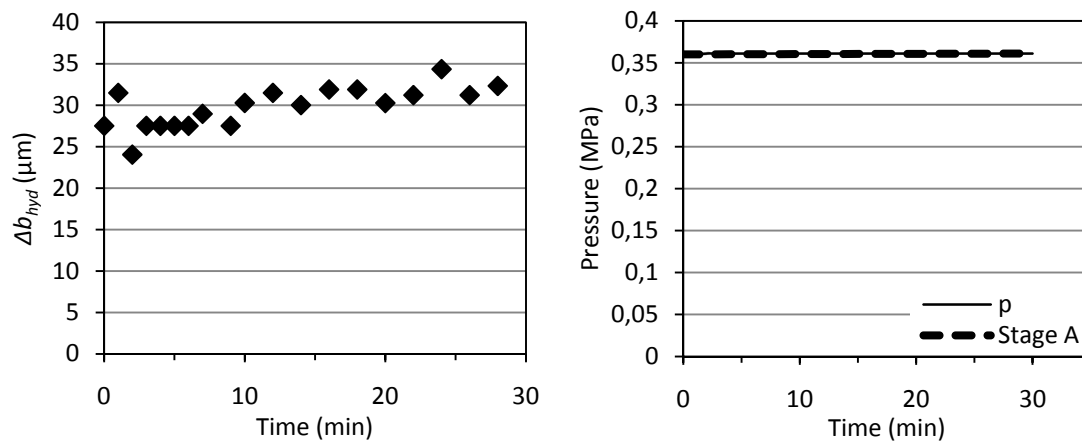


*Figure A.V-9: WPT, performed on 2010-03-03 at 10:00*

# Appendix V

## Correlation of deformation sensors

The deformation was measured with two different sensors. The digital sensor was set to log every second and the data was stored to a computer. The analog sensor was observed during the tests and the deformation was written in a protocol. These two observations were then compared in order to evaluate the differences between the sensors. For validation of the analog and digital deformation sensors the deformation measured by both methods were plotted in the same plot, and synchronized for start time, see Figure A.V-1 - Figure A.V-7.

The correlation between the two sensors seems to be quite good, the shape of the curves and the magnitude match almost perfectly. The difference that can be noticed at some parts is around 10 µm.
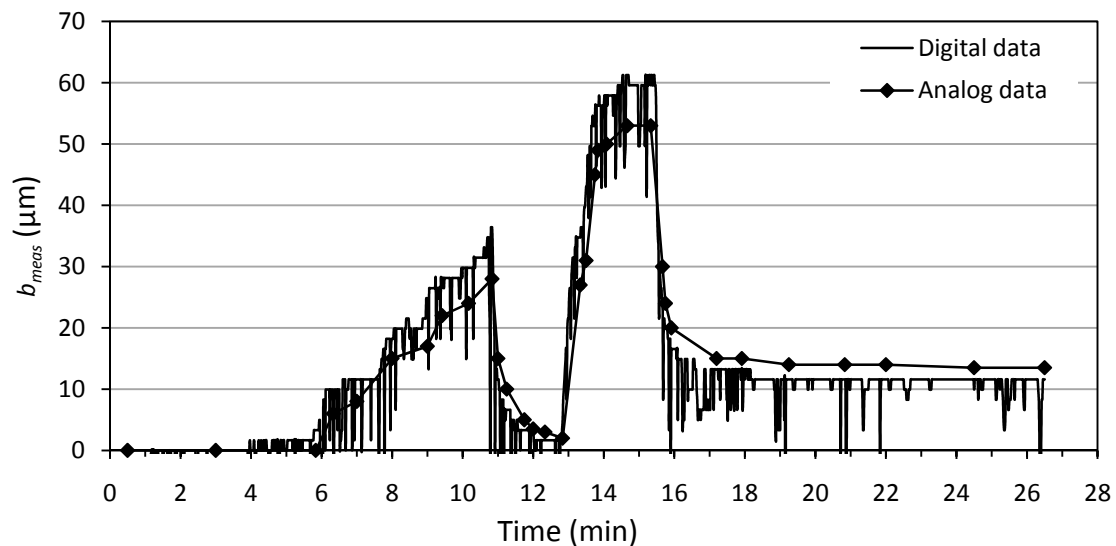


*Figure A.V-1: Deformation logged at water pressure test 2010-03-17 20:50.*
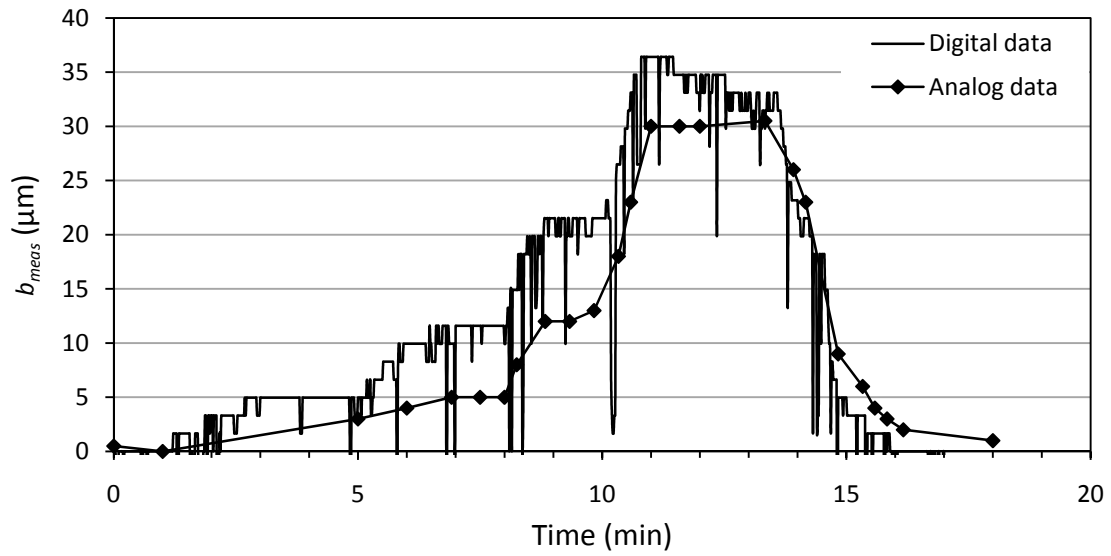
*Figure A.V-2: Deformation logged at water pressure test 2010-03-17 21:20.*
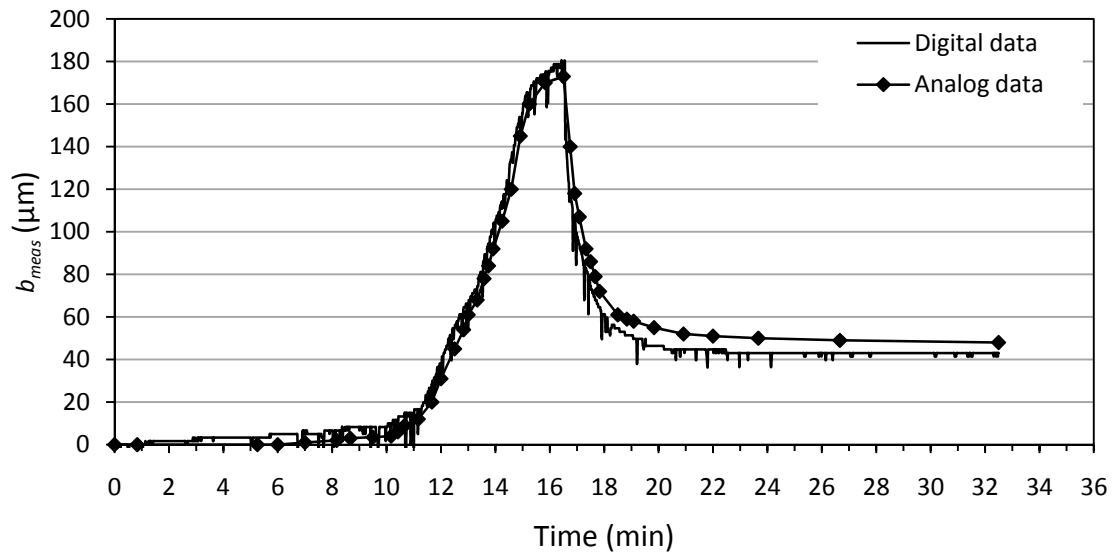


*Figure A.V-3: Deformation logged at water pressure test 2010-03-18 10:20.*
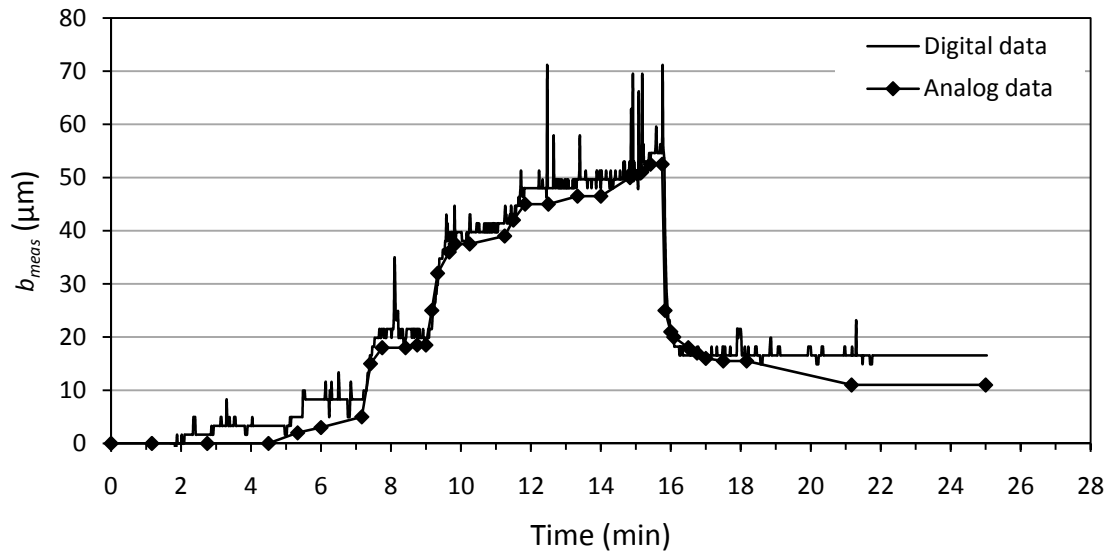
*Figure A.V-4: Deformation logged at water pressure test 2010-03-18 12:20.*
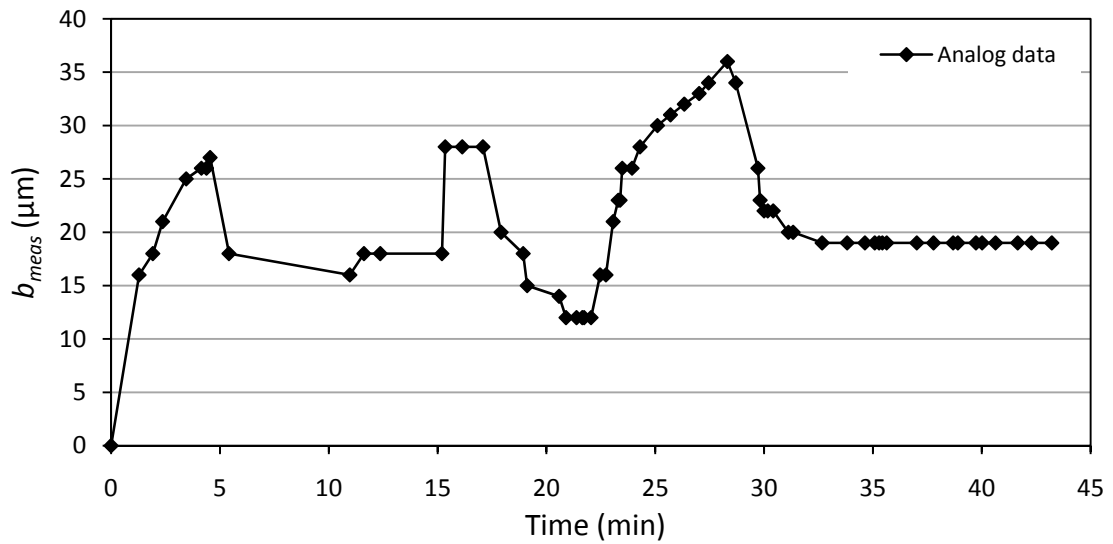


*Figure A.V-5: Deformation logged at the grouting of BH9, 2010-03-31 16:50. No digital data was obtained.*
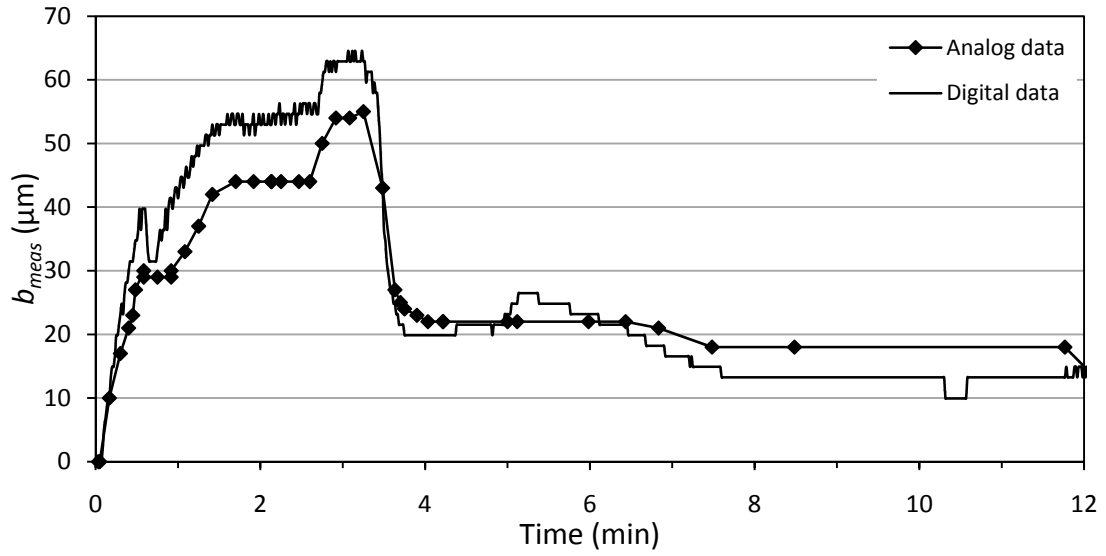
*Figure A.V-6: Deformation logged at the grouting of BH9, 2010-03-31 21:40*
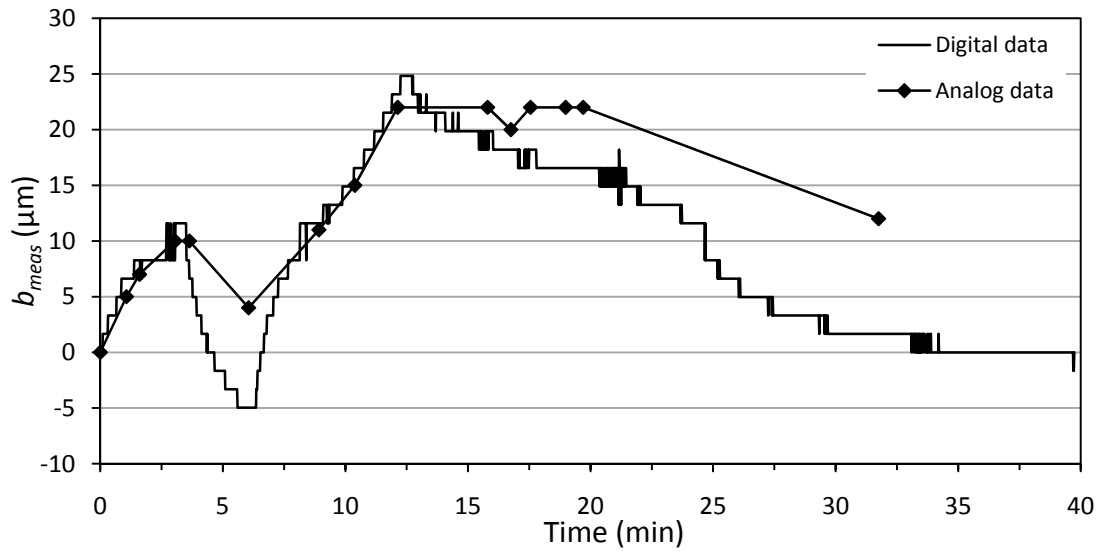


*Figure A.V-7: Deformation logged at the grouting of BH7, 2010-03-31 22:30*

# Appendix VI

## Flow dimension analysis

Results from the deformation measurement in BH8 in Hallandsås are presented in Figure A.VI-1-Figure A.VI-4 left. Flow dimension analysis was evaluated from the pump data and the result is presented in Figure A.VI-1-Figure A.VI-4, right. The pressure steps plotted is the total pressure, i.e. the pump pressure. Because of difficulties with the packer in BH28, a leakage from this hole was observed. This might be the reason for the high values in the dimension analysis. Although the trend is that when a deformation occur the flow dimension is increased. The four tests were performed in the same sequence as shown, starting with Figure A.VI-1.
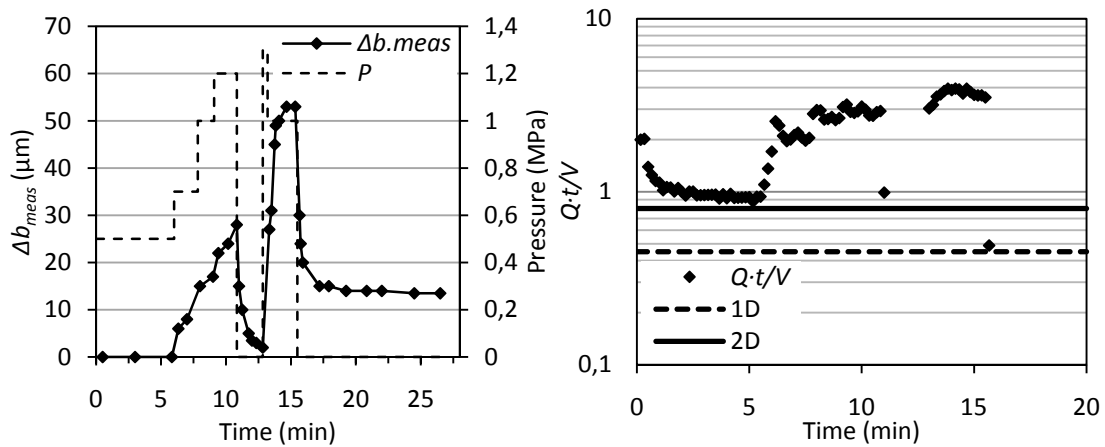


*Figure A.VI-1: Left: Deformation measured during water pressure test in BH28. Right: The dimensionality analysis for the water flow. An increase of the Q·t/V-value corresponds to a deformation.*
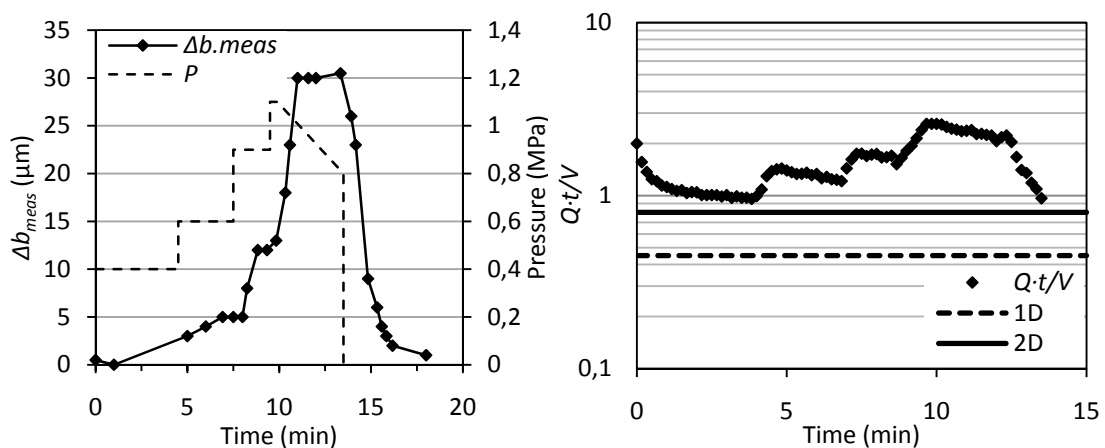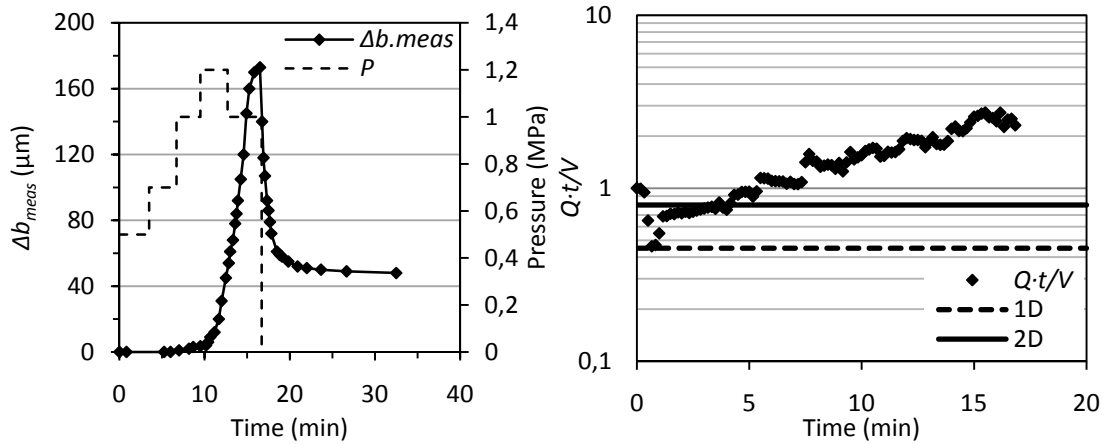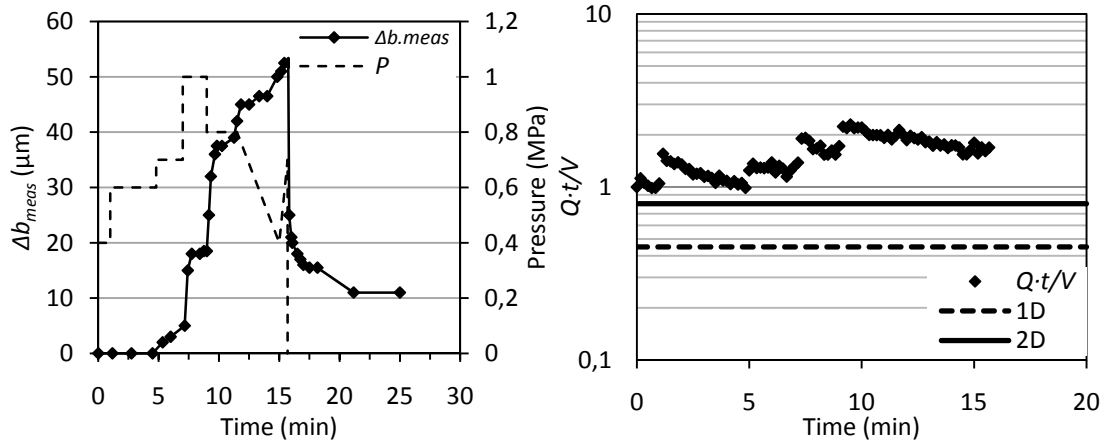


*Figure A.VI-2: Deformation measured during water pressure test in BH28. Right: The dimensionality analysis for the water flow. An increase of the Q·t/V-value corresponds to a deformation.*

*Figure A.VI-3: Deformation measured during water pressure test in BH28. Right: The dimensionality analysis for the water flow. An increase of the Q·t/V-value corresponds to a deformation.*



*Figure A.VI-4: Deformation measured during water pressure test in BH28. Right: The dimensionality analysis for the water flow. An increase of the Q·t/V-value corresponds to a deformation.*

Below the deformation measurements during grouting, performed in BH9, BH28 and BH7, in Hallandsås are shown (Figure A.VI-5-Figure A.VI-7). For each deformation graph, the corresponding flow dimensionality analysis is shown. As stated in chapter 2.2.6, a Q·t/V-value larger than 1.0 indicates a 3D flow, which could be either flow in a well connected 3D fracture network, deformation of fractures, or both. The general feature is that the flow dimension is at 3D when an increasing deformation is registered and 2D or lower when a regression is registered. The grouting of BH9 does not fully follow this trend (Figure A.VI-5).
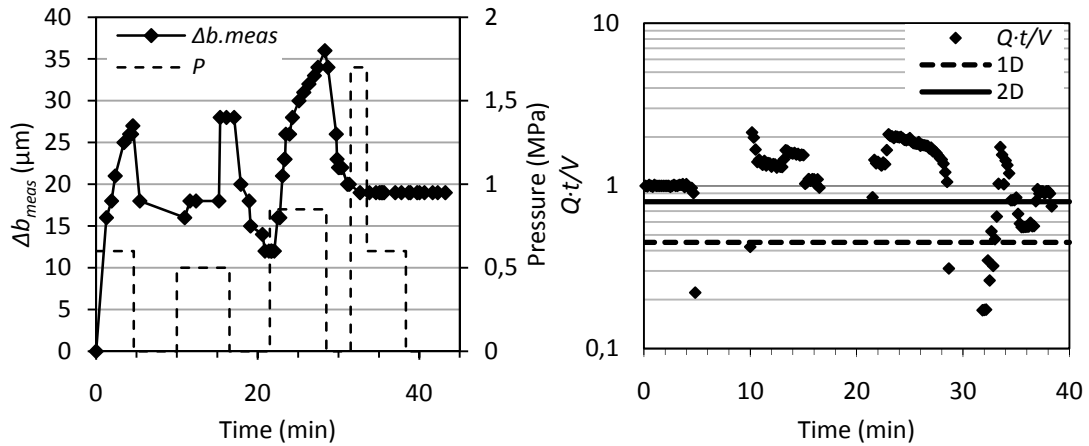
*Figure A.VI-5: Left: Deformation measured during the grouting of BH9. Right: The dimensionality analysis for the grout flow. The Q·t/V-value is above 0.8 when deformation occurs, which indicates 3D-flow.The gel time for the first grout batch was 25 min.*



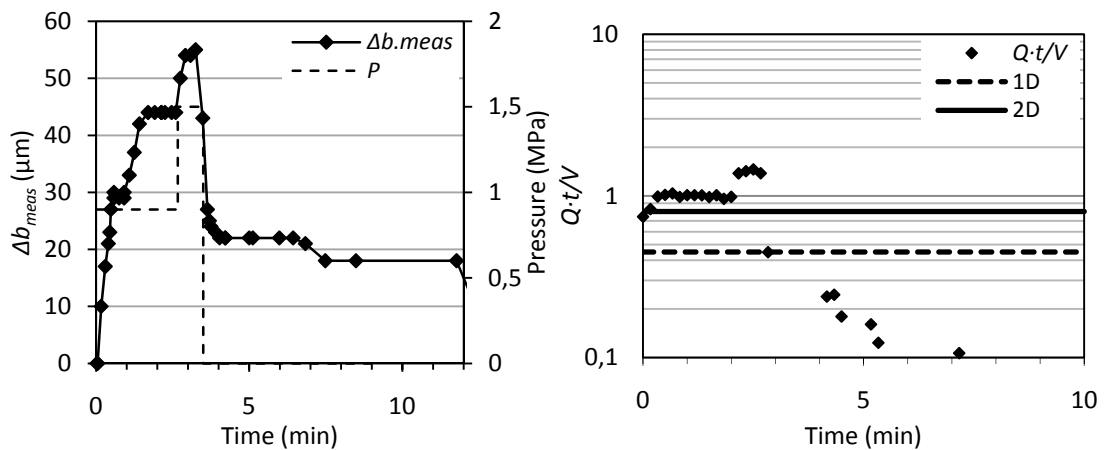*Figure A.VI-6: Left: Deformation measured during the grouting of BH28. Right: The dimensionality analysis for the grout flow. The Q·t/V-value is above 0.8 when deformation occurs, which indicates 3D-flow.The gel time for this grout batch was 7 min, which might be the reason for the reduced flow after 3.5 min.*
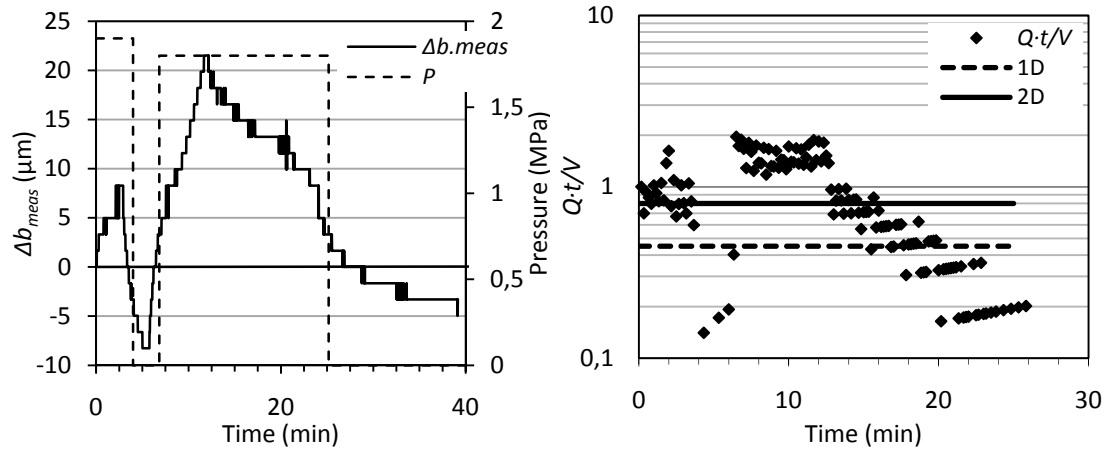
*Figure A.VI-7: Left: Deformation measured during the grouting of BH7. Right: The dimensionality analysis for the grout flow. The Q·t/V-value is about 0.8 when the first deformation occurs, and above 1.0 when the second deformation occurs, which indicates 3D-flow. The gel time for this grout batch is 25 min.*